N 62 11267

NASA TN D-1232

NASA TN D-1232

TECHNICAL NOTE

D-1232

STATIC AERODYNAMIC CHARACTERISTICS OF A TWO-STAGE AND A THREE-STAGE ROCKET VEHICLE AT MACH NUMBERS FROM 1.47 TO 4.63

By Clarence A. Brown, Jr., and Ausley B. Carraway

Langley Research Center
Langley Station, Hampton, Va.

NATIONAL AERONAUTICS AND SPACE ADMINISTRATION

WASHINGTON April 1962

1F

NATIONAL AERONAUTICS AND SPACE ADMINISTRATION

TECHNICAL NOTE D-1232

STATIC AERODYNAMIC CHARACTERISTICS OF A TWO-STAGE AND A THREE-STAGE ROCKET VEHICLE AT MACH NUMBERS FROM 1.47 TO 4.63

By Clarence A. Brown, Jr., and Ausley B. Carraway

L
1
9
6
7

SUMMARY

An investigation has been conducted in the Langley Unitary Plan wind tunnel to determine the effects of fin cant and fin size on the static aerodynamic characteristics of a 0.081-scale model of a three-stage and a two-stage Trailblazer II configuration. Tests were performed at Mach numbers from 1.47 to 4.63 and at a Reynolds number per foot of 3.0×10^6. The angle-of-attack range varied from approximately -5° to 5° and angle of sideslip varied from approximately -4° to 4°.

The results showed that all first-stage fins tested gave adequate static stability when the center-of-gravity travel of the flight model is taken into account. The presence of the auxiliary rocket motors in the lateral plane decreased the effectiveness of the fins in the pitch plane at the lower Mach number and increased the fin effectiveness at the higher Mach numbers. Removal of the auxiliary rocket motors from the first stage of the two-stage configuration reduced the axial force about 25 percent at the low Mach numbers and about 15 percent at the high Mach numbers. The first-stage fins were effective in producing about 90 percent of the rolling moment of the three-stage configuration when both of the stages had 2° cant in two of each set of fins.

INTRODUCTION

The National Aeronautics and Space Administration, in conjunction with Massachussetts Institute of Technology Lincoln Laboratory, is currently investigating the effects of dissociation and ionization of atmospheric gases on bodies reentering the atmosphere. These disturbed gases surrounding the body create problems in communications and also change the radar cross section of the reentering object. The lack of laboratory facilities capable of simulating conditions experienced by these high-speed bodies has led to the development of rocket vehicles for this purpose. The rocket vehicles use their first stages to boost a velocity package to altitude and the last stages to project it earthward at hypersonic speeds. The vehicle used previously in the reentry

physics program is known as Trailblazer I and wind-tunnel tests of the static stability characteristics of scale models are reported in references 1 and 2.

As a continuing effort in this field, a larger rocket vehicle, Trailblazer II, has been designed to boost a larger velocity package to altitude. Trailblazer II is a three-stage configuration of rather unconventional design; that is, its last stage is blunt and of larger diameter than the preceding stage. The effect of this blunt final stage on stability and fin roll could not be predicted with sufficient certainty and, therefore, it was considered necessary to conduct wind-tunnel tests to define these characteristics more accurately. The static stability characteristics of the combined second and third stages have already been reported in reference 3.

L
1
9
6
7

The present paper is concerned with tests of a 0.081-scale three-stage and a two-stage configuration of Trailblazer II to determine the effects of fin size and fin cant on the static stability characteristics. The two-stage configuration was tested because preliminary calculations had indicated the possibility that the second-stage booster of the three-stage configuration may not be necessary in some instances to obtain the altitude needed for full-scale flight test. Tests were conducted at Mach numbers from 1.47 to 4.63 at a constant Reynolds number per foot of 3.0×10^6. The angle-of-attack range was from about -5° to 5° and the angle of sideslip was varied from approximately -4° to 4°.

SYMBOLS

The coefficients of forces and moments are referred to the body-axis system. (See fig. 1.) Aerodynamic moments for the three-stage configuration and the two-stage configuration are presented about points located 34.55 inches and 22.38 inches aft of the model nose, respectively, for these configurations. The moment centers given above would correspond to the loaded center-of-gravity locations for the full-scale Trailblazer II configurations. Symbols used in this paper are as follows:

A exposed fin aspect ratio

C_A axial-force coefficient, $\frac{\text{Axial force}}{qS}$

$C_{A,o}$ axial-force coefficient at 0° angle of attack

L
1
9
6
7

C_l rolling-moment coefficient, $\frac{\text{Rolling moment}}{qSd}$

$C_{l,o}$ rolling-moment coefficient at 0° angle of sideslip

C_m pitching-moment coefficient, $\frac{\text{Pitching moment}}{qSd}$

C_{m_α} slope of pitching-moment curve through 0° angle of attack

C_N normal-force coefficient, $\frac{\text{Normal force}}{qS}$

C_{N_α} slope of normal-force curve through 0° angle of attack

C_n yawing-moment coefficient, $\frac{\text{Yawing moment}}{qSd}$

C_{n_β} slope of yawing-moment curve through 0° angle of sideslip

C_Y side-force coefficient, $\frac{\text{Side force}}{qS}$

C_{Y_β} slope of side-force curve through 0° angle of sideslip

d diameter of first stage of test configuration, 2.501 in.

M free-stream Mach number

q free-stream dynamic pressure, lb/sq ft

S cross-sectional area of first stage of test configuration, 0.03416 sq ft

x_{cp} center-of-pressure location, in. aft of model nose

α angle of attack of model center line, deg

β angle of sideslip of model center line, deg

δ_I angle of cant of first-stage fin, deg

δ_{II} angle of cant of second-stage fin, deg

MODELS

Three-Stage Configuration

Photographs of the three-stage Trailblazer II configuration are shown in figures 2(a) and 2(b). A two-view drawing with dimensional details of the model tested is presented in figure 2(c). The $\frac{1}{12.4}$-scale model consisted of the first-stage booster with auxiliary rocket motors, the second-stage booster, and the velocity package of the Trailblazer II configuration. In the full-scale vehicle, the velocity package houses the rearward-firing third and fourth stages as well as necessary instrumentation.

L
1
9
6
7

The first-stage booster was equipped with cruciform modified double-wedge-shaped fins with a leading-edge sweep of $18^{\circ}24'$. Three sets of fins, which are illustrated in figure 3, were provided for this first stage. One set represented full-scale fins with an exposed area (outboard of the body) of 12 square feet and an aspect ratio of 1.5. A second set, in which the fin design was obtained by clipping the tips from the first fin design, represented full-scale fins with an exposed area of 10 square feet and an aspect ratio of 0.985. The third set represented full-scale fins with an exposed area of 10 square feet and an aspect ratio of 1.5. For convenient reference, the fin configurations are identified herein as the 12-sq-ft, $A = 1.5$ fins, the 10-sq-ft, $A = 0.985$ fins, and the 10-sq-ft, $A = 1.5$ fins. The model was orientated in the tunnel so that two fins were located in the lateral (pitch) plane and two fins were located in the vertical (yaw) plane. The two vertical fins (fig. 2(c)) were capable of being canted 0°, 1°, and 2° to produce positive roll for the vehicle. The 10-sq-ft, $A = 0.985$ fins were tested with 0° angle of cant. The other sets of vertical fins of this stage were canted to produce positive rolling moment.

The first-stage booster also had two auxiliary rocket motors mounted on the side. Sketches of these motors, along with the short adapters with launching lugs used to connect the first- and second-stage boosters, are shown in figure 4.

The second-stage booster was equipped with cruciform wedge-shaped fins (fig. 4) with a leading-edge sweep angle of 30°. These fins were alined with the first-stage booster fins. The wedge half-angle for these fins was 4° and the fins were 0.081-scale of 4-sq-ft fins. Two sets of horizontal fins were provided for this stage with cant angles of 0° and 2°; the fins canted 2° produced positive rolling moment.

The nose of the velocity package is a hemispherical segment tangent to a 17° cone frustum. Another cone frustum of approximately 1° half-angle forms the tube section of the velocity package. The maximum diameter of the velocity package is larger than that of the second-stage booster, so that an inverse cone-frustum adapter is required to connect these stages.

Two-Stage Configuration

L
1
9
6
7

Photographs of the two-stage configuration are shown in figures 5(a), 5(b), and 5(c). A two-view drawing with dimensional details of the model tested is presented in figure 5(d).

The first-stage booster, auxiliary rocket motors, and fins are identical to those of the first stage of the three-stage configuration. The adapter used in this configuration to connect the first-stage booster and velocity package is identified in figure 4 as the long first-stage adapter. The velocity package is also identical to that of the three-stage configuration.

MEASUREMENTS

Aerodynamic forces and moments were measured by means of a six-component electrical strain-gage balance housed within the model. The balance, in turn, was rigidly fastened to a sting-support system. Schlieren photographs were taken at various model attitudes and Mach numbers; some of these photographs are presented in figure 6. Static pressure was measured in the vicinity of the balance chamber for each model and test condition.

ACCURACY

The accuracy of the individual measured quantities, based on calibration and repeatability of data, is estimated to be within the following limits:

C_A	±0.002
C_l	±0.01
C_m	±0.05
C_n	±0.05
C_N	±0.05

C_Y . . . . . ±0.05
Mach number:
For range from M = 1.57 to 3.96 . . . . . ±0.015
For M = 4.63 . . . . . ±0.05

α, deg . . . . . ±0.10
β, deg . . . . . ±0.10

CORRECTIONS

L
1
9
6
7

Angles of attack were corrected for average tunnel-flow angularity and for deflection of model and sting support as a result of aerodynamic loads. The axial-force data were adjusted to corresponding free-stream static conditions or zero chamber axial-force coefficient.

APPARATUS AND METHODS

Wind Tunnel

The tests were conducted in both the low and high Mach number test sections of the Langley Unitary Plan wind tunnel, which is a variable-pressure, continuous-flow tunnel. Each of the test sections is approximately 4 feet square and 7 feet long. The nozzles leading to each test section are of the asymmetric sliding-block type, which permits a continuous variation of Mach number from approximately 1.5 to 2.9 in the low Mach number test section, and from approximately 2.3 to 4.7 in the high Mach number test section.

Test Conditions

The test conditions were as follows:

Mach number	Stagnation temperature, °F	Stagnation pressure, lb/sq ft abs
1.47	125	10.87
1.97	125	12.85
2.36	150	16.39
2.86	150	21.28
3.96	175	40.11
4.63	175	54.74

All configurations were tested through an angle-of-attack range of approximately -5° to 5° at an angle of sideslip of 0° and through an angle-of-sideslip range of about -4° to 4° at angles of attack of -4°, 0°, and 4°. The Reynolds number per foot was 3.0×10^{6} and stagnation dewpoint was maintained at -30° F in order to avoid condensation effects.

In an attempt to obtain turbulent flow over the model, a transition strip was fixed around the model, 1 inch rearward of the nose. The transition strip was about $\frac{1}{8}$ inch wide and consisted of 0.012-inch carborundum grains imbedded in shellac.

L
1
9
6
7

PRESENTATION OF RESULTS

The results of this investigation are presented in the following figures:

	Figure
Typical schlieren photographs of models tested	6
Aerodynamic characteristics:	
Three-stage configuration	7 to 14
Two-stage configuration	15 to 22
Summary plots:	
Three-stage configuration	23 to 25
Two-stage configuration	26 to 28
Effect of Mach number and fin configuration on center of pressure:	
Three-stage configuration	29(a)
Two-stage configuration	29(b)

DISCUSSION

Although the results presented in this paper are for a specific vehicle, the data can be used for other similar configurations.

Figure 23 shows $C_{m_{\alpha}}$, $C_{N_{\alpha}}$, and $C_{A,o}$ as functions of Mach number for the three-stage configuration with fins of different sizes on the first stage. These derivatives and coefficients varied smoothly with Mach number and, as expected, the configuration with 12-sq-ft, $A = 1.5$ fins showed greater pitching-moment and normal-force slopes.

It should be noted that the configuration with the 10-sq-ft, $A = 0.985$ fins showed greater pitching-moment and normal-force slopes than did that with the 10-sq-ft, $A = 1.5$ fins. This difference could be due to the difference in downwash on the two sets of fins and/or the interference effects of the auxiliary rocket motors and is within the accuracy of the data. Very little difference in the axial-force coefficient could be noted for the different fin sizes.

Figure 24 shows the variation of C_{n_β} and C_{Y_β} with Mach number for this model. Comparison of figure 23 with figure 24 shows that at the lowest test Mach number, values of C_{n_β} were larger for the model with 12-sq-ft and 10-sq-ft, $A = 1.5$ fins than were the values of the equivalent parameter in the pitch plane C_{m_α}. It can also be seen that the model with the 10-sq-ft, $A = 1.5$ fins had a higher C_{n_β} than C_{m_α} at the higher Mach numbers. This result is probably caused by the presence of two auxiliary rocket motors in the lateral plane for this test.

L
1
9
6
7

Figure 25 shows the variation of C_l with Mach number due to canting the first-stage fins in the vertical plane and canting the second-stage fins in the horizontal plane. These data show that the 10-sq-ft, $A = 0.985$ fins produced more rolling moment than did the 10-sq-ft, $A = 1.5$ fins. It should also be noted that canting the second-stage fins had a negligible effect on the rolling moment. This result is attributed in part to the larger fins on the first-stage booster.

Presented in figure 26 is the variation of C_{N_α}, C_{m_α}, and $C_{A,o}$ with Mach number for the two-stage configuration with 10-sq-ft and 12-sq-ft, $A = 1.5$ fins. Also included are data for the configuration with the 12-sq-ft, $A = 1.5$ fins with the auxiliary rocket motors removed. Very little difference is noted in pitching-moment and normal-force derivatives as a result of the removal of the auxiliary rocket motors, but a reduction of axial force by about 25 percent at the low Mach numbers and 15 percent at the high Mach numbers occurred.

Figure 27 shows the variation of C_{n_β} and C_{Y_β} with Mach number for the two-stage configuration with 10-sq-ft and 12-sq-ft, $A = 1.5$ fins and also with 12-sq-ft, $A = 1.5$ fins without the auxiliary rocket motors. In this case, removal of the auxiliary rocket motors tended to decrease the fin effectiveness at the lower Mach numbers, probably because of the presence of the auxiliary rocket motors in the yaw plane.

Figure 28 shows the rolling-moment coefficient C_l for 0° and 2° of fin cant on the vertical fins of the two-stage configuration. Comparison of figure 28 with figure 25 shows that the first-stage fins are

effective in producing approximately 90 percent of the rolling moment of the three-stage configuration when both of the stages have 2° incidence in two of each set of the fins.

Presented in figure 29 is the center-of-pressure location for each of the configurations tested. In all cases, the moment center was taken as the loaded center-of-gravity location. As is shown in figure 29(a) for the three-stage configuration, the model with 10-sq-ft, A = 0.985 fins had a center-of-pressure location farther aft than did that with the 10-sq-ft, A = 1.5 fins. This difference could be due to the differences in downwash on the two sets of fins and/or the interference effects of the auxiliary rocket motors and is within the accuracy of the data. As expected, the 12-sq-ft, A = 1.5 fins had the center-of-pressure location in the most rearward position.

L
1
9
6
7

Since the full-scale vehicle has a large center-of-gravity shift during thrusting of the rocket motor, only one moment center was selected. This moment center was taken as the loaded center of gravity of the full-scale vehicle. In flight, the center-of-gravity travel represents a distance of 2.9 diameters forward. For the three-stage configuration, the model with 10-sq-ft, A = 1.5 fins showed a center of pressure ahead of the moment center at Mach numbers greater than 4.3. Since this center-of-pressure condition can never exist during flight of the full-scale vehicle, the 10-sq-ft fins will give adequate static stability for all Mach numbers of interest.

CONCLUSIONS

An investigation has been conducted in the Langley Unitary Plan wind tunnel to determine the effects of fin cant and fin size on the aerodynamic characteristics of a 0.081-scale model of a three-stage and two-stage Trailblazer II configuration. This investigation was conducted at Mach numbers from 1.47 to 4.63 and at a Reynolds number per foot of 3.0×10^{6}. Aerodynamic moments were taken about a point 34.55 inches and 22.38 inches aft of the model nose for the three- and two-stage Trailblazer II configuration, respectively.

This investigation indicated the following conclusions:

1. All first-stage fins tested gave adequate static stability when the center-of-gravity travel of the flight model was taken into account.

2. The presence of the auxiliary rocket motors in the lateral plane decreased the effectiveness of the fins in the pitch plane at the lower Mach numbers and increased the fin effectiveness at the higher Mach numbers.

3. Removal of the auxiliary rocket motors from the first stage of the two-stage configuration reduced the axial force about 25 percent at the low Mach numbers and about 15 percent at the high Mach numbers.

4. The first-stage fins were effective in producing approximately 90 percent of the rolling moment of the three-stage configuration when both of the stages had 2° cant in two of each set of fins.

Langley Research Center,
National Aeronautics and Space Administration,
Langley Air Force Base, Va., January 19, 1962.

L
1
9
6
7

REFERENCES

1. Gregory, Donald T., and Carraway, Ausley B.: Investigation of the Static Longitudinal Stability and Roll Characteristics of a Three-Stage Missile Configuration at Mach Numbers From 1.77 to 2.87. NASA TM X-124, 1959.

2. Robinson, Ross B.: Effects of Body and Fin Deflections on the Aerodynamic Characteristics in Pitch of a 0.065-Scale Model of a Four-Stage Rocket Configuration at Mach Numbers of 1.41 and 1.82. NASA TN D-37, 1959.

3. Carraway, Ausley B., Edwards, Frederick G., and Keating, Jean C.: Investigation of the Static Stability Characteristics of Two Stages of a Three-Stage Missile at a Mach Number of 4.00. NASA TN D-651, 1961.

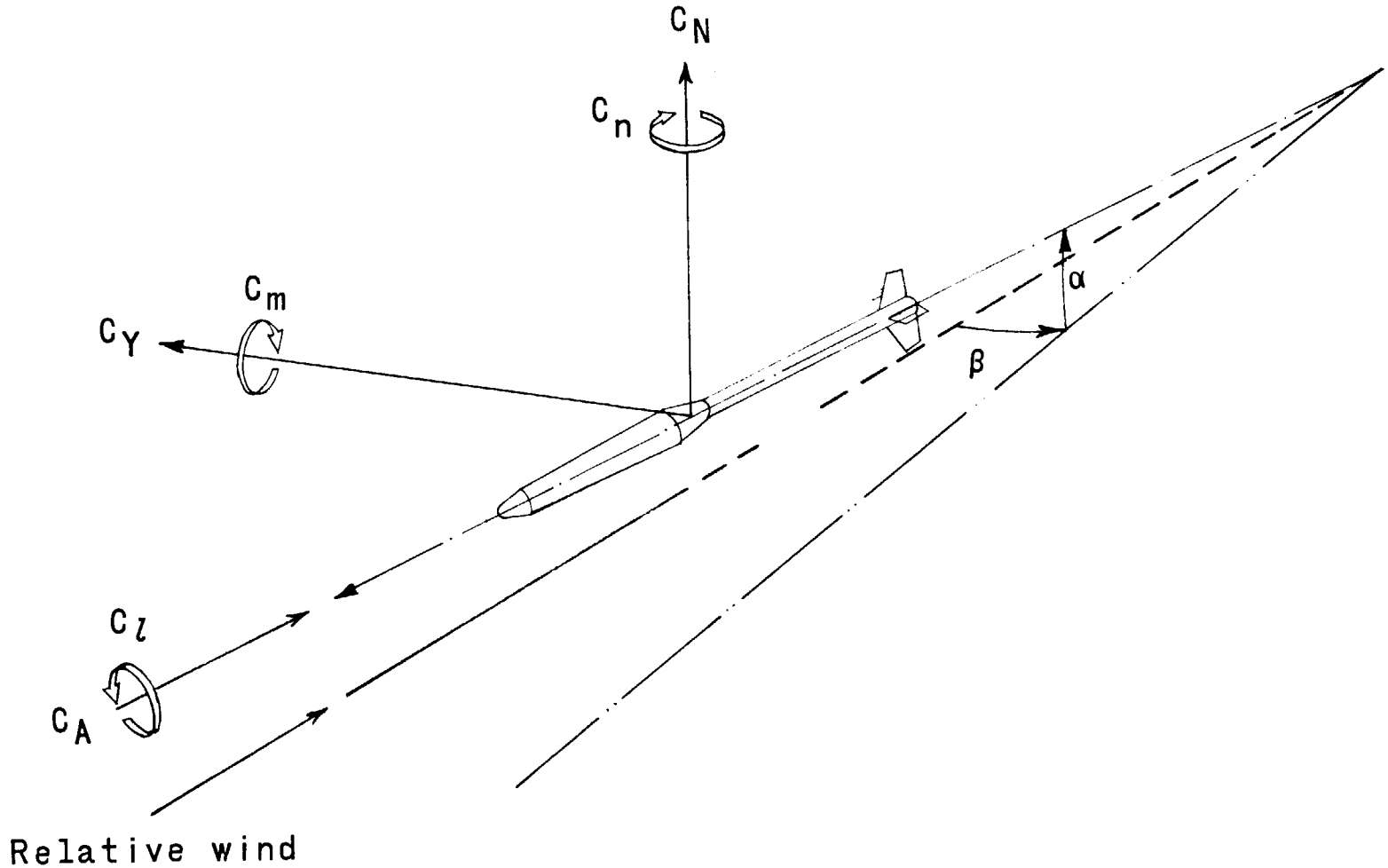

Figure 1.- Body-axis system. Arrows indicate positive direction.

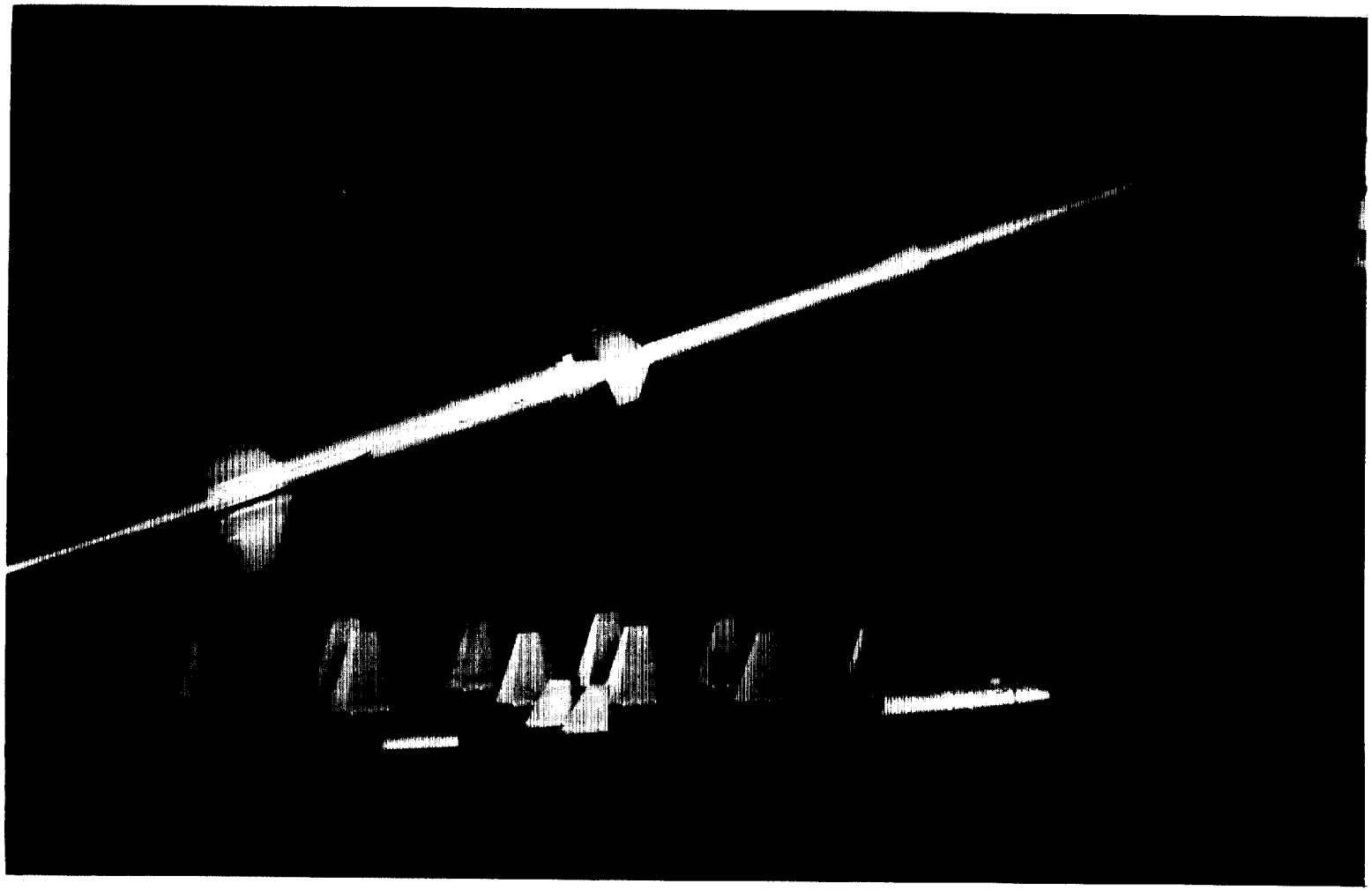

(a) Sideview of three-stage model. L-60-7279

Figure 2.- Photographs and sketch of three-stage model Trailblazer II configuration tested.

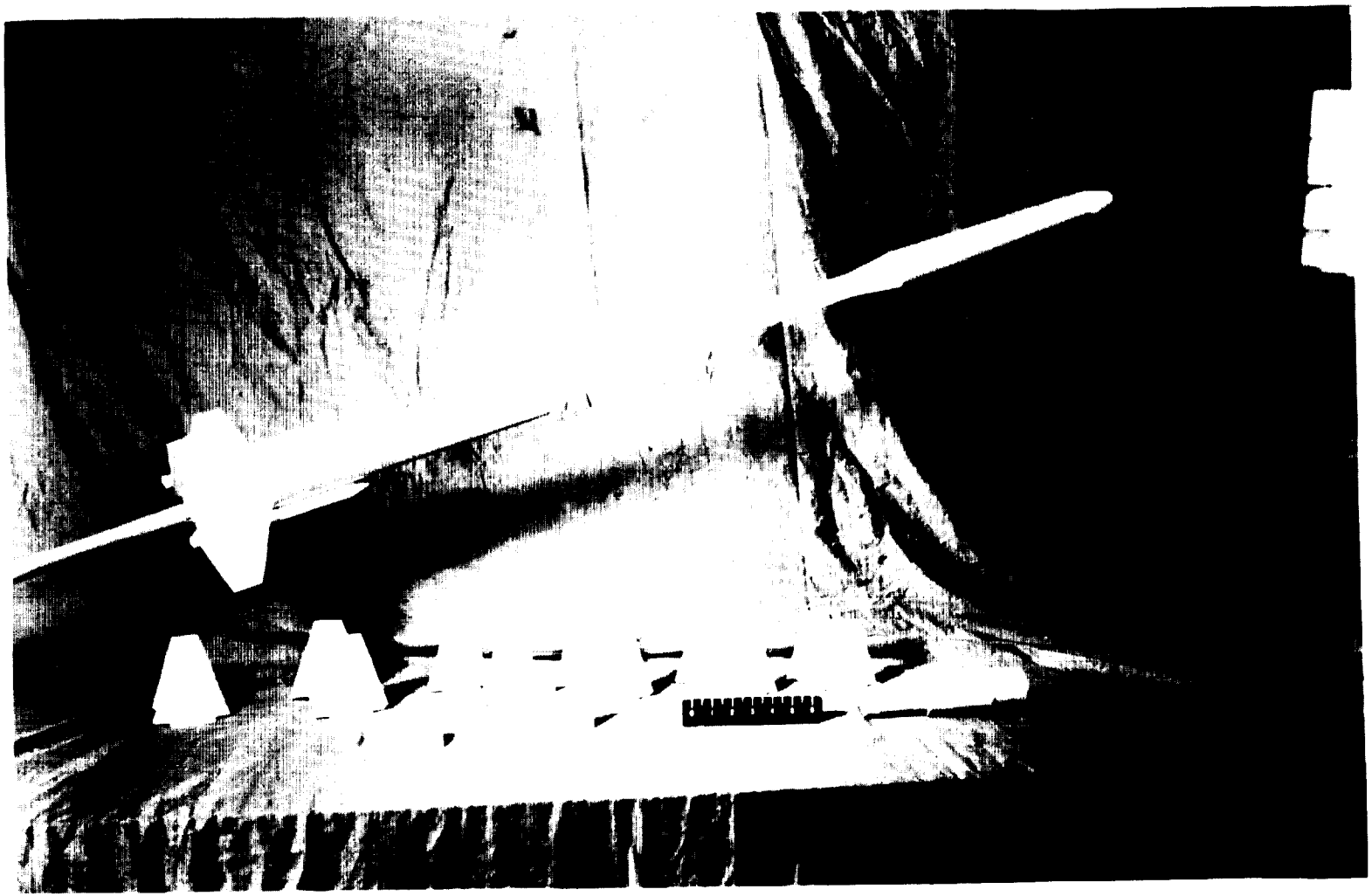

(b) Planview of three-stage model. L-60-7280

Figure 2.- Continued.

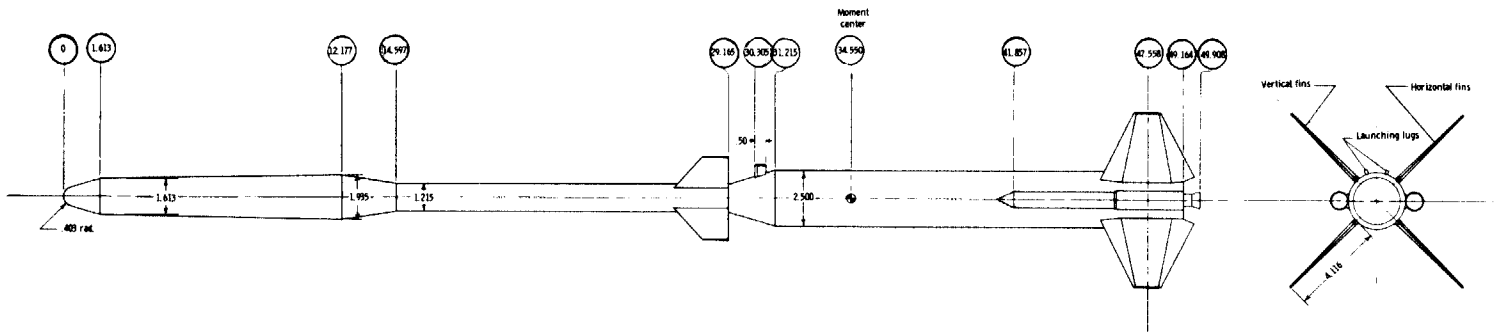

(c) Sketch of a three-stage model of Trailblazer II configuration. All dimensions are in inches. Circled numbers indicate stations in inches.

Figure 2.- Concluded.

L-1967

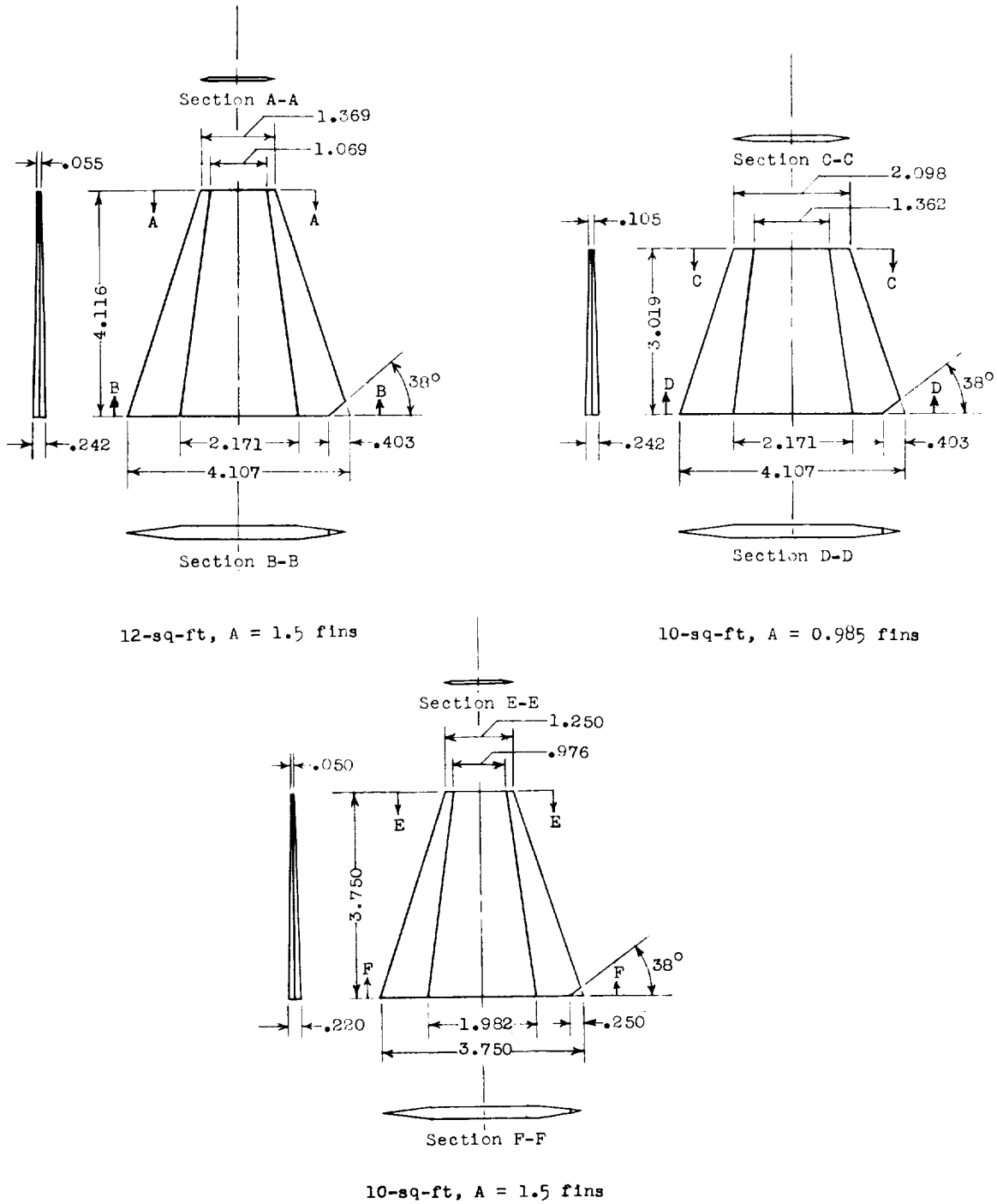

Figure 3.- Sketch of 0.081-scale model of first-stage booster fins. All dimensions are in inches.

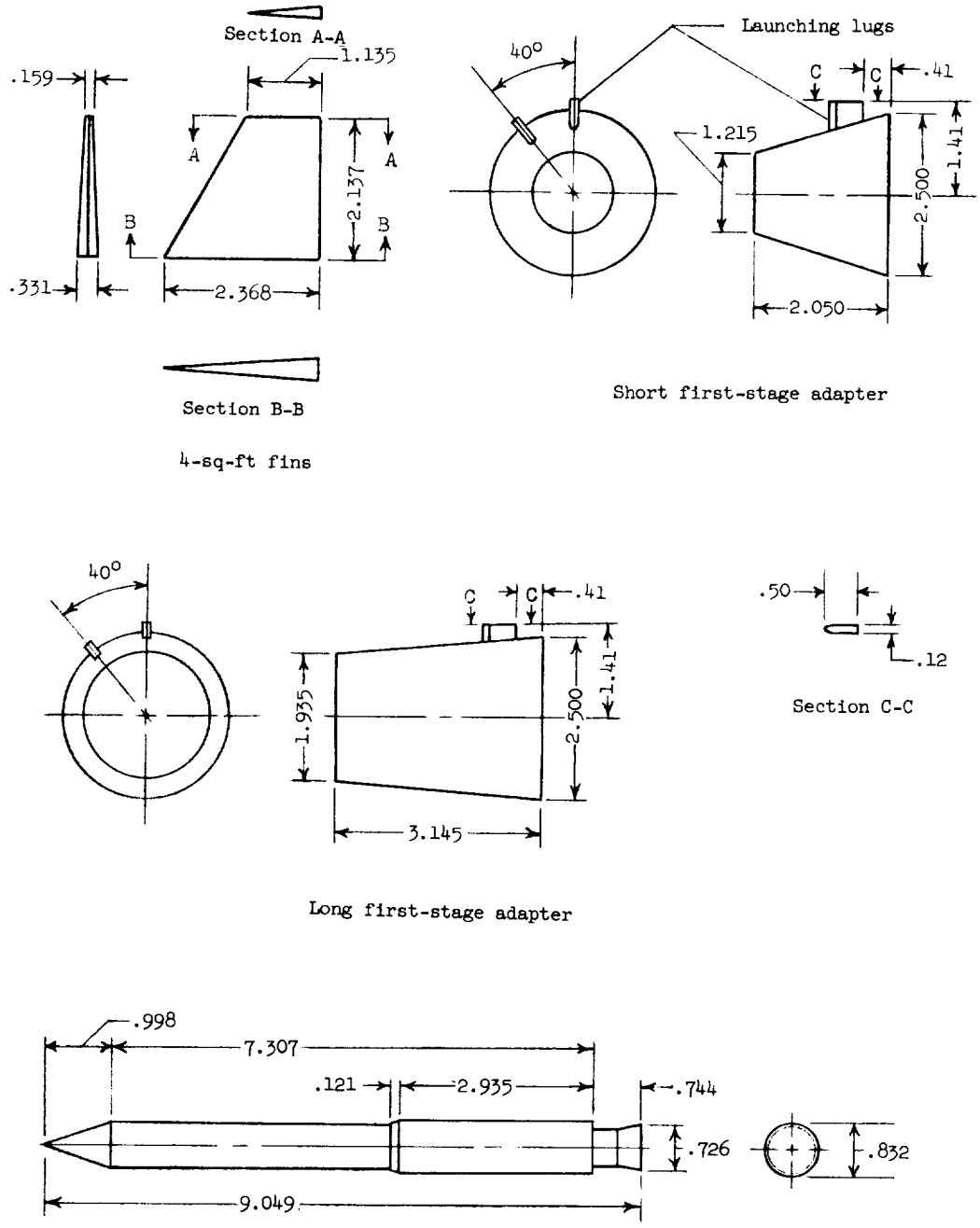

Figure 4.- Sketch of second-stage booster fins, long and short first-stage adapters, and first-stage auxiliary rocket motor. All dimensions are in inches.

L-1967

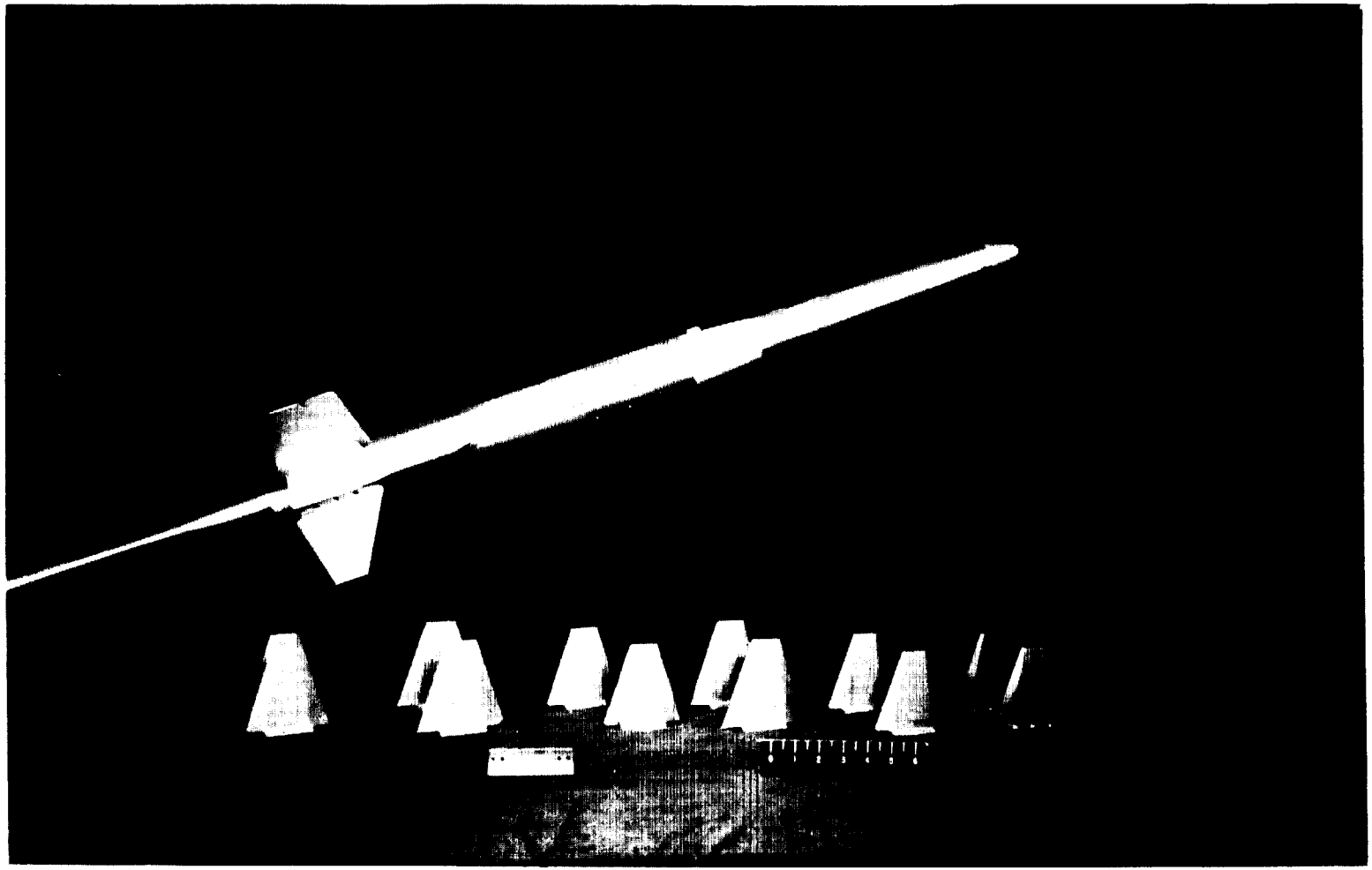

(a) Sideview of two-stage model. L-60-7283

Figure 5.- Photographs and sketch of two-stage model of Trailblazer II configuration.

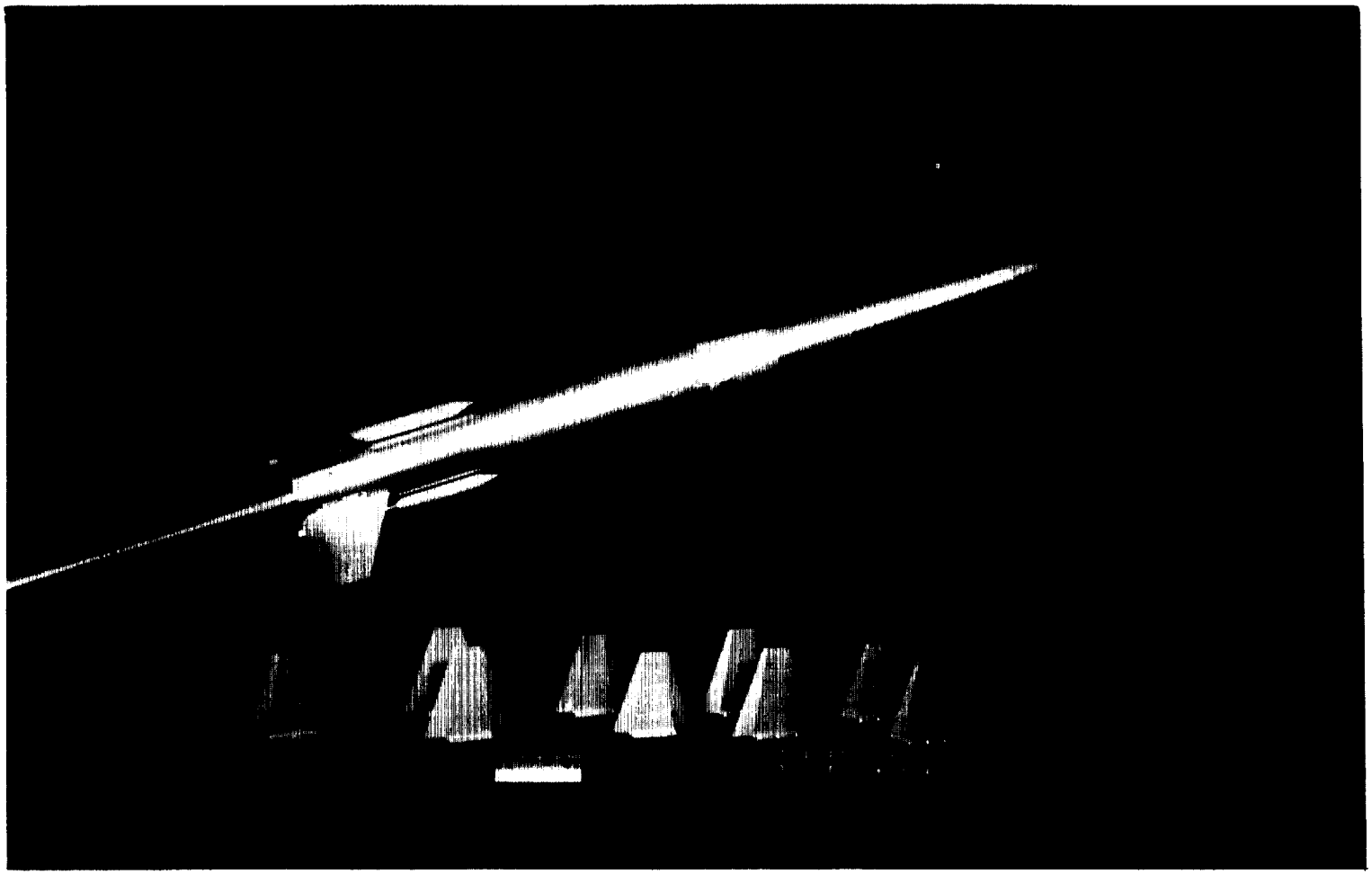

(b) Planview of two-stage model. L-60-7281

Figure 5.- Continued.

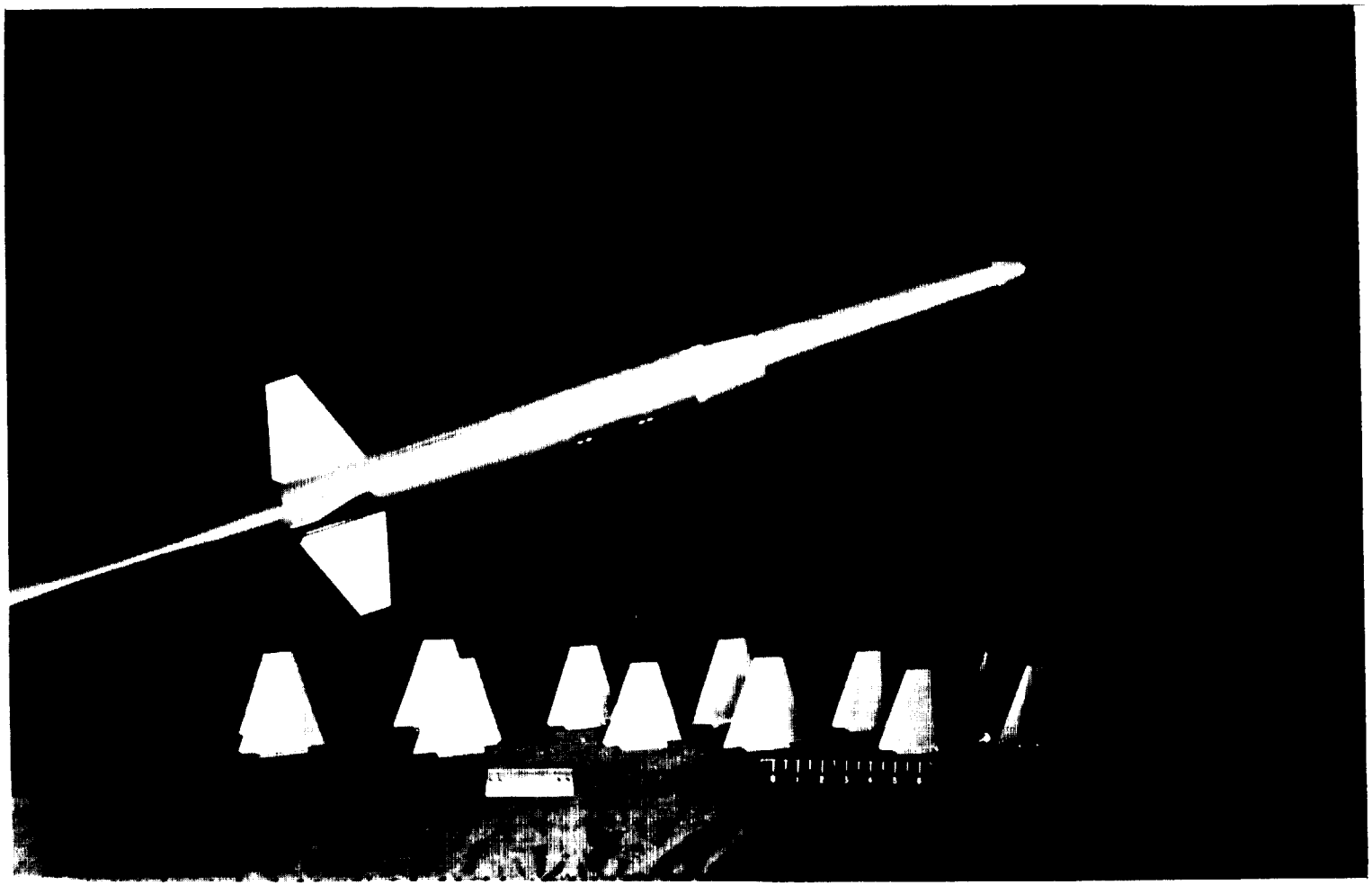

(c) Two-stage model without auxiliary rocket motors. L-60-7282

Figure 5.- Continued.

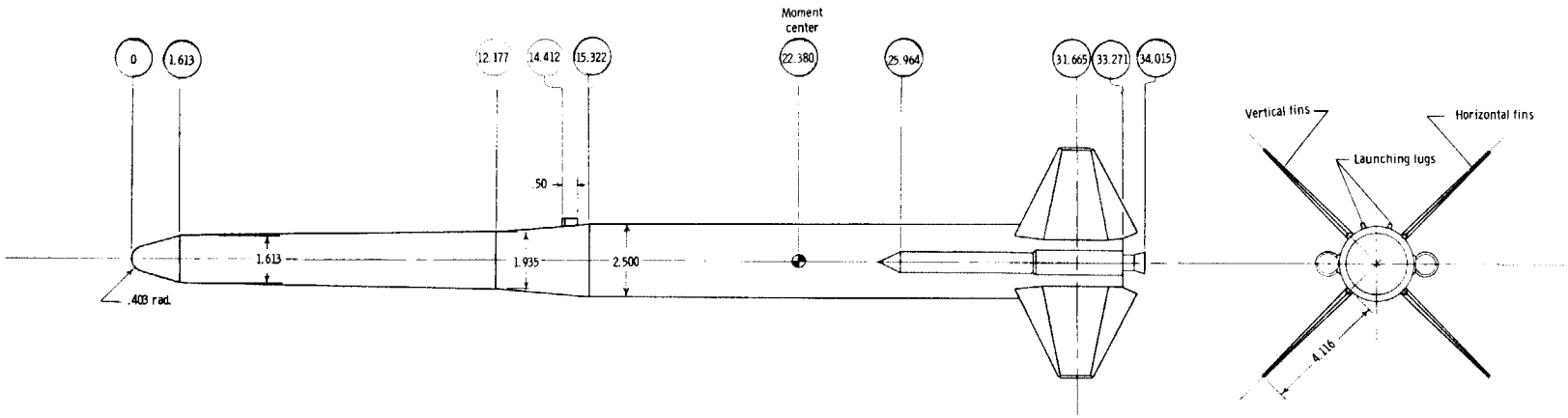

(d) Sketch of two-stage model of Trailblazer II configuration. All dimensions in inches. Circled numbers indicate stations in inches.

Figure 5.- Concluded.

L-1967

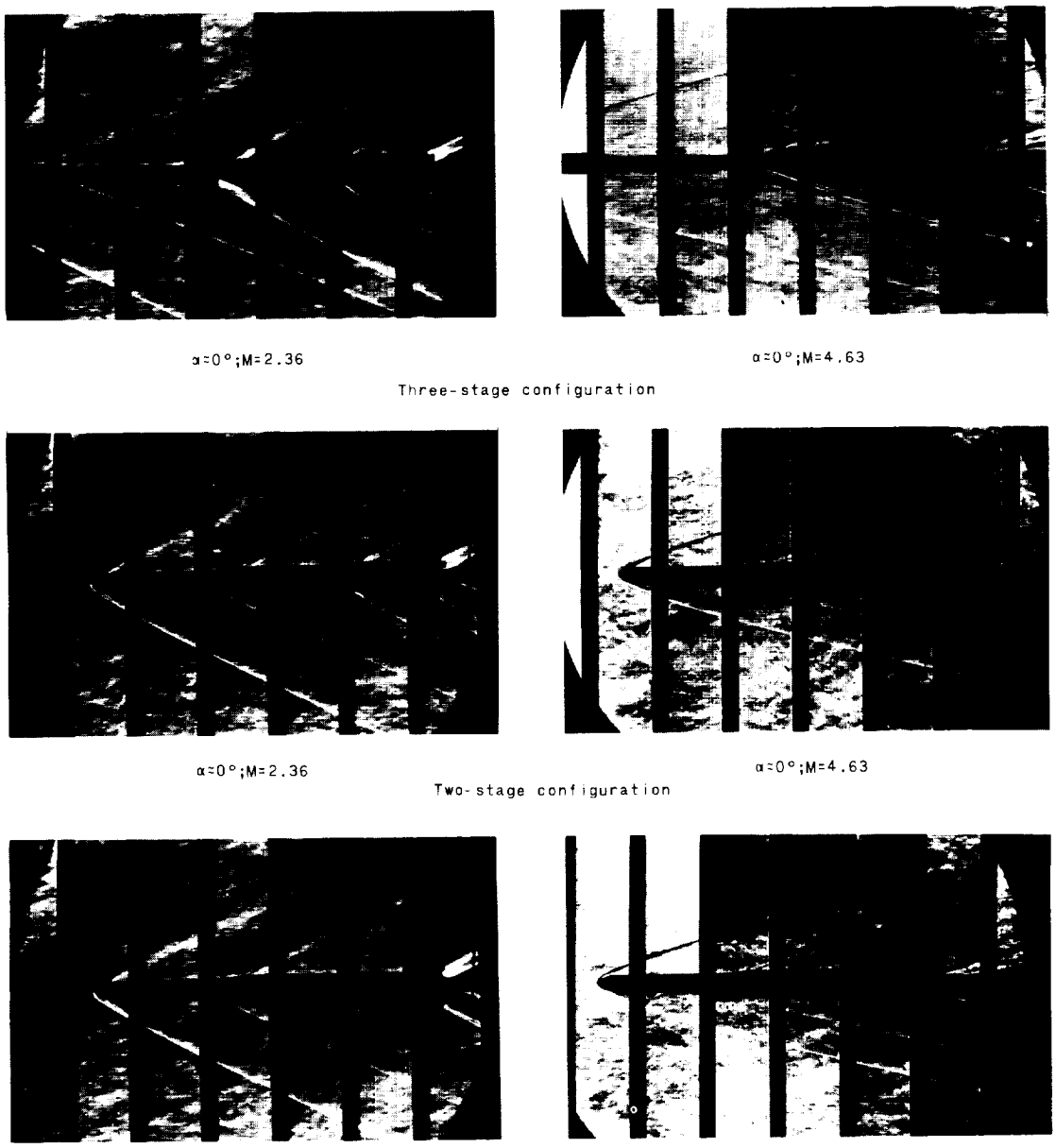

L-62-26

Figure 6.- Typical schlieren photographs of models tested.

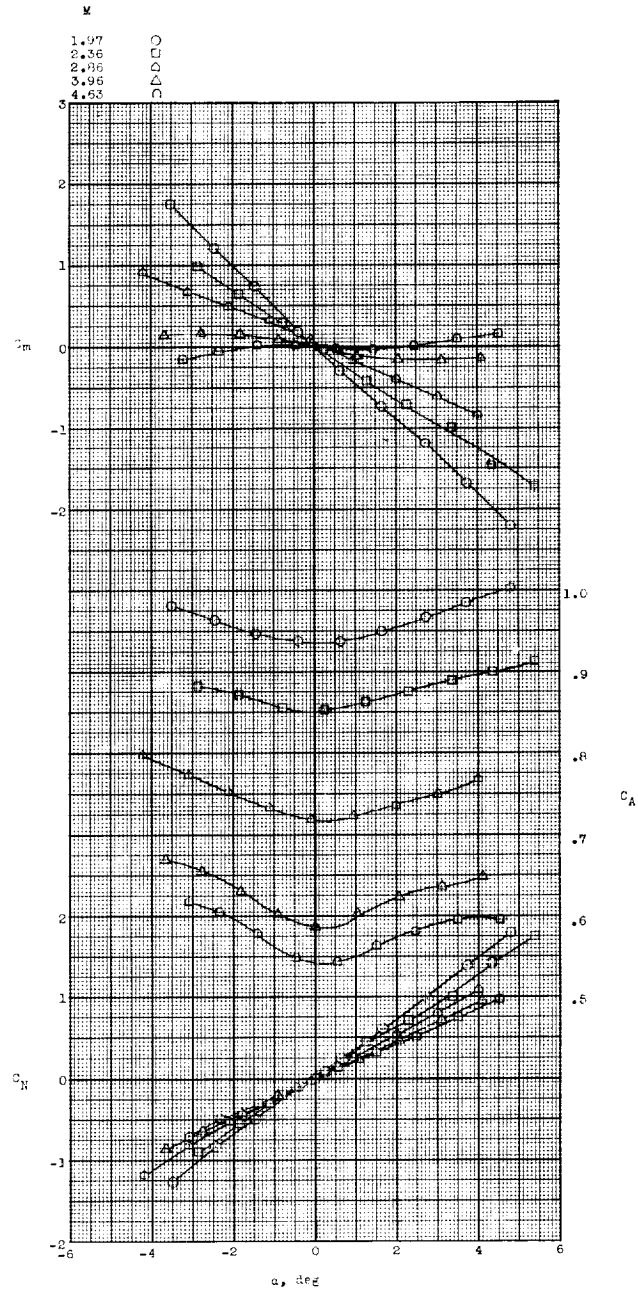

(a) $\delta_I = 0^o$; $\delta_{II} = 0^o$; $\beta = 0^o$.

Figure 7.- Variation of pitch characteristics with angle of attack at five Mach numbers for three-stage configuration. 12-sq-ft, A = 1.5 fins.

L-1967

L-1967

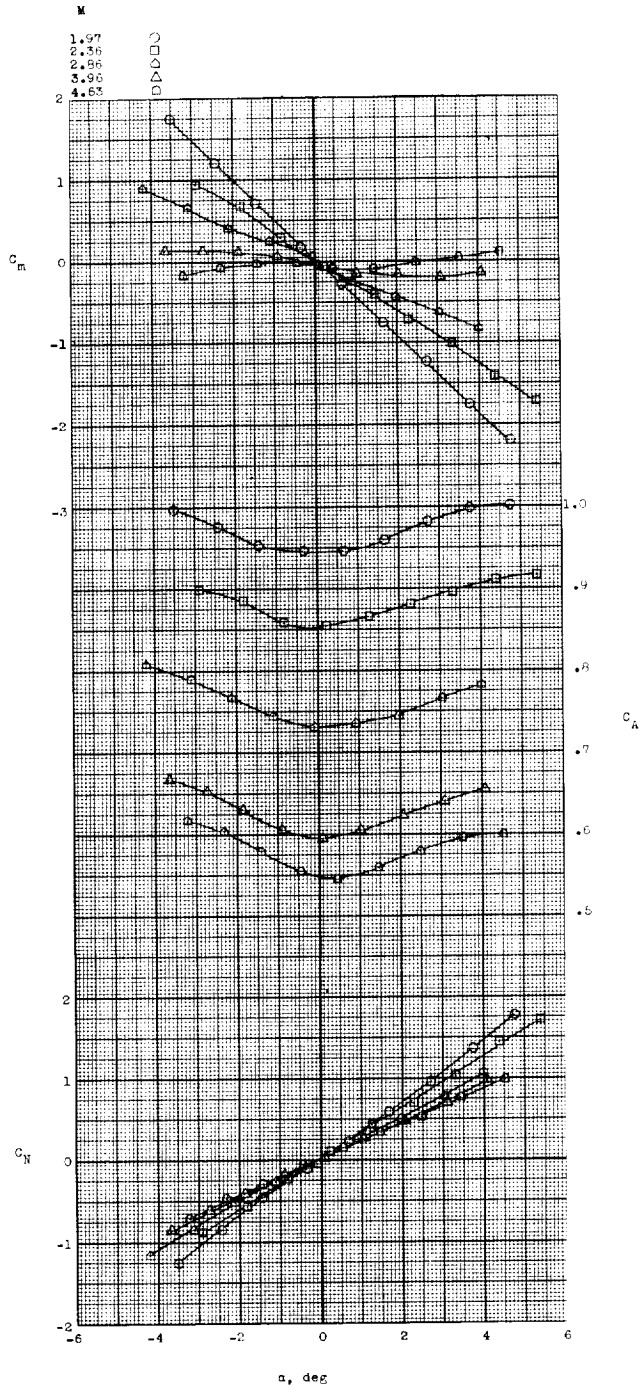

(b) $\delta_I = 1^o$; $\delta_{II} = 0^o$; $\beta = 0^o$.

Figure 7.- Continued.

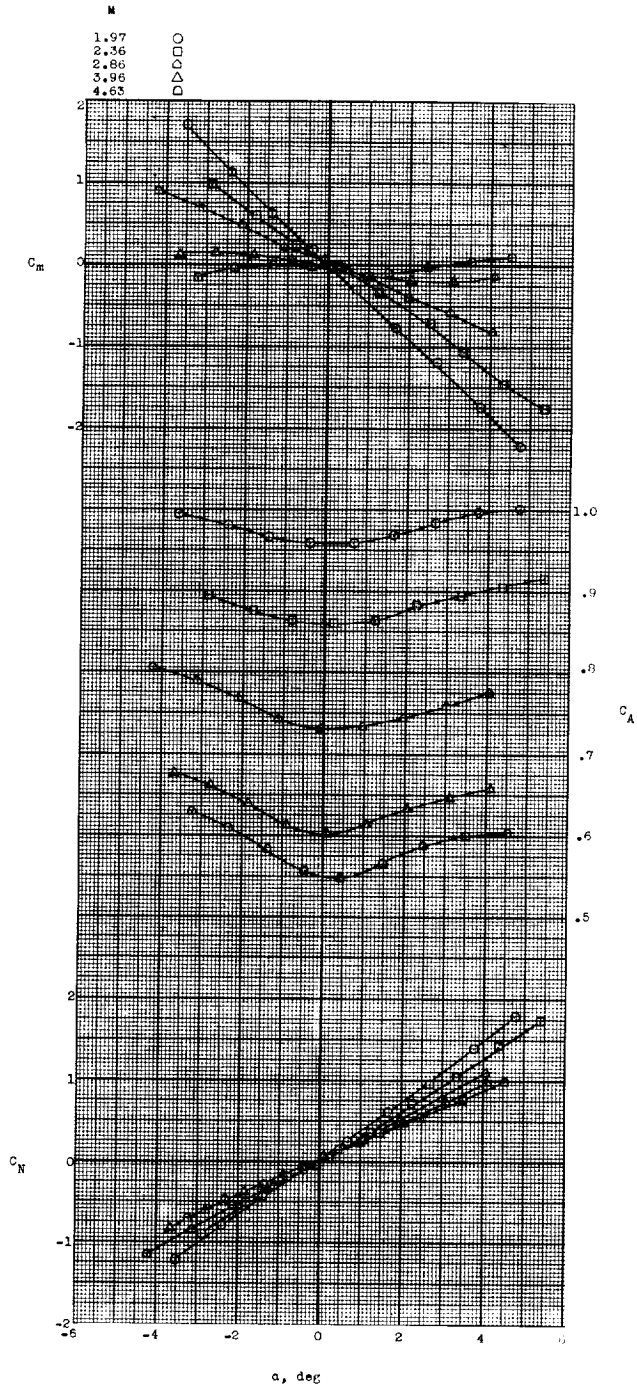

(c) $\delta_I = 1^o$; $\delta_{II} = 2^o$; $\beta = 0^o$.

Figure 7.- Continued.

L-1967

L-1967

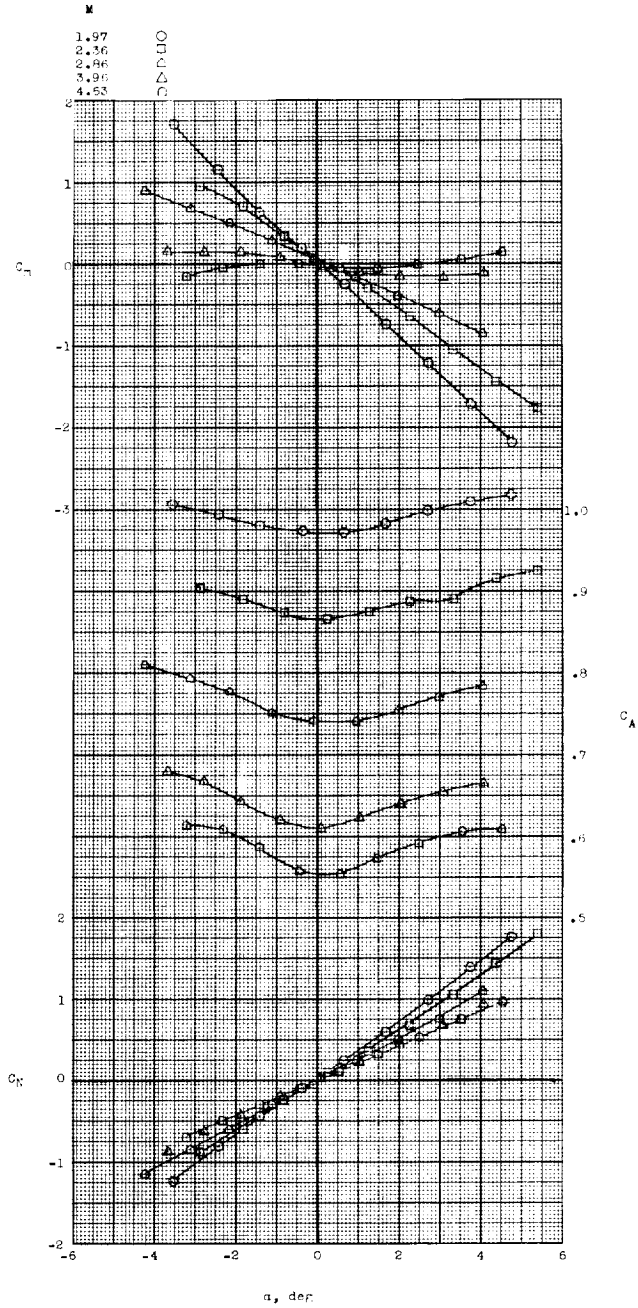

(d) $\delta_I = 2^o$; $\delta_{II} = 2^o$; $\beta = 0^o$.

Figure 7.- Concluded.

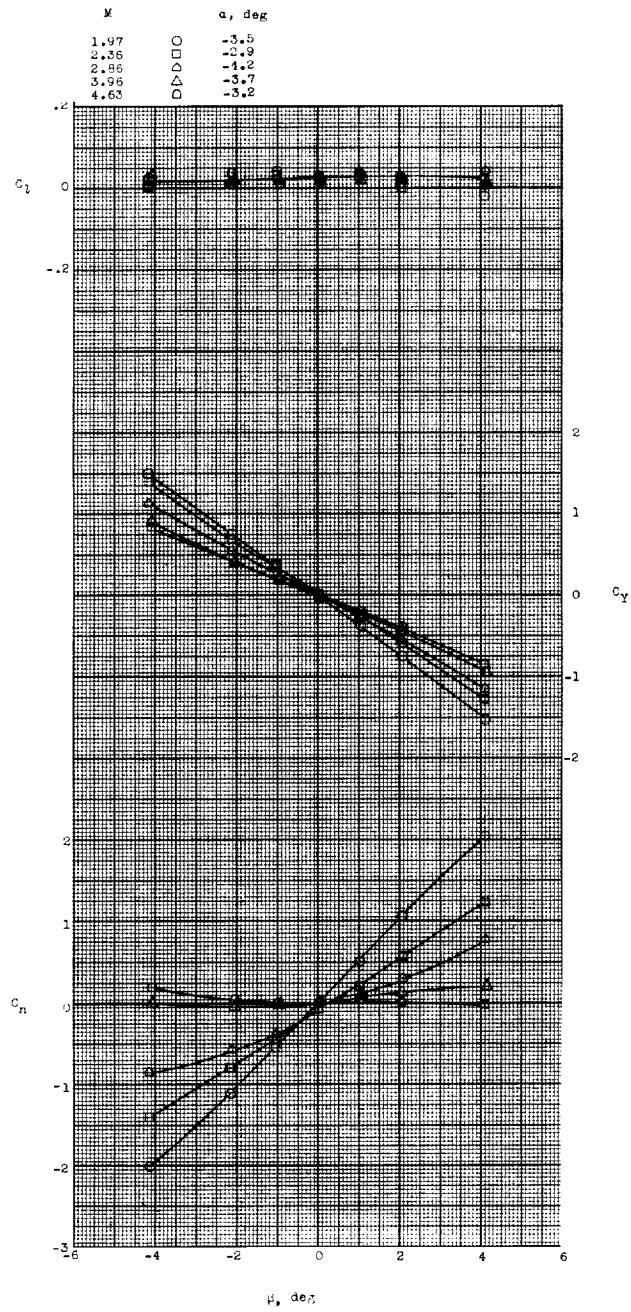

(a) $\delta_I = 0^\circ$; $\delta_{II} = 0^\circ$; $\alpha \approx -4^\circ$.

Figure 8.- Variation of lateral characteristics with angle of sideslip at Mach numbers for three-stage configuration. 12-sq-ft, A = 1.5 fins.

L-1967

L-1967

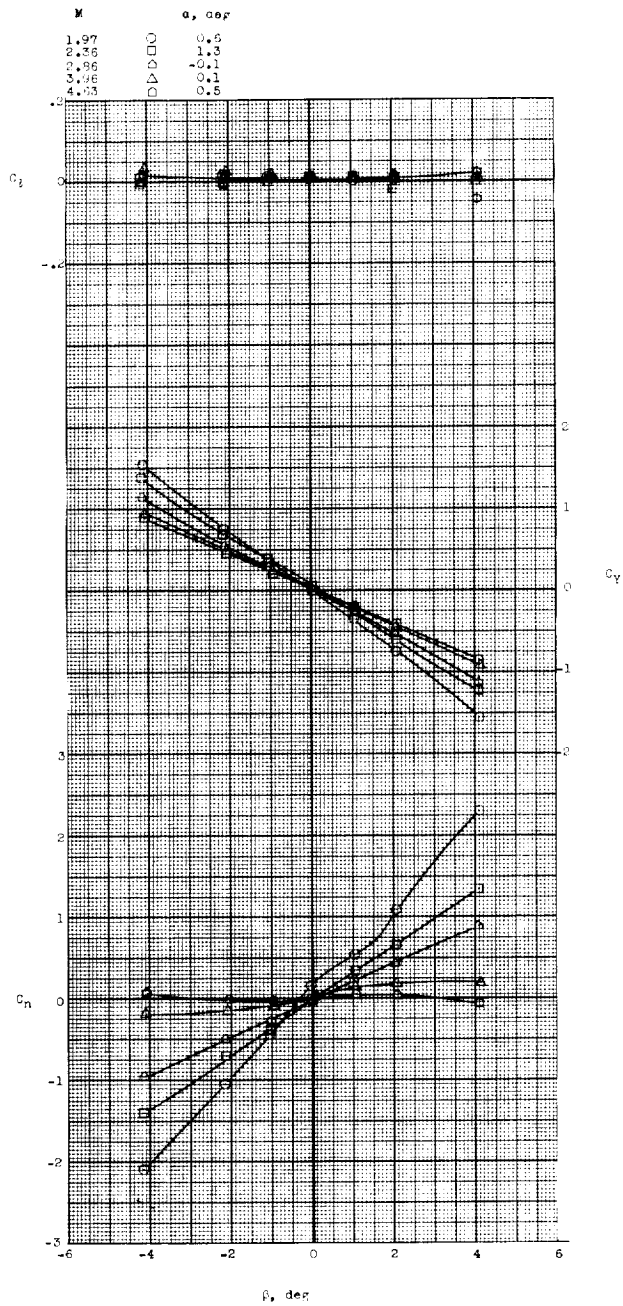

(b) $\delta_I = 0^o$; $\delta_{II} = 0^o$; $\alpha \approx 0^o$.

Figure 8.- Continued.

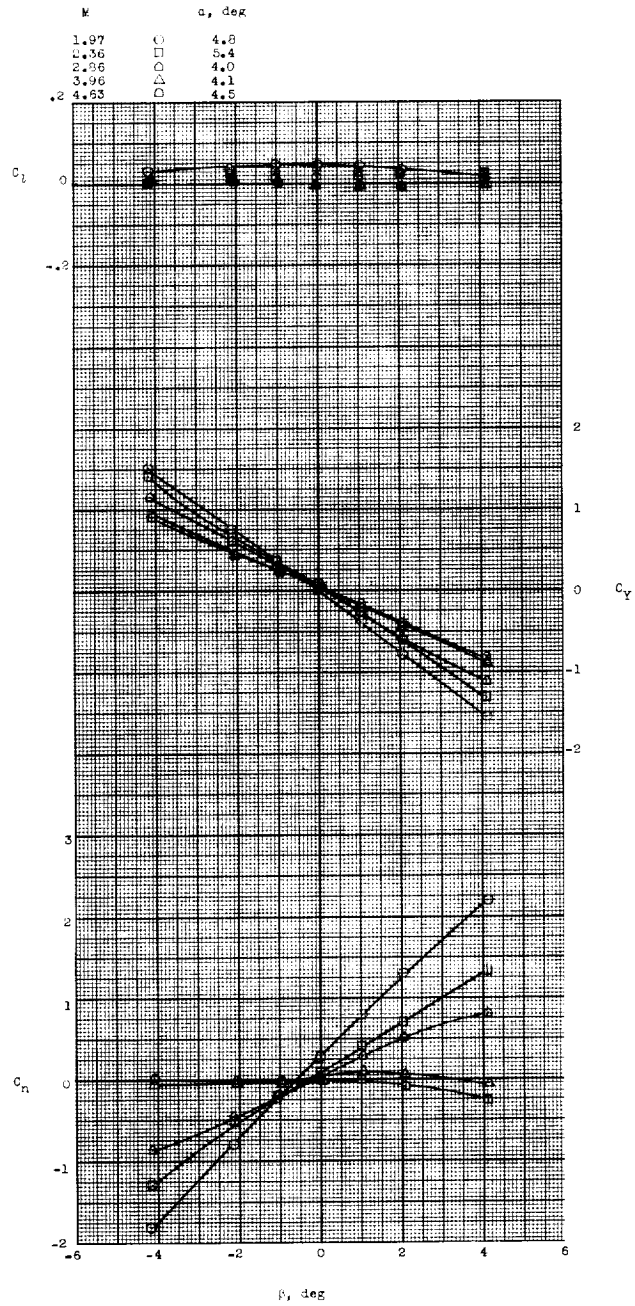

(c) $\delta_I = 0^\circ$; $\delta_{II} = 0^\circ$; $\alpha \approx 4^\circ$.

Figure 8.- Continued.

L-1967

L-1967

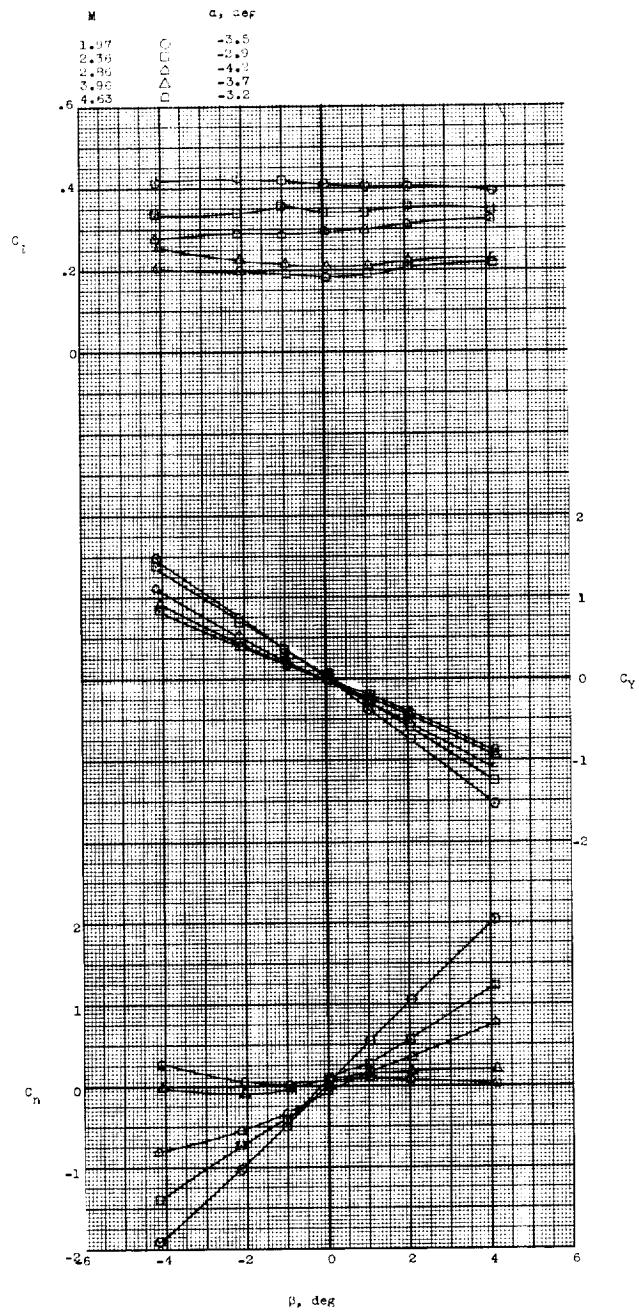

(d) $\delta_I = 2^o$; $\delta_{II} = 2^o$; $\alpha \approx -4^o$.

Figure 8.- Continued.

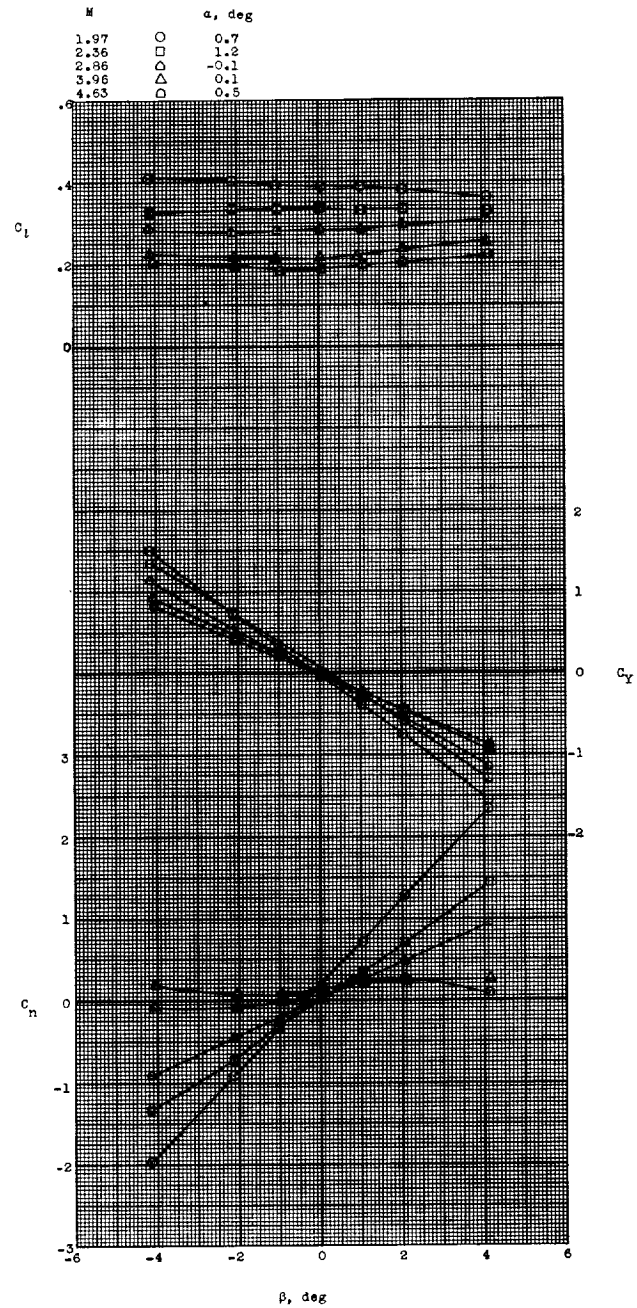

(e) $\delta_I = 2^o$; $\delta_{II} = 2^o$; $\alpha \approx 0^o$.

Figure 8.- Continued.

L-1967

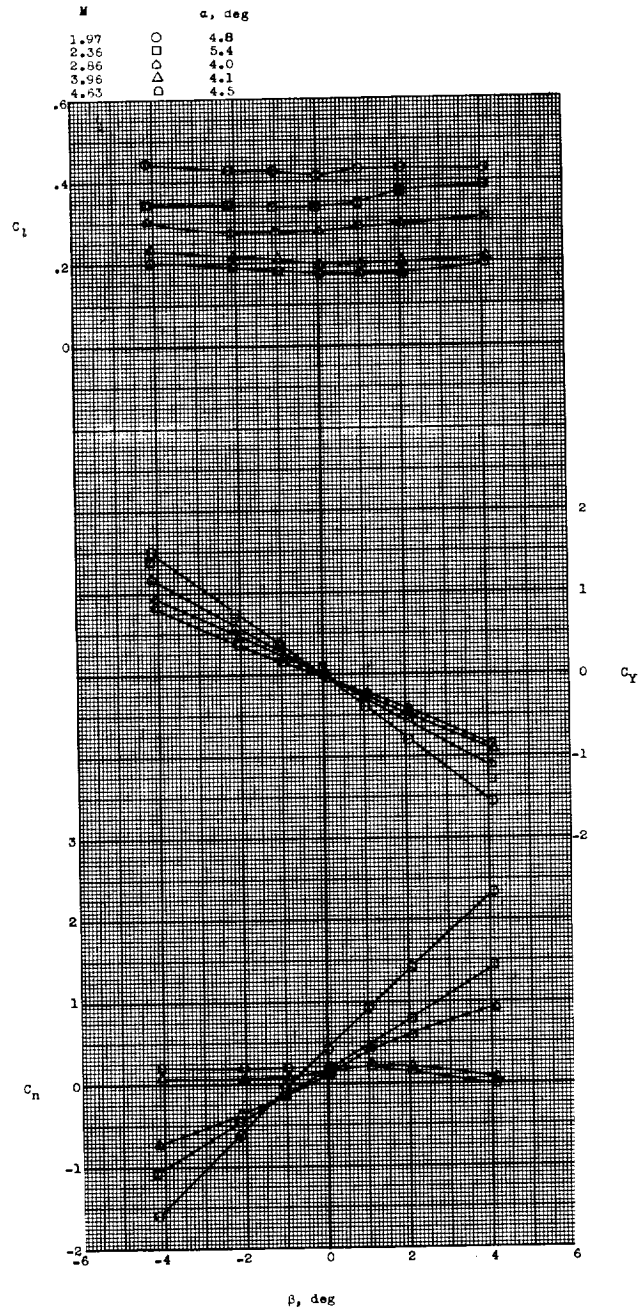

(f) $\delta_I = 2^o$; $\delta_{II} = 2^o$; $\alpha \approx 4^o$.

Figure 8.- Concluded.

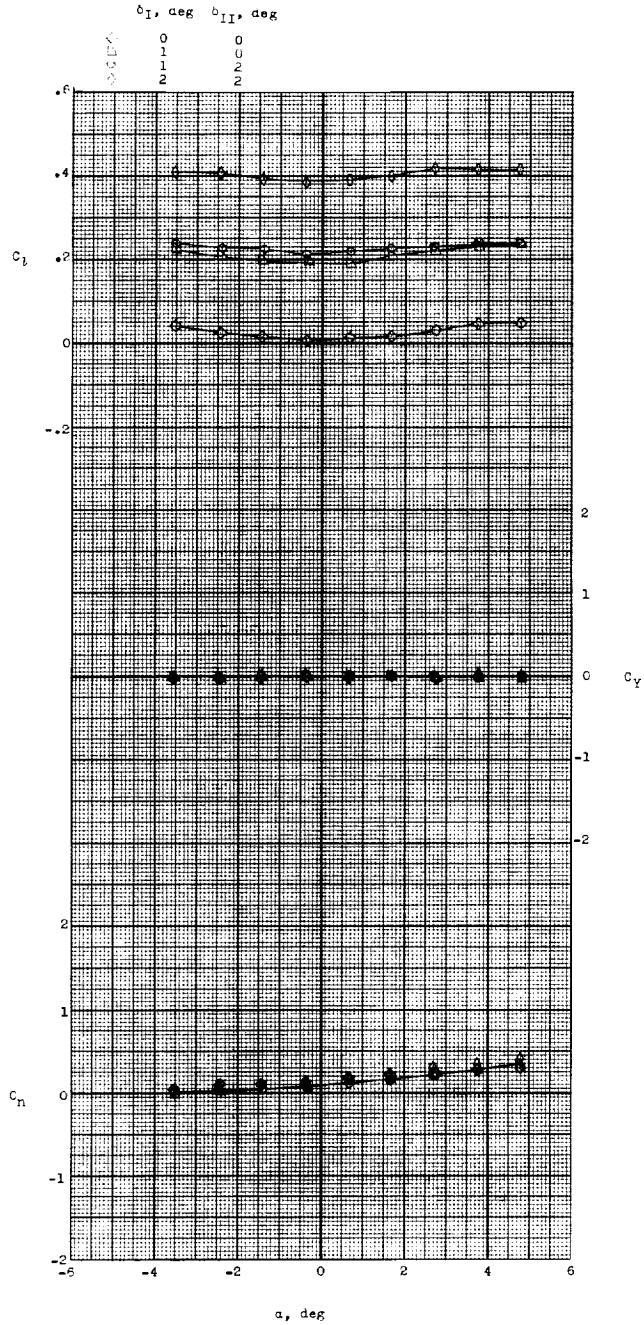

(a) M = 1.97; β = 0°.

Figure 9.- Variation of lateral characteristics with angle of attack for three-stage configuration with fin cant. 12-sq-ft, A = 1.5 fins.

L-1967

L-1967

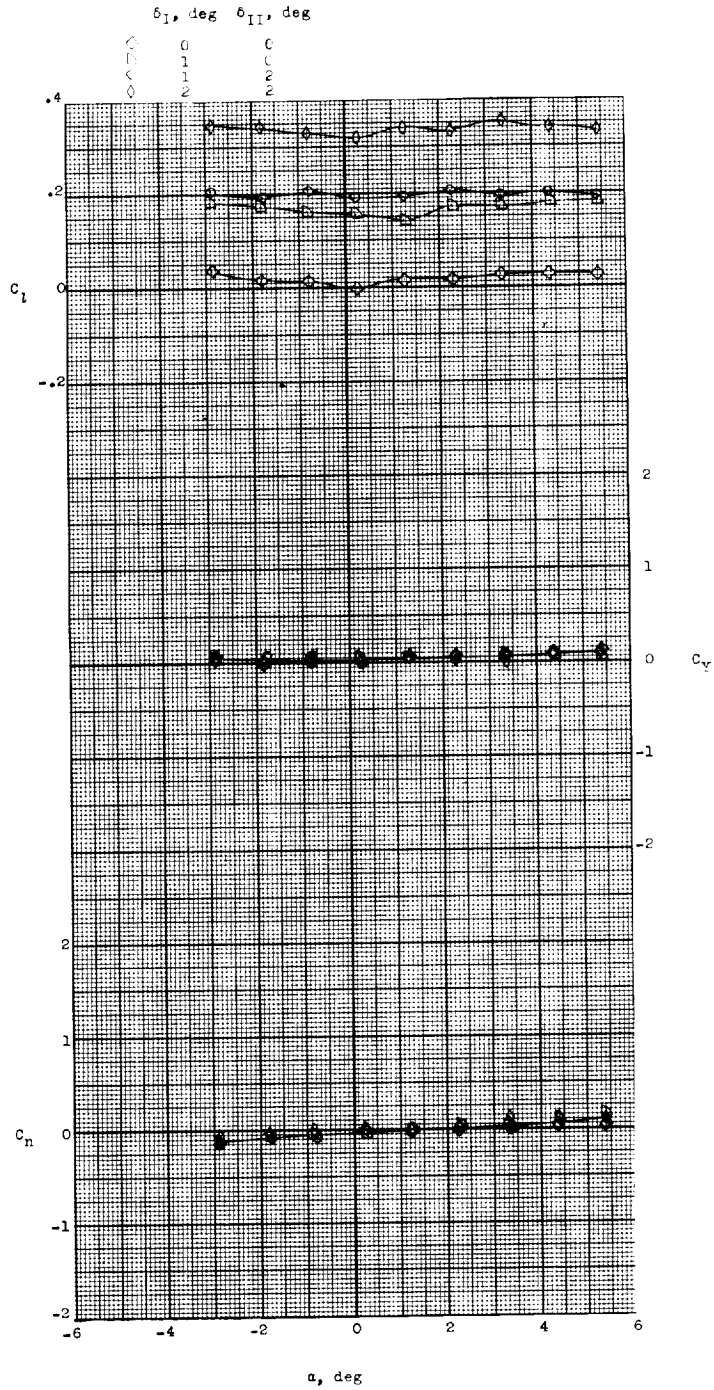

(b) M = 2.36; β = 0°.

Figure 9.- Continued.

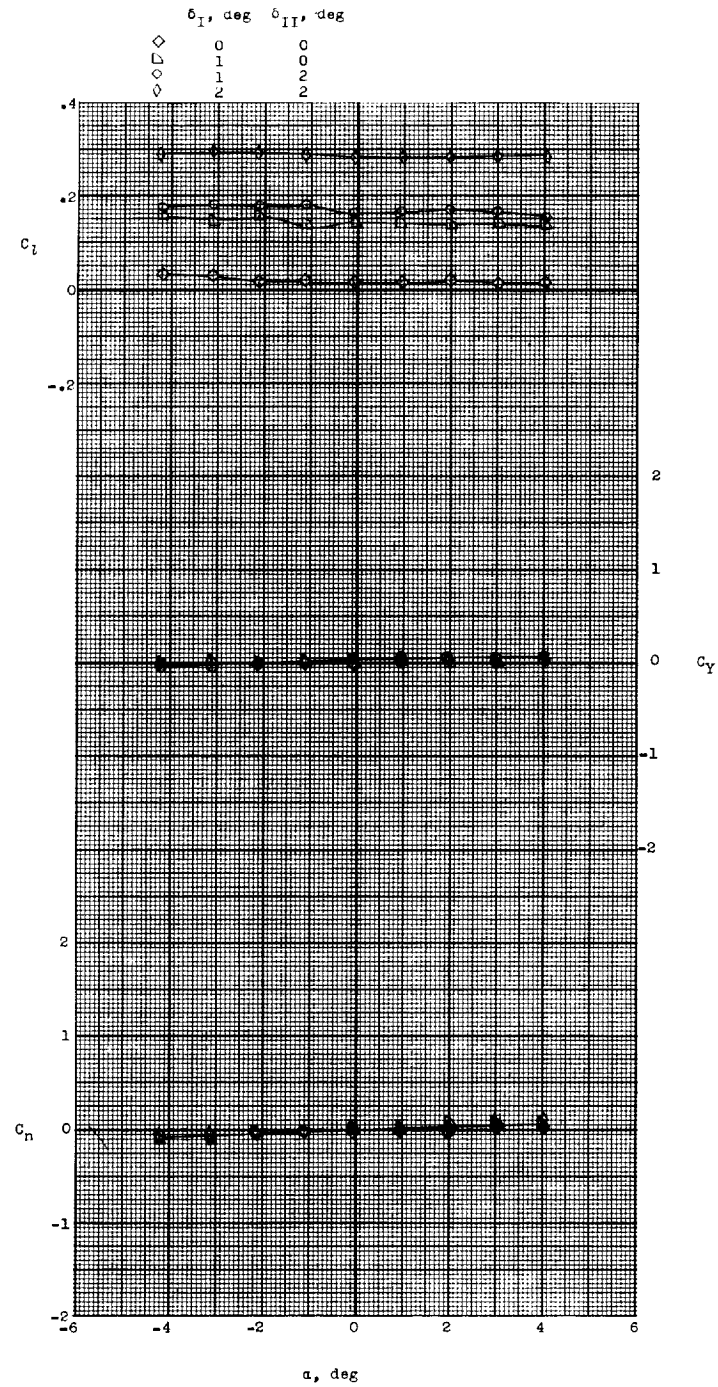

(c) M = 2.86; β = 0°.

Figure 9.- Continued.

L-1967

L-1967

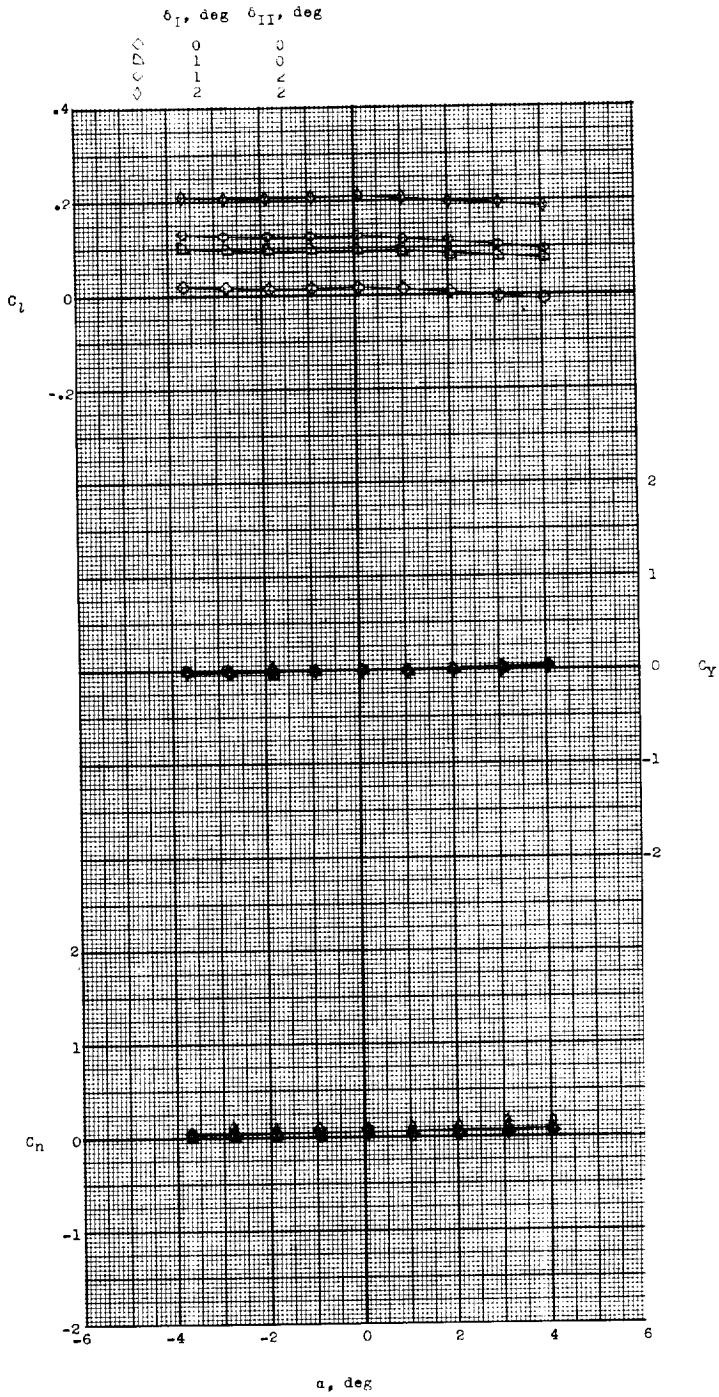

(d) M = 3.96; β = 0°.

Figure 9.- Continued.

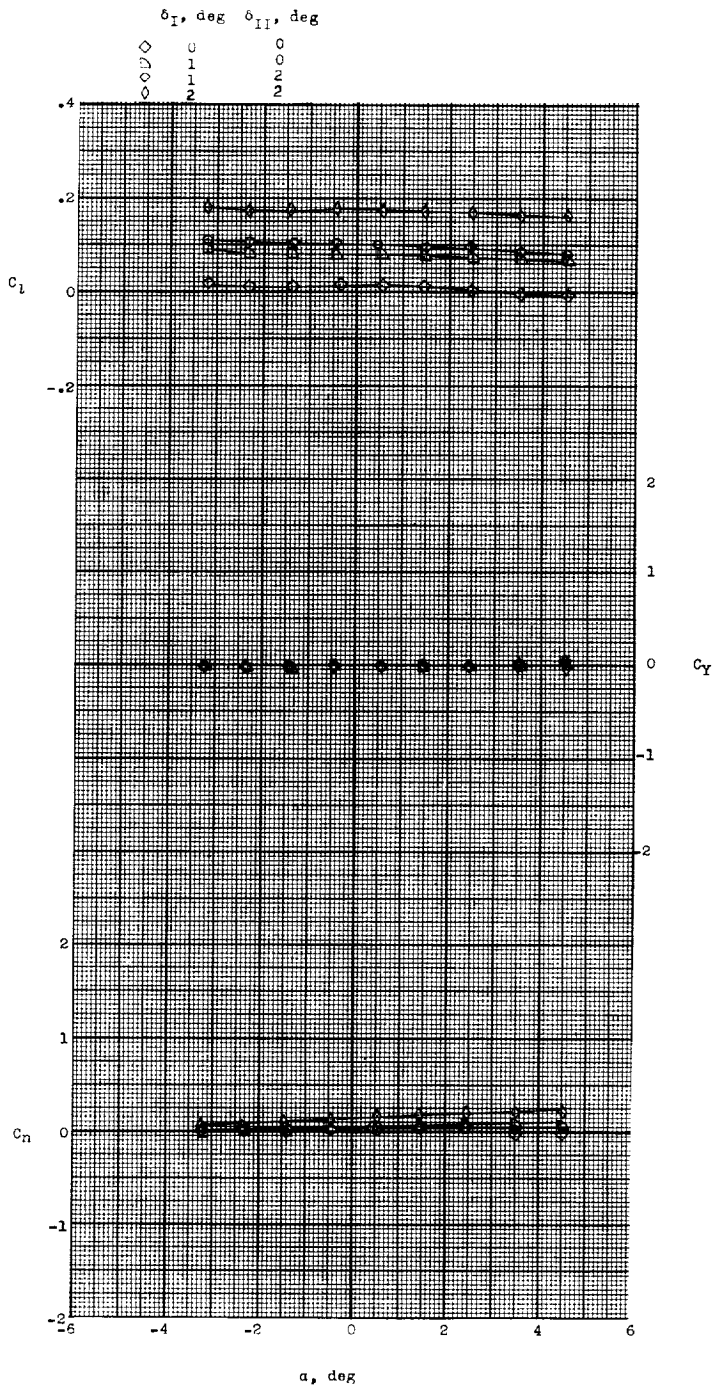

(e) M = 4.63; β = 0°.

Figure 9.- Concluded.

L-1967

L-1967

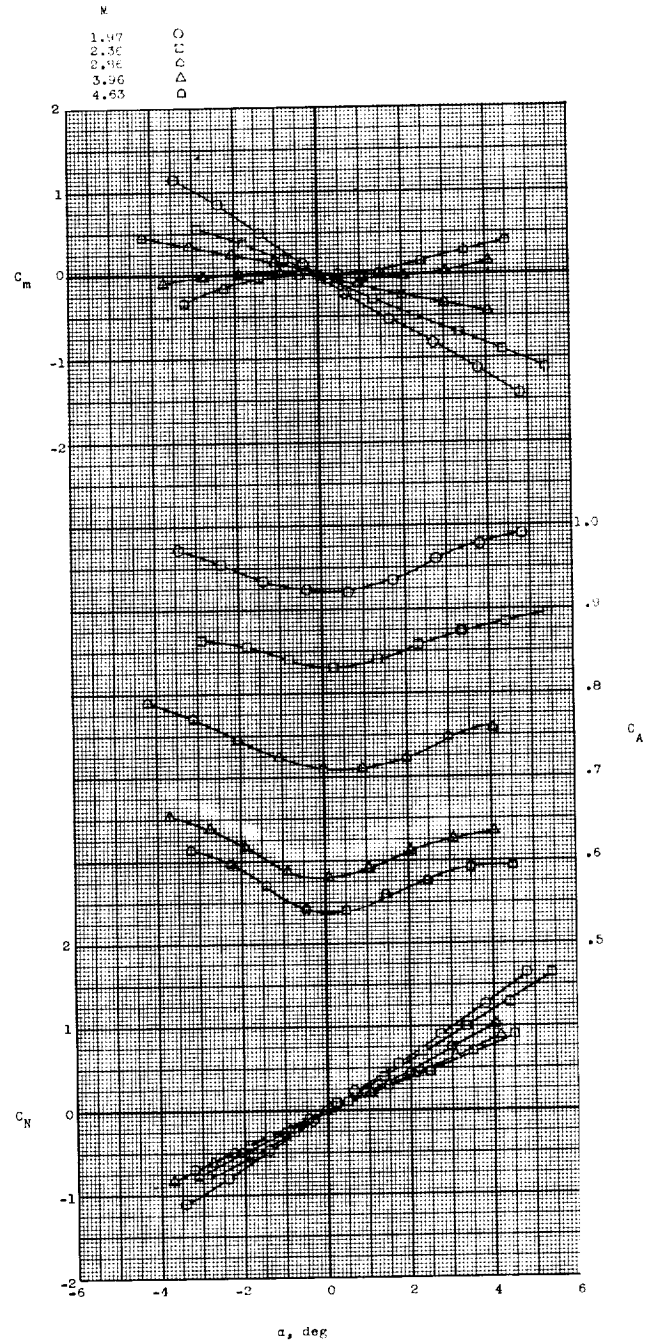

(a) $\delta_I = 0^o$; $\delta_{II} = 0^o$; $\beta = 0^o$.

Figure 10.- Variation of pitch characteristics with angle of attack at five Mach numbers for three-stage configuration. 10-sq-ft, A = 1.5 fins.

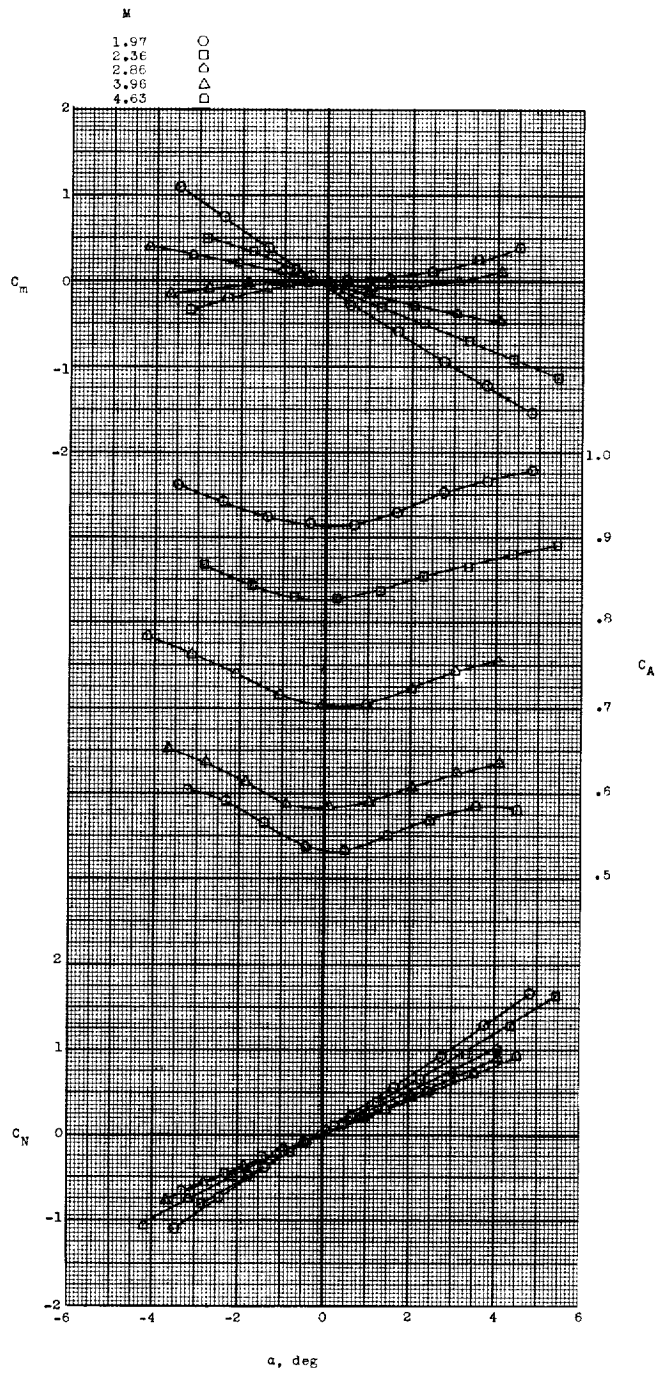

(b) $\delta_I = 1^o$; $\delta_{II} = 0^o$; $\beta = 0^o$.

Figure 10.- Continued.

L-1967

L-1967

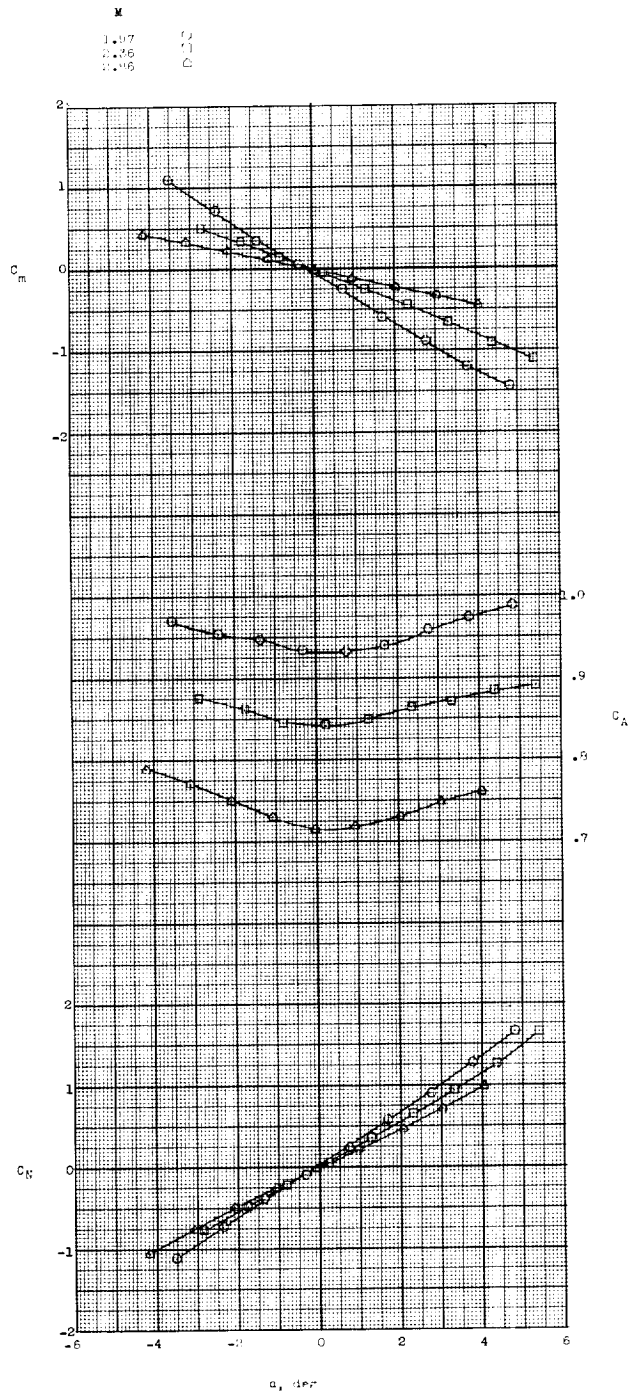

(c) $\delta_I = 1^o$; $\delta_{II} = 2^o$; $\beta = 0^o$.

Figure 10.- Continued.

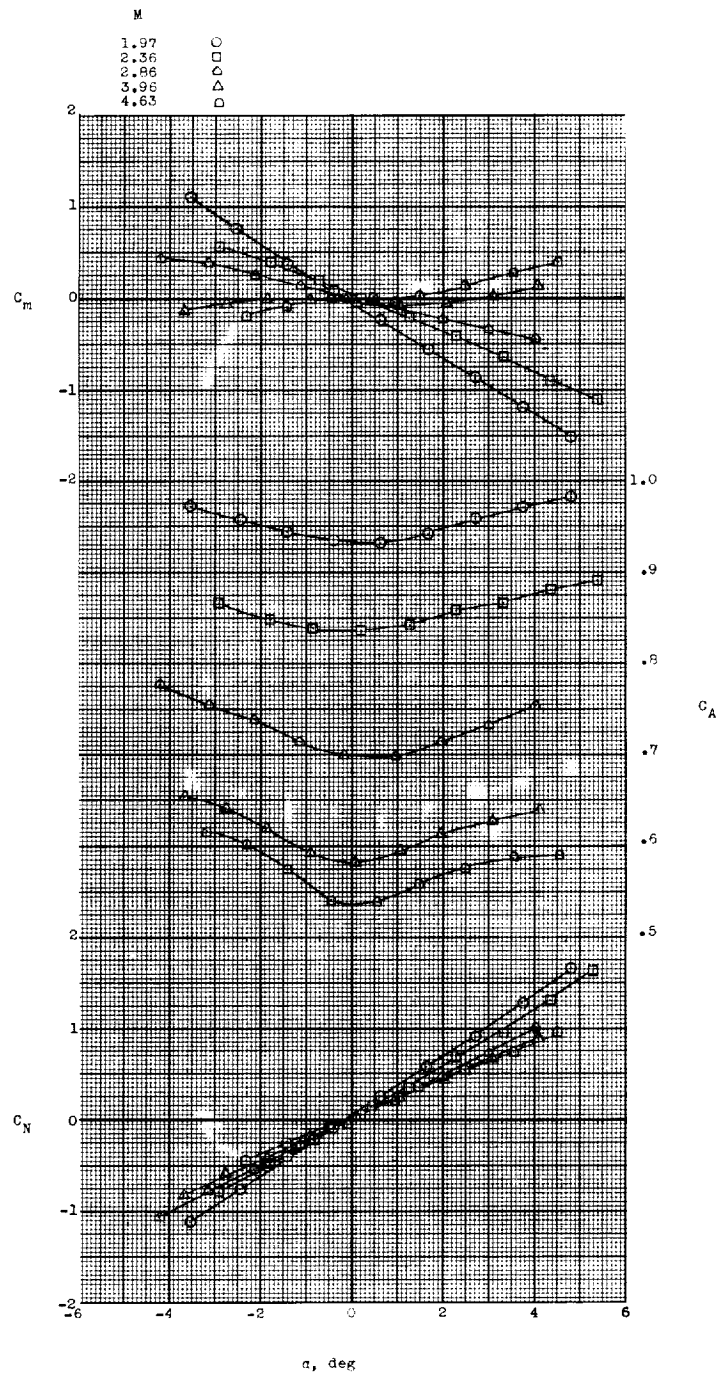

(d) $\delta_I = 2^o$; $\delta_{II} = 2^o$; $\beta = 0^o$.

Figure 10.- Concluded.

L-1967

L-1967

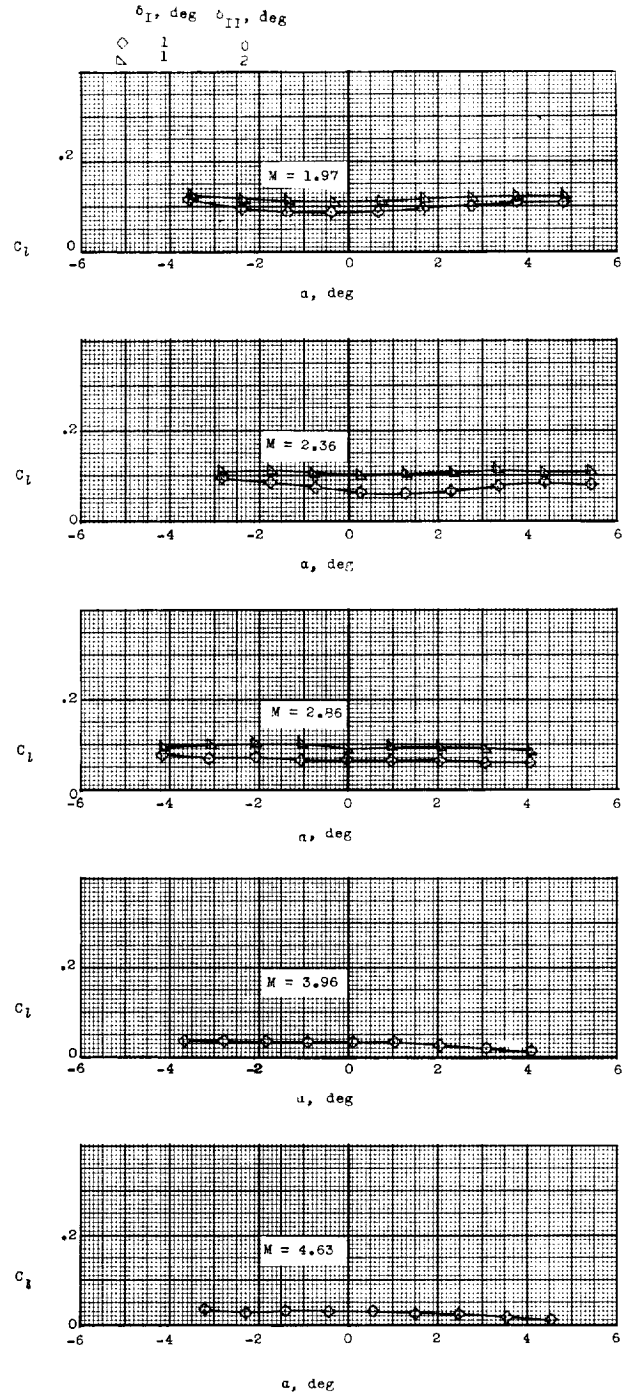

Figure 11.- Variation of rolling moment C_l with angle of attack at various Mach numbers for three-stage configuration with fin cant. 10-sq-ft, A = 1.5 fins; $\beta = 0^{\circ}$.

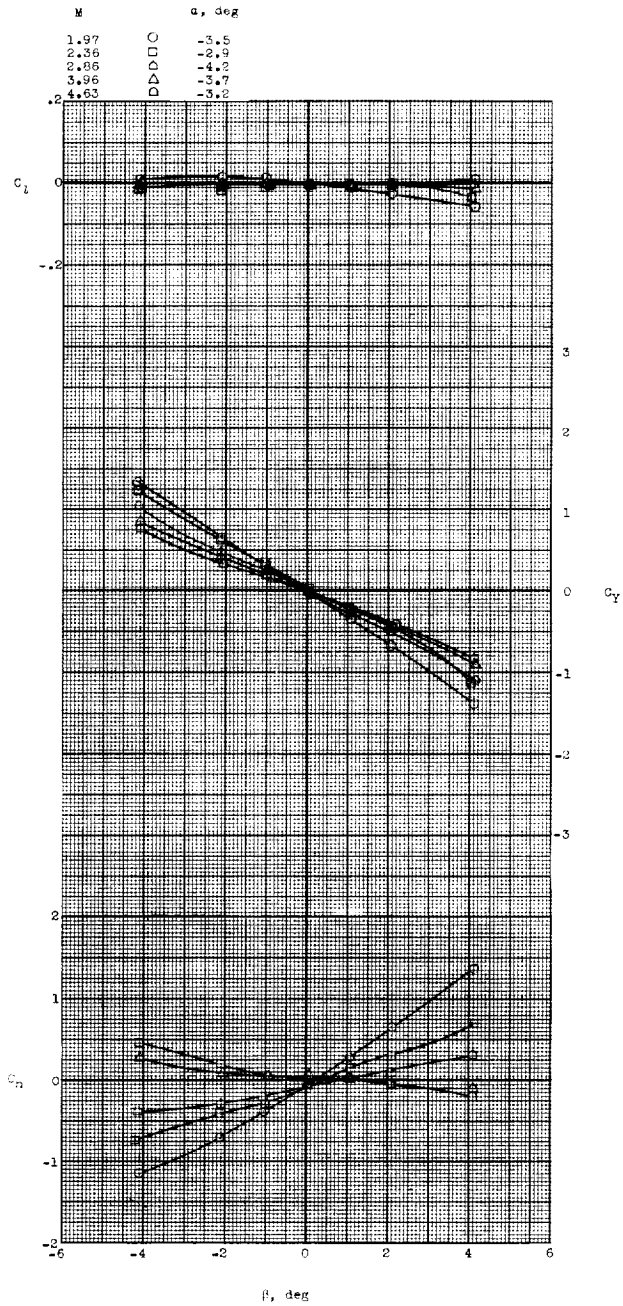

(a) $\delta_I = 0^o$; $\delta_{II} = 0^o$; $\alpha \approx -4^o$.

Figure 12.- Variation of lateral characteristics with angle of sideslip at five Mach numbers for three-stage configuration. 10-sq-ft, A = 1.5 fins.

L-1967

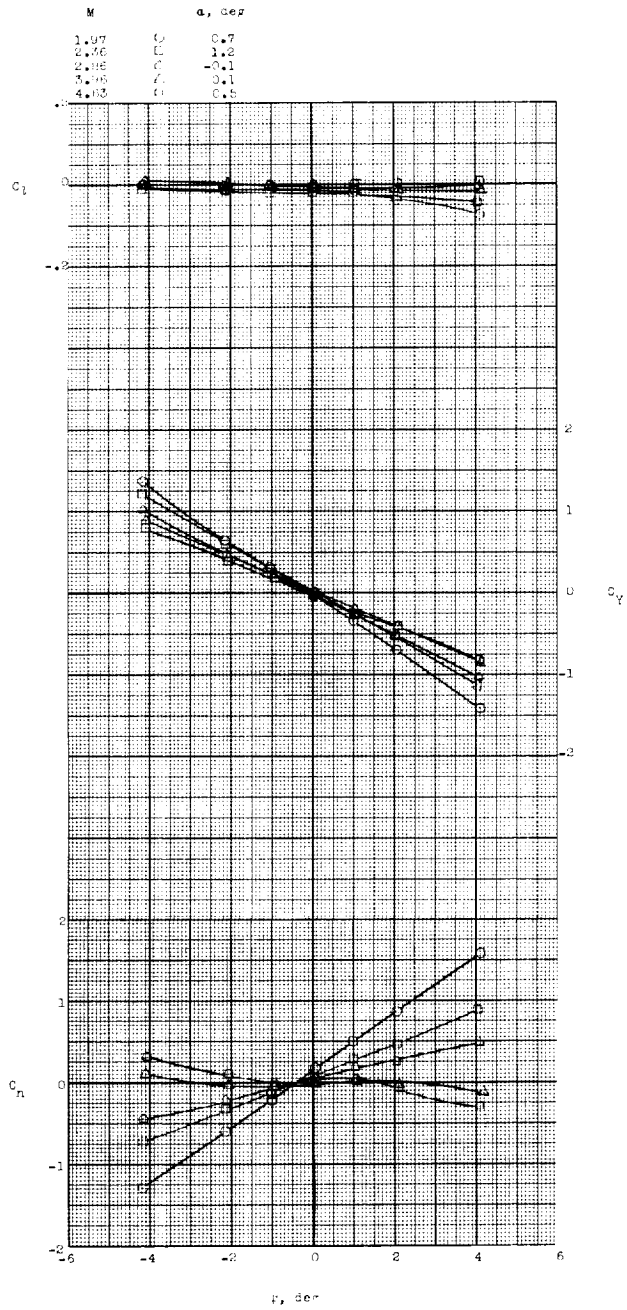

(b) $\delta_I = 0^o$; $\delta_{II} = 0^o$; $\alpha \approx 0^o$.

Figure 12.- Continued.

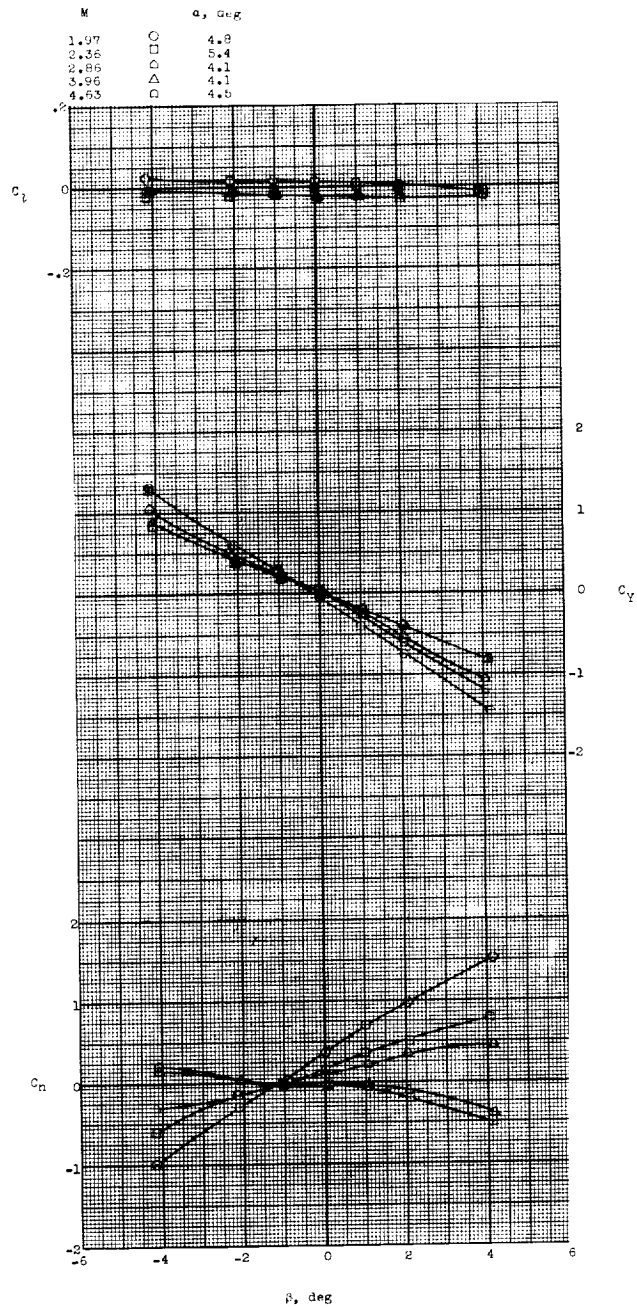

(c) $\delta_I = 0^o$; $\delta_{II} = 0^o$; $\alpha \approx 4^o$.

Figure 12.- Continued.

L-1967

L-1967

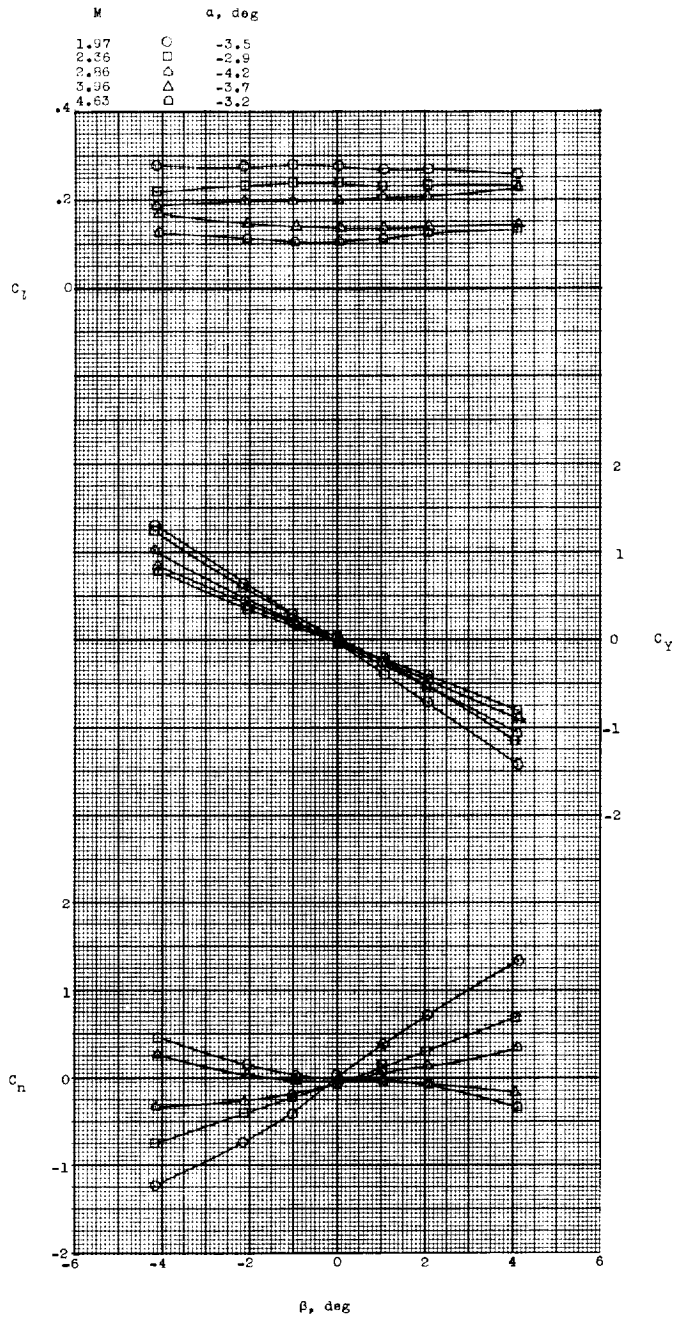

(d) $\delta_I = 2^o$; $\delta_{II} = 2^o$; $\alpha \approx -4^o$.

Figure 12.- Continued.

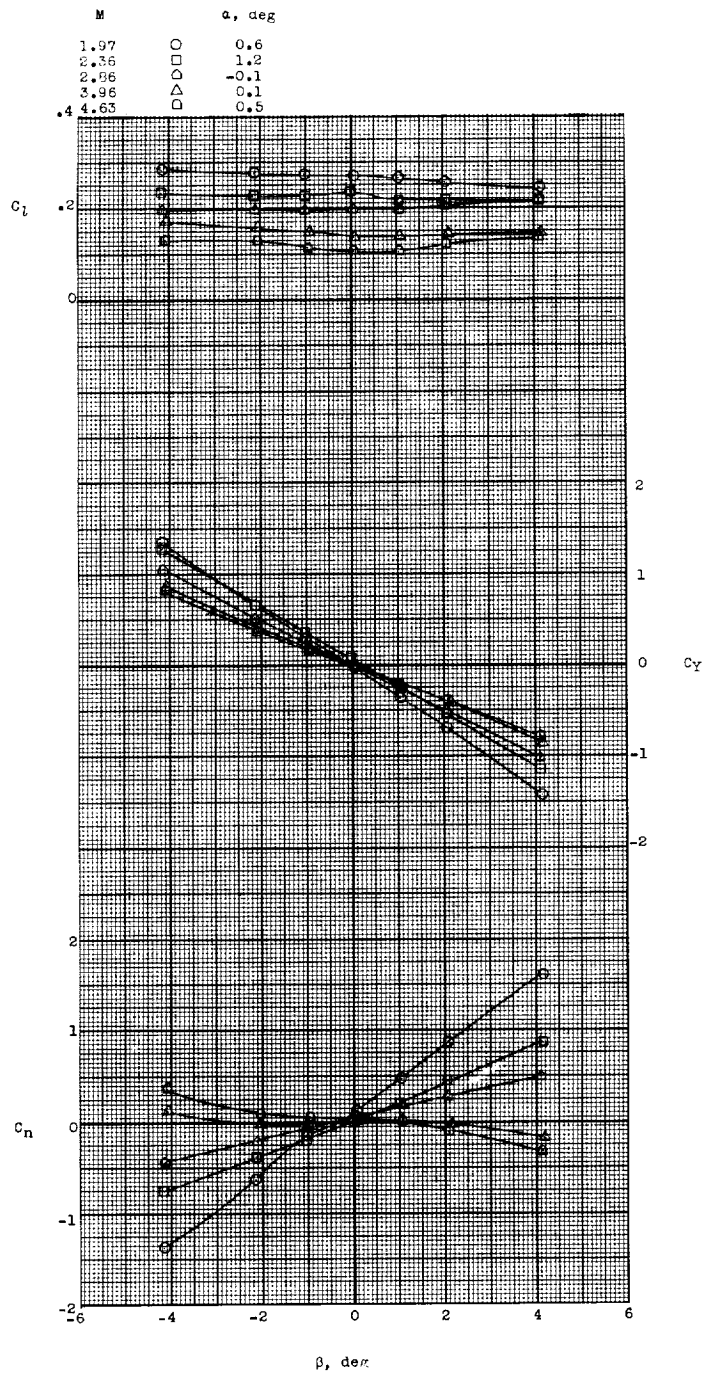

(e) $\delta_I = 2^o$; $\delta_{II} = 2^o$; $\alpha \approx 0^o$.

Figure 12.- Continued.

L-1967

L-1967

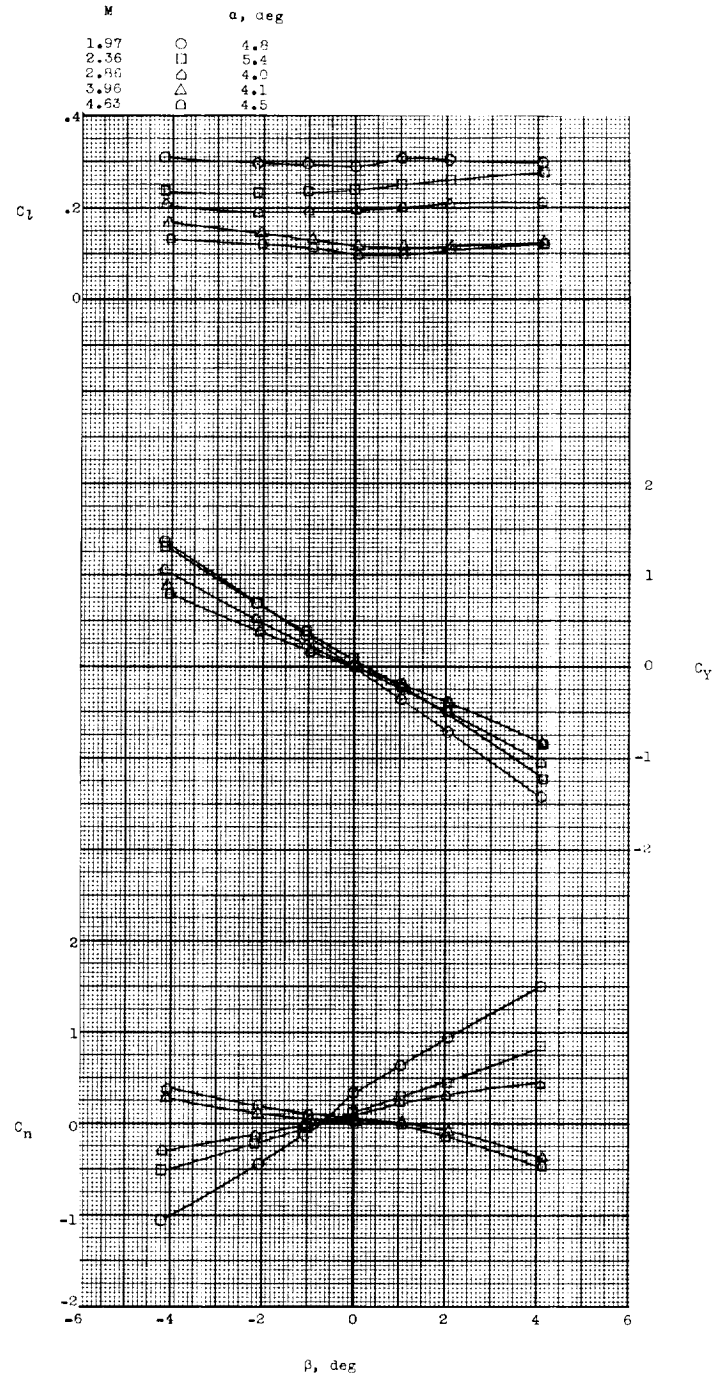

(f) $\delta_I = 2^o$; $\delta_{II} = 2^o$; $\alpha \approx 4^o$.

Figure 12.- Concluded.

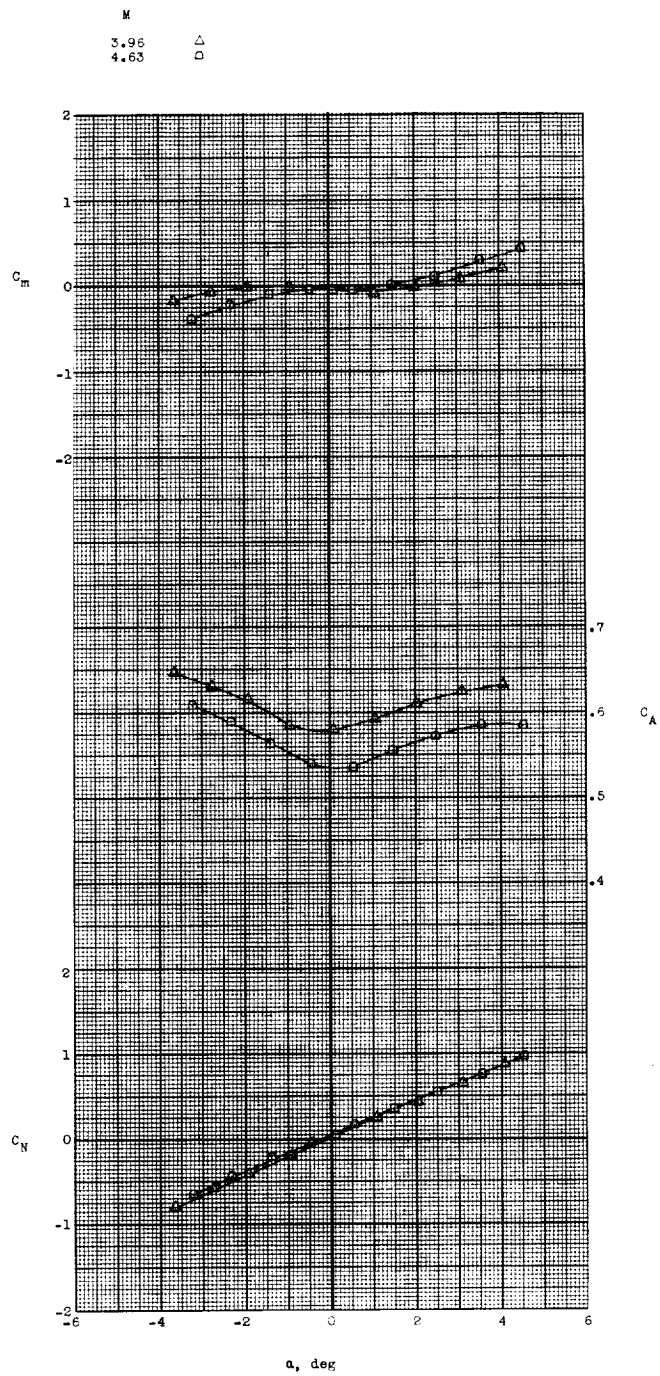

Figure 13.- Variation of pitching characteristics with angle of attack at two Mach numbers for three-stage configuration. 10-sq-ft, A = 0.985 fins; $\delta_I = 2^o$; $\delta_{II} = 2^o$; $\beta = 0^o$.

L-1967

L-1967

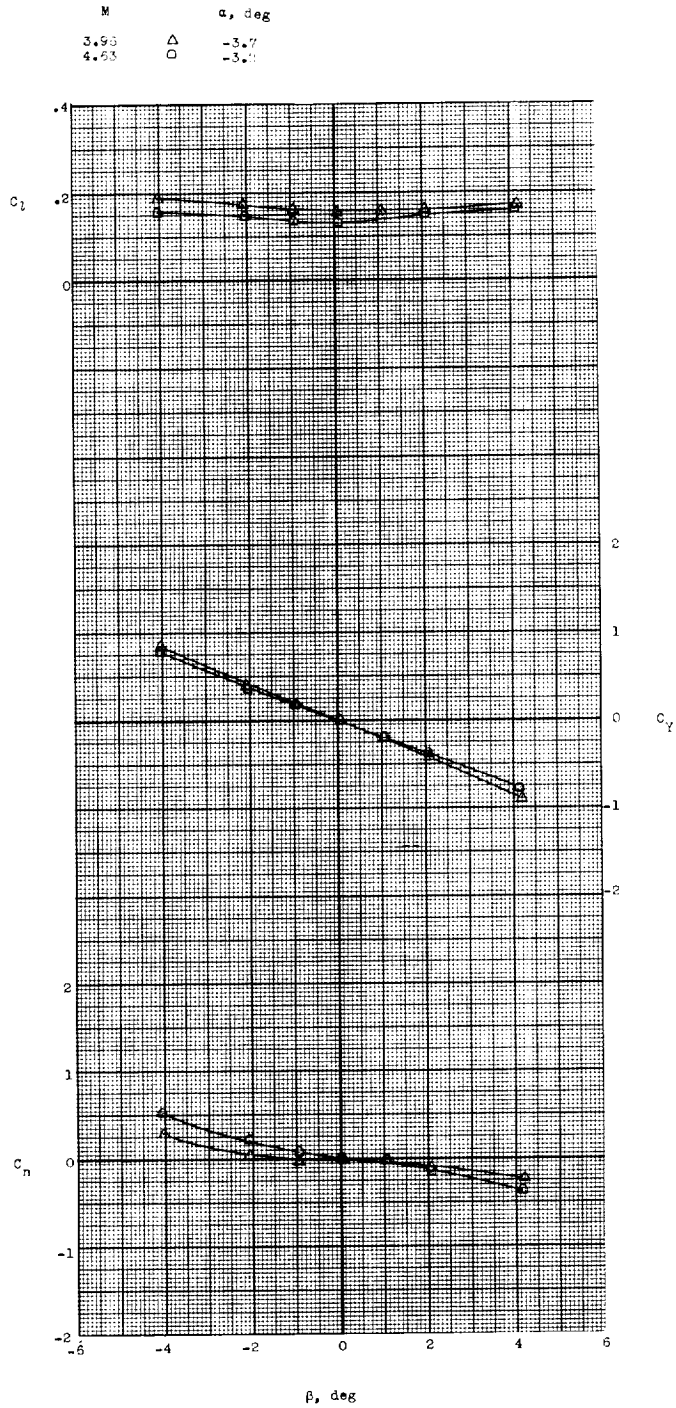

(a) $\delta_I = 2^o$; $\delta_{II} = 2^o$; $\alpha \approx -4^o$.

Figure 14.- Variation of lateral characteristics with angle of sideslip at two Mach numbers for three-stage configuration. 10-sq-ft, A = 0.985 fins.

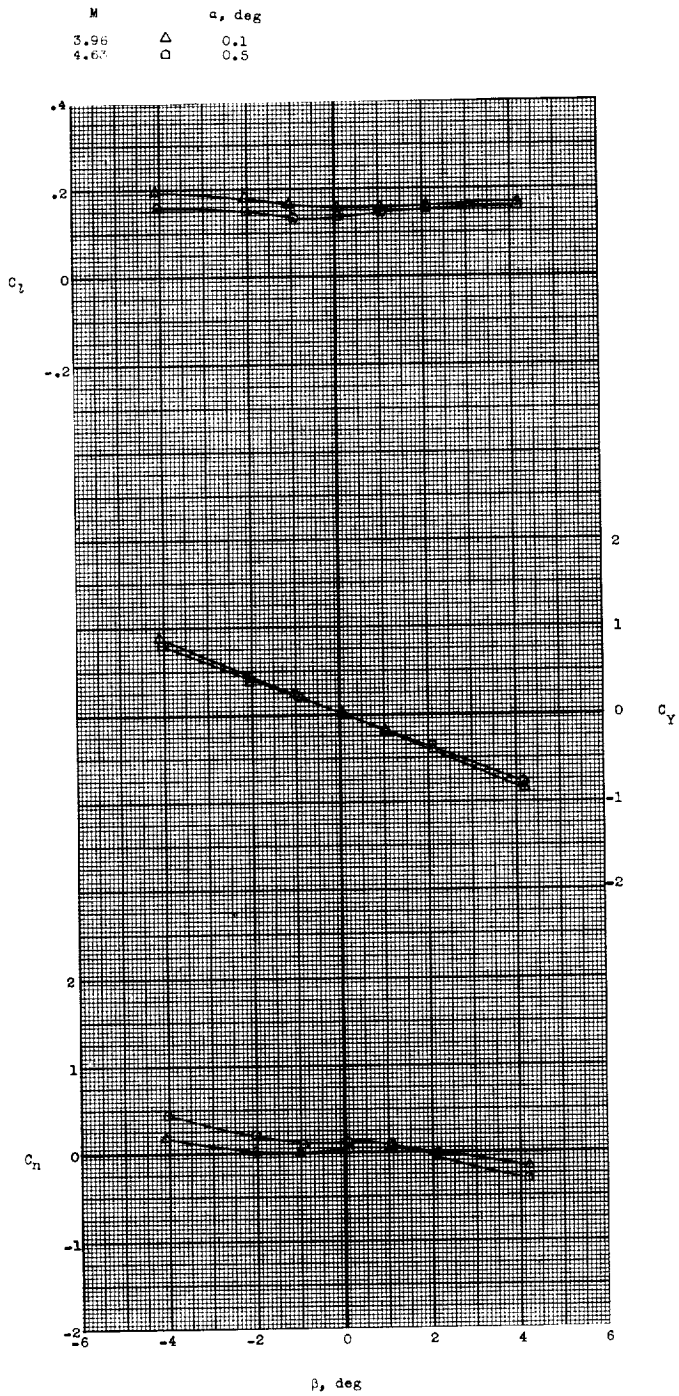

(b) $\delta_I = 2^\circ$; $\delta_{II} = 2^\circ$; $\alpha \approx 0^\circ$.

Figure 14.- Continued.

L-1967

L-1967

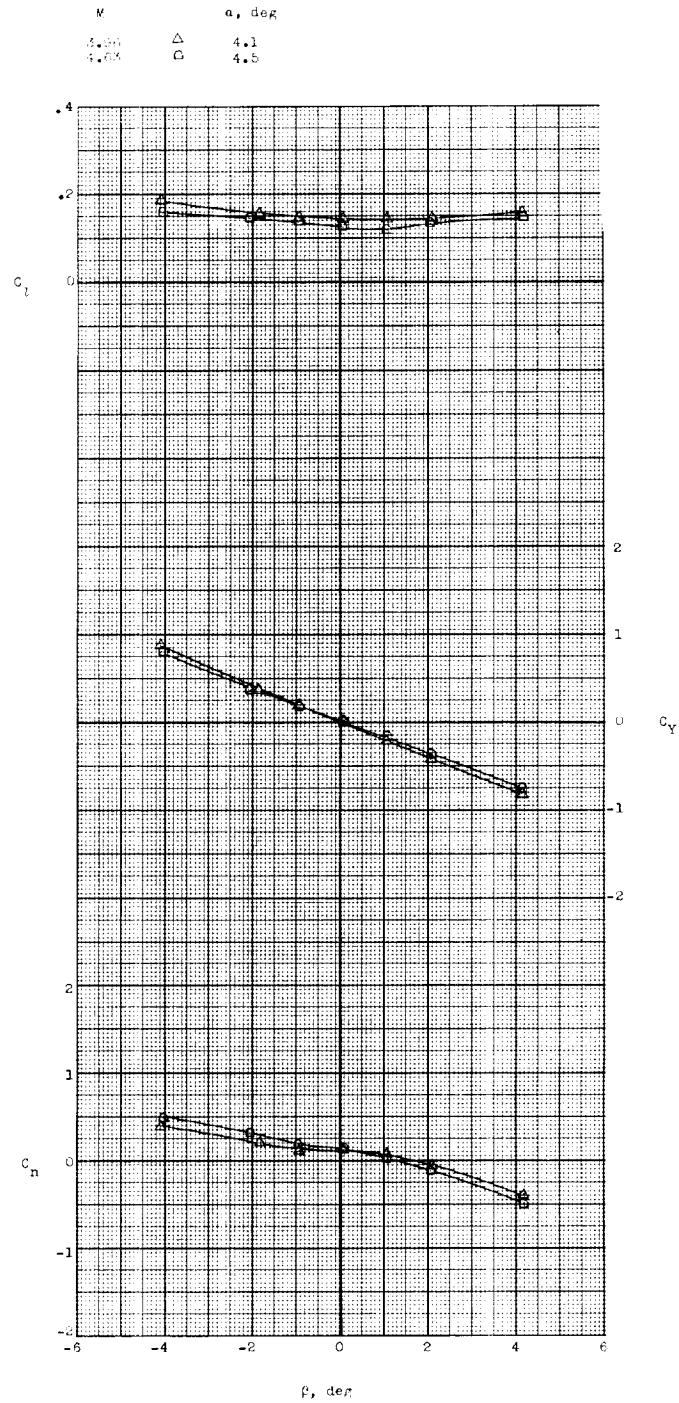

(c) $\delta_I = 2^o$; $\delta_{II} = 2^o$; $\alpha \approx 4^o$.

Figure 14.- Concluded.

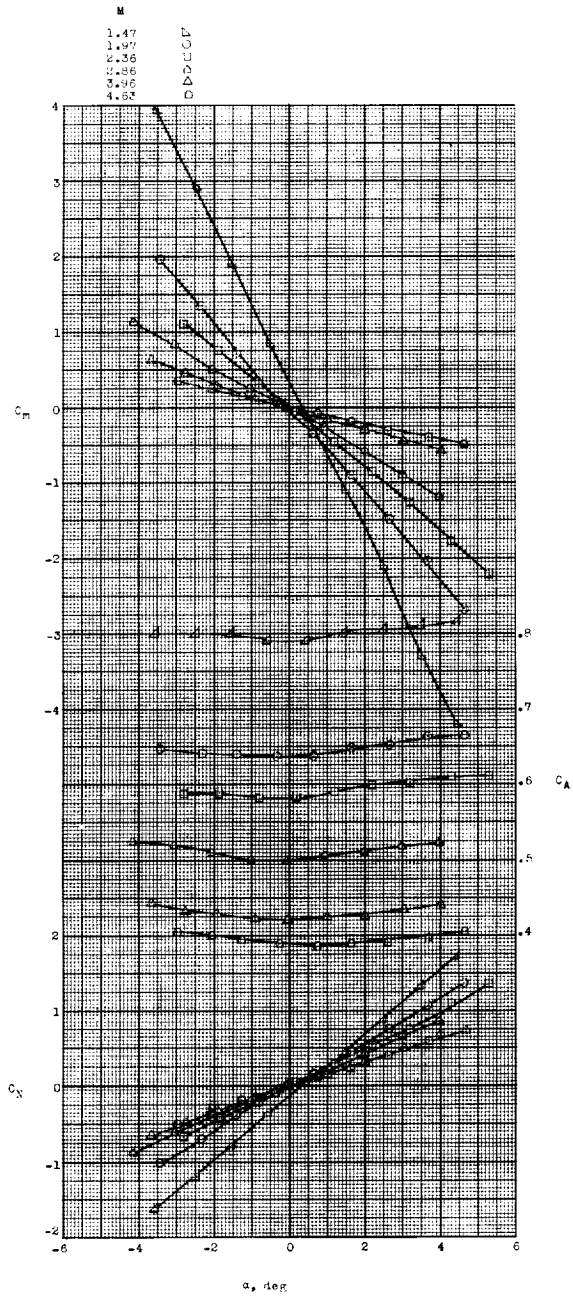

(a) $\delta_I = 0^o$; $\beta = 0^o$.

Figure 15.- Variation of pitch characteristics with angle of attack at six Mach numbers for two-stage configuration. 12-sq-ft, A = 1.5 fins.

L-1967

L-1967

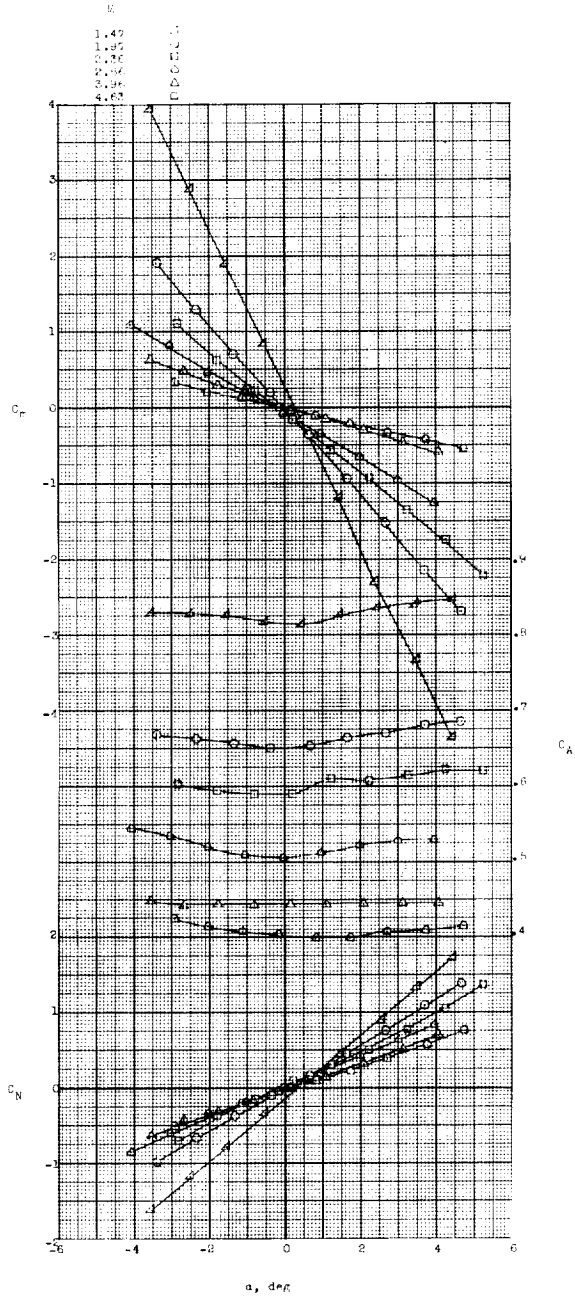

(b) $\delta_I = 2^o$; $\beta = 0^o$.

Figure 15.- Concluded.

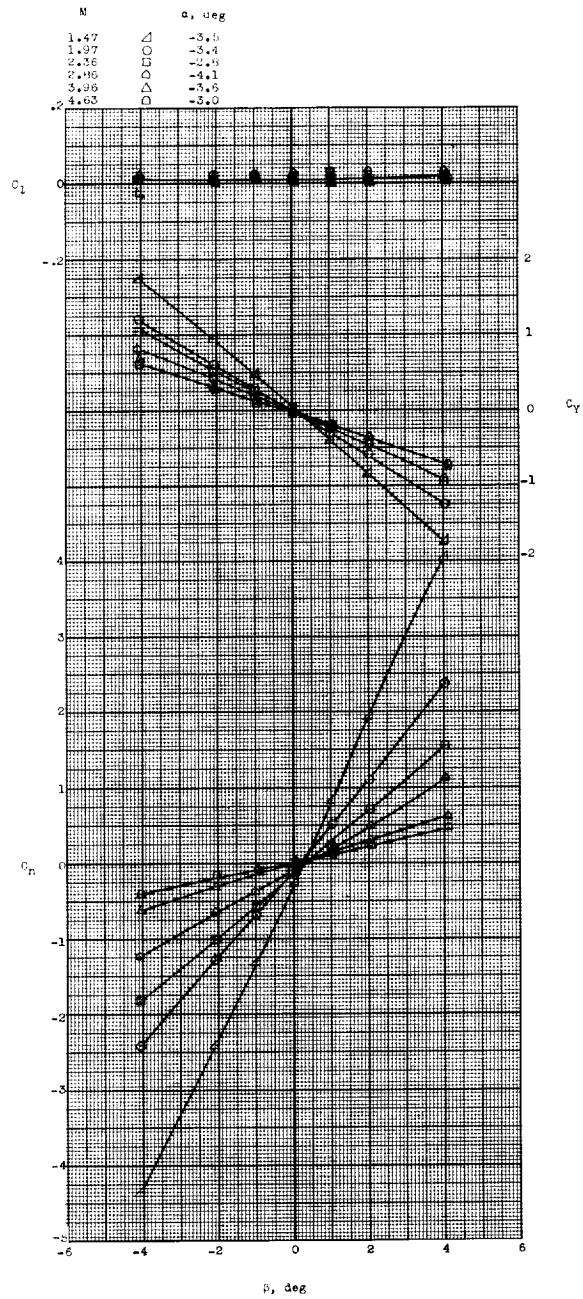

(a) $\delta_I = 0^o$; $\alpha \approx -4^o$.

Figure 16.- Variation of lateral characteristics with angle of sideslip at six Mach numbers for two-stage configuration. 12-sq-ft, A = 1.5 fins.

L-1967

L-1967

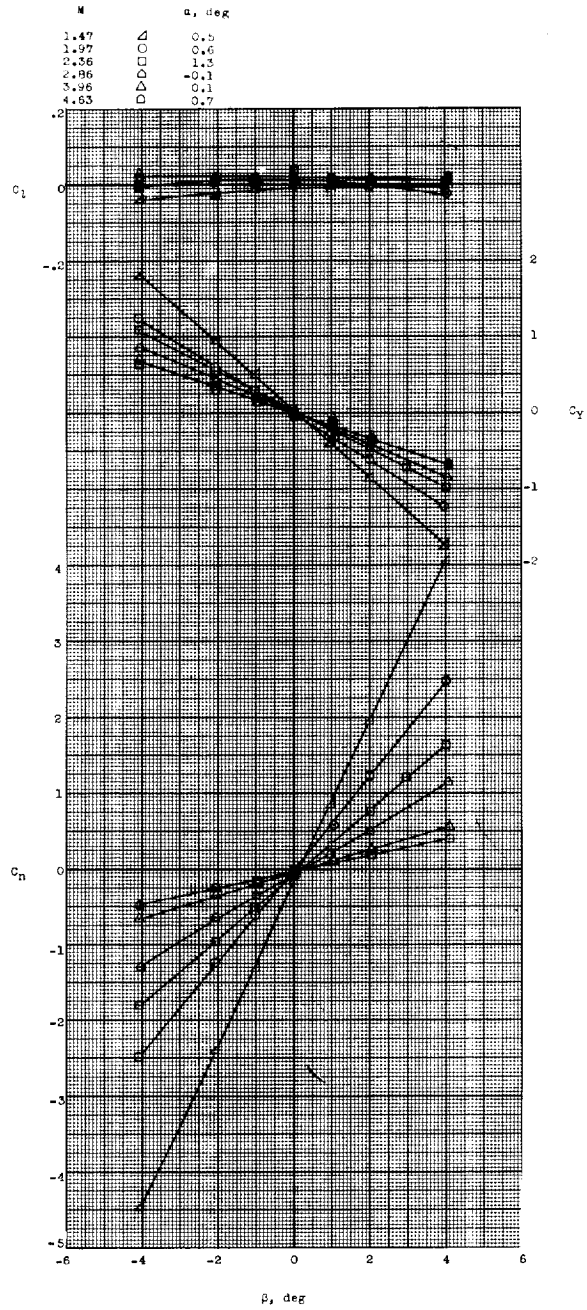

(b) $\delta_I = 0^\circ$; $\alpha \approx 0^\circ$.

Figure 16.- Continued.

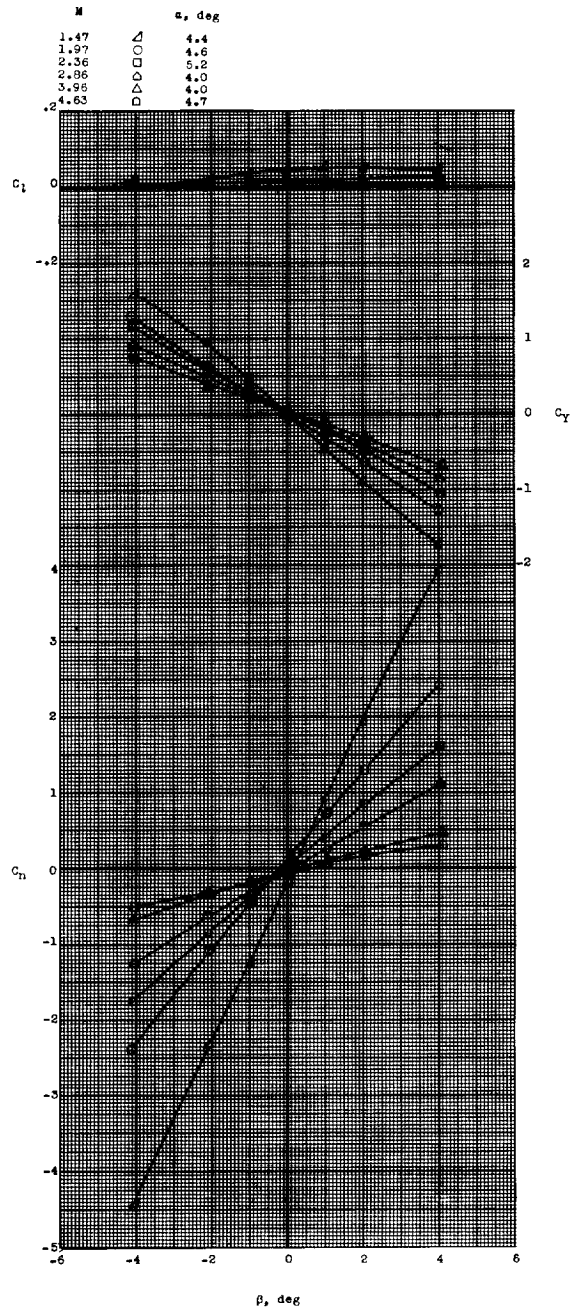

(c) $\delta_I = 0^\circ$; $\alpha \approx 4^\circ$.

Figure 16.- Concluded.

L-1967

L-1967

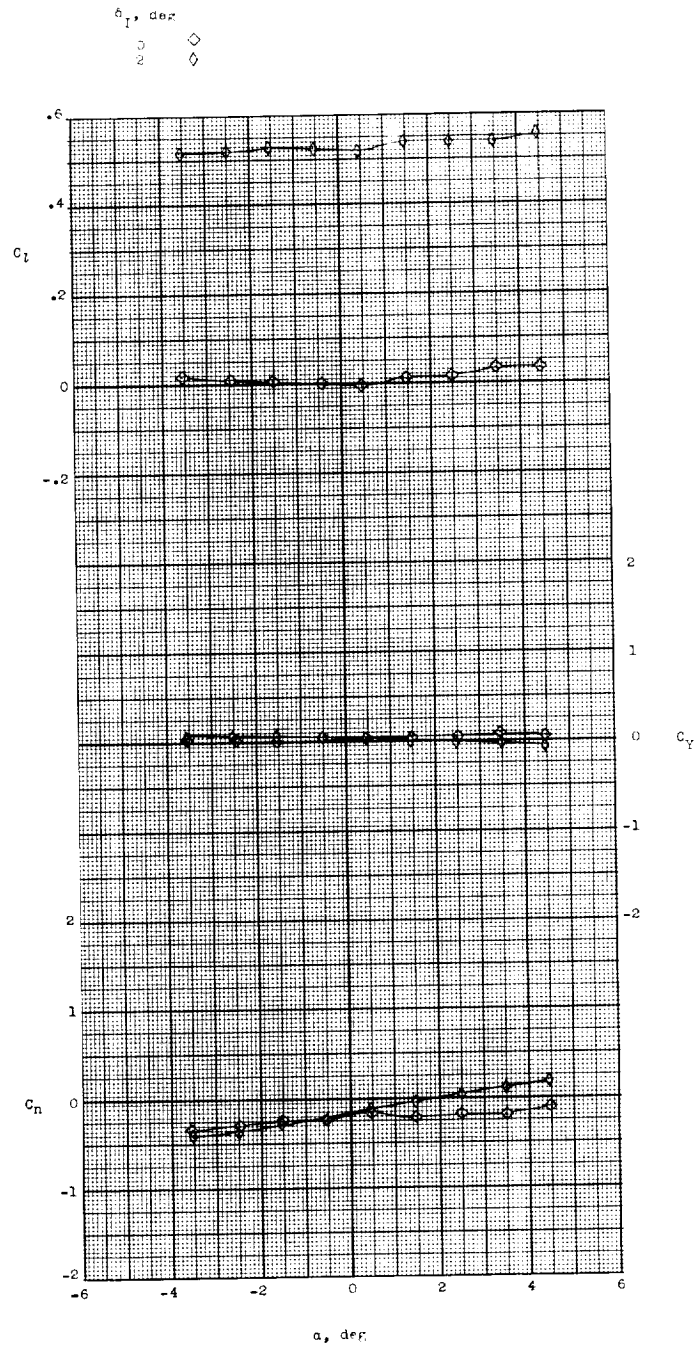

(a) M = 1.47; β = 0°.

Figure 17.- Variation of lateral characteristics with angle of attack for two-stage configuration with fin cant.

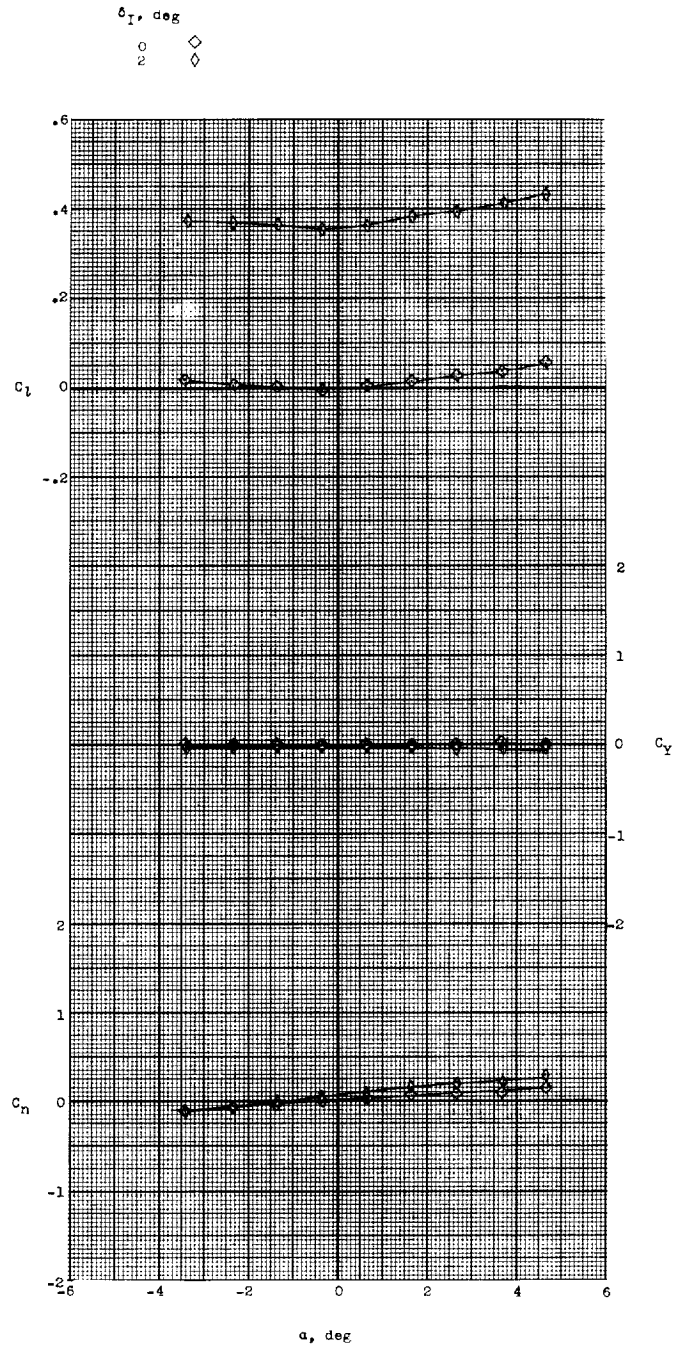

(b) M = 1.97; β = 0°.

Figure 17.- Continued.

L-1967

L-1967

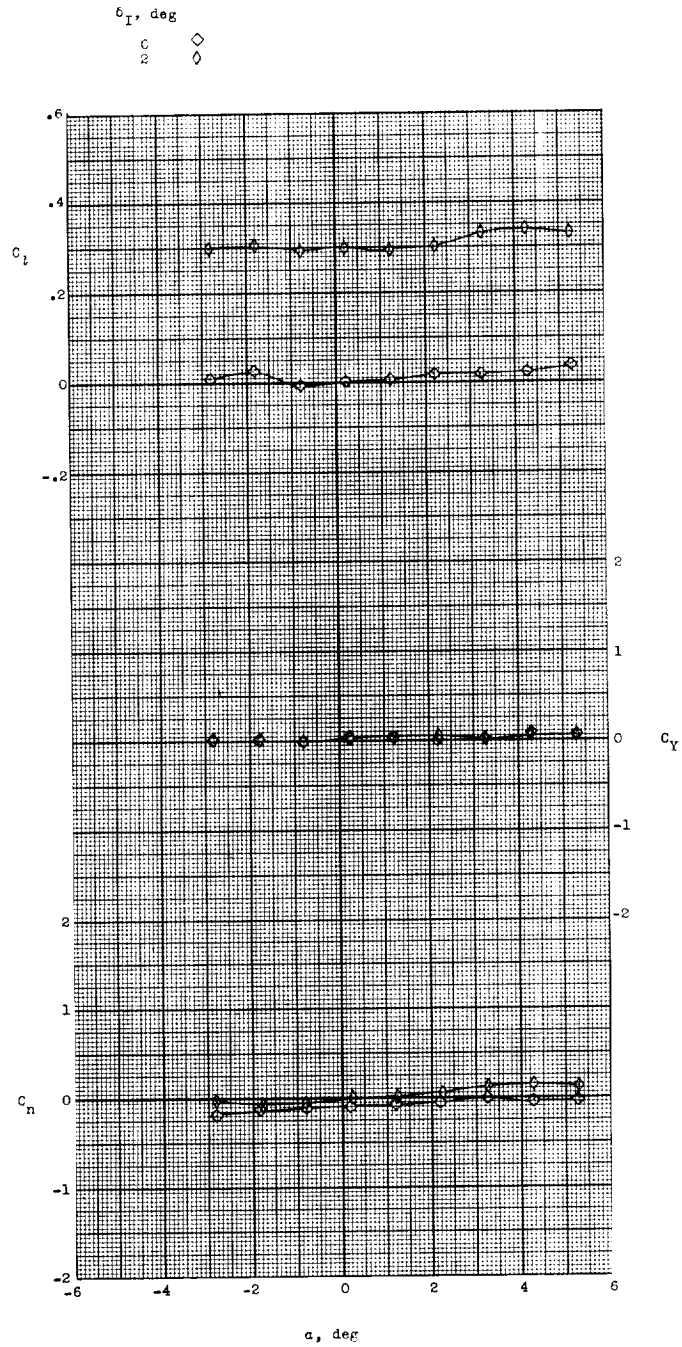

(c) M = 2.36; $\beta = 0^{\circ}$.

Figure 17.- Continued.

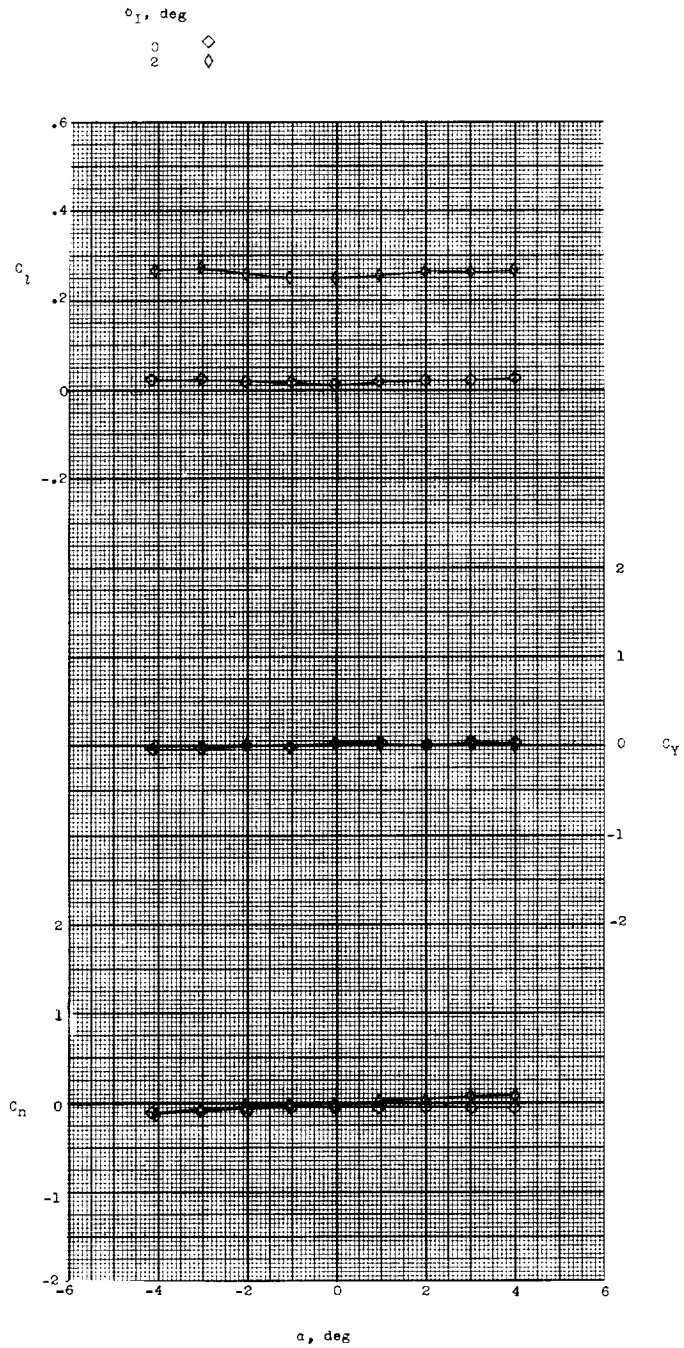

(d) M = 2.86; β = 0°.

Figure 17.- Continued.

L-1967

L-1967

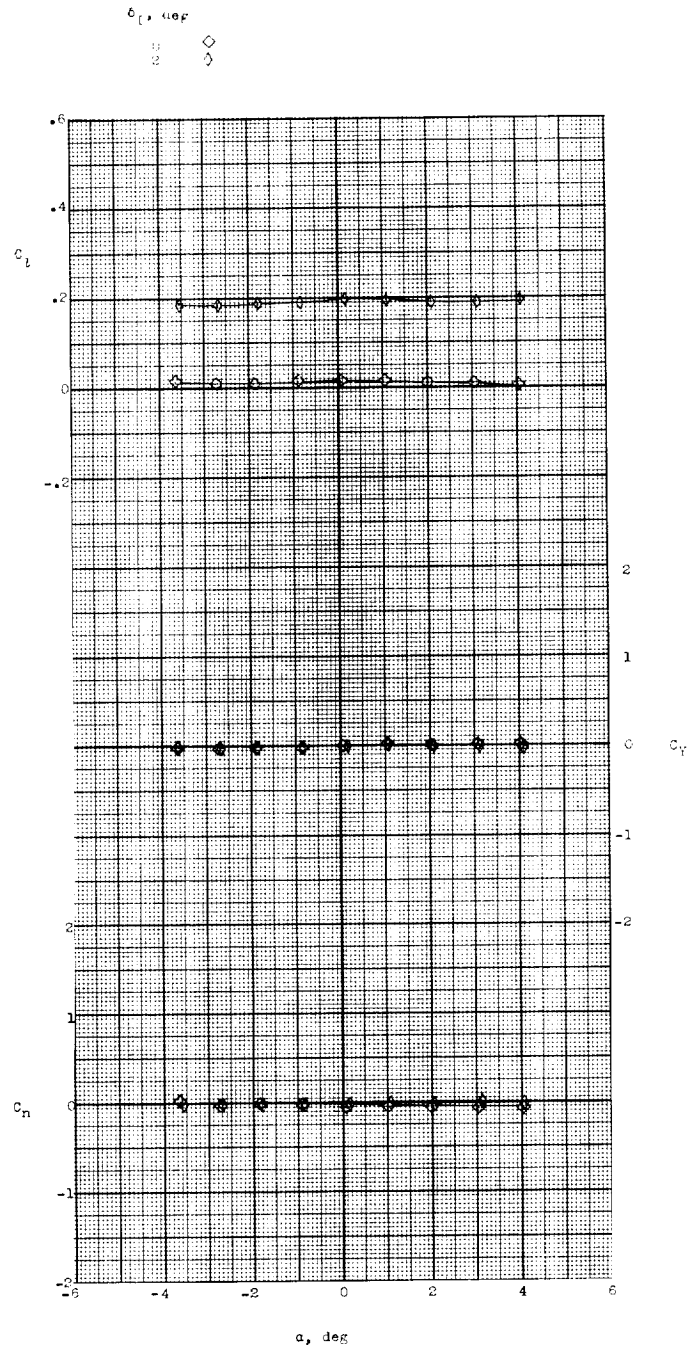

(e) M = 3.96; β = 0°.

Figure 17.- Continued.

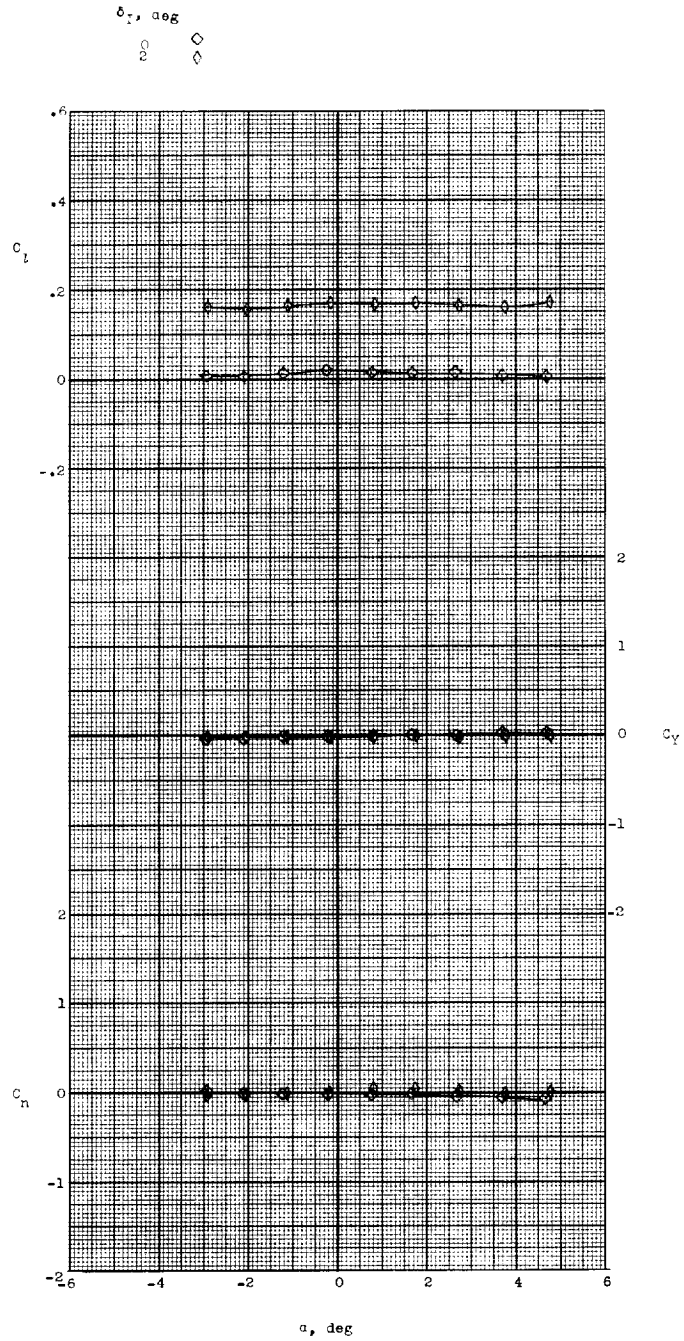

(f) M = 4.63; $\beta = 0^{\circ}$.

Figure 17.- Concluded.

L-1967

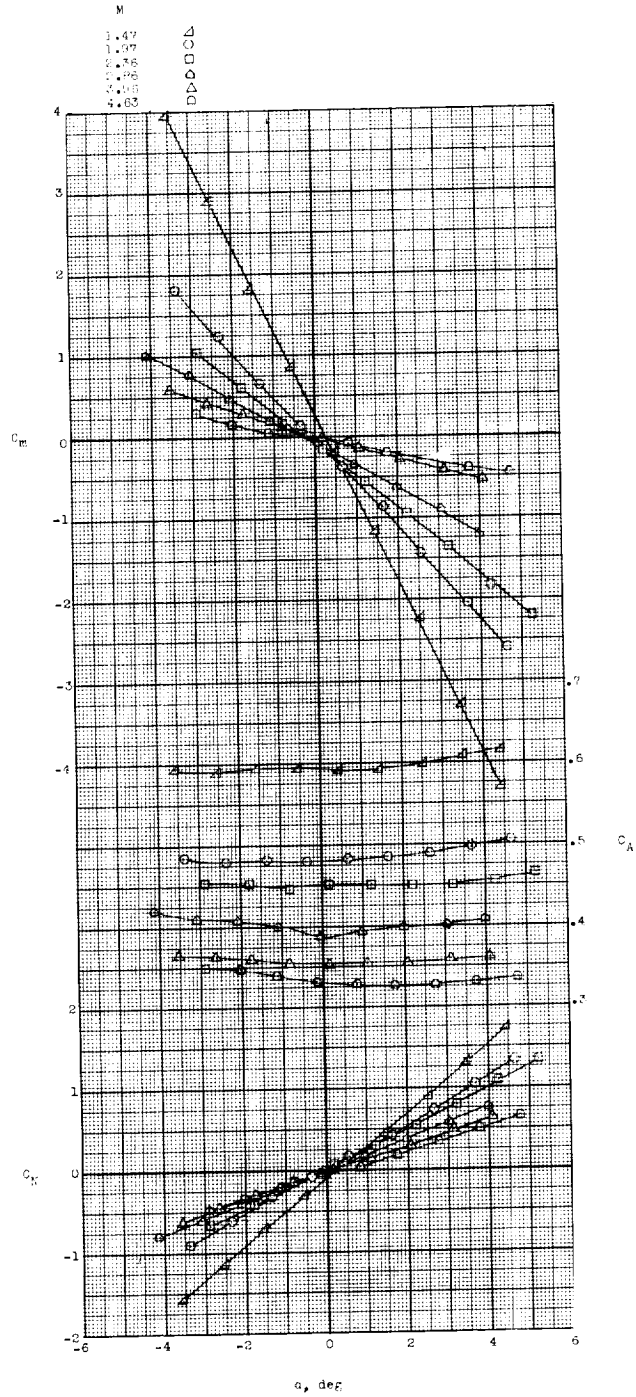

Figure 18.- Variation of pitch characteristics with angle of attack at six Mach numbers for two-stage configuration without auxiliary rocket motors. 12-sq-ft, A = 1.5 fins; $\delta_I = 0^o$; $\beta = 0^o$.

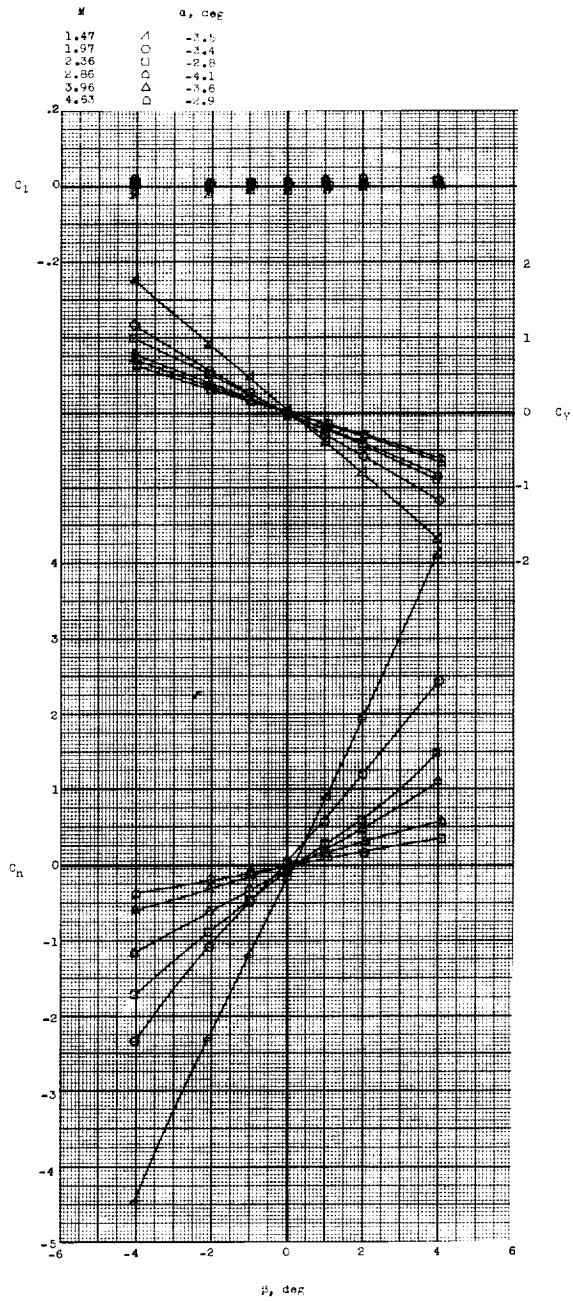

(a) $\delta_I = 0^o$; $\alpha \approx -4^o$.

Figure 19.- Variation of lateral characteristics with angle of sideslip at six Mach numbers for two-stage configuration without auxiliary rocket motors. 12-sq-ft, A = 1.5 fins.

L-1967

L-1967

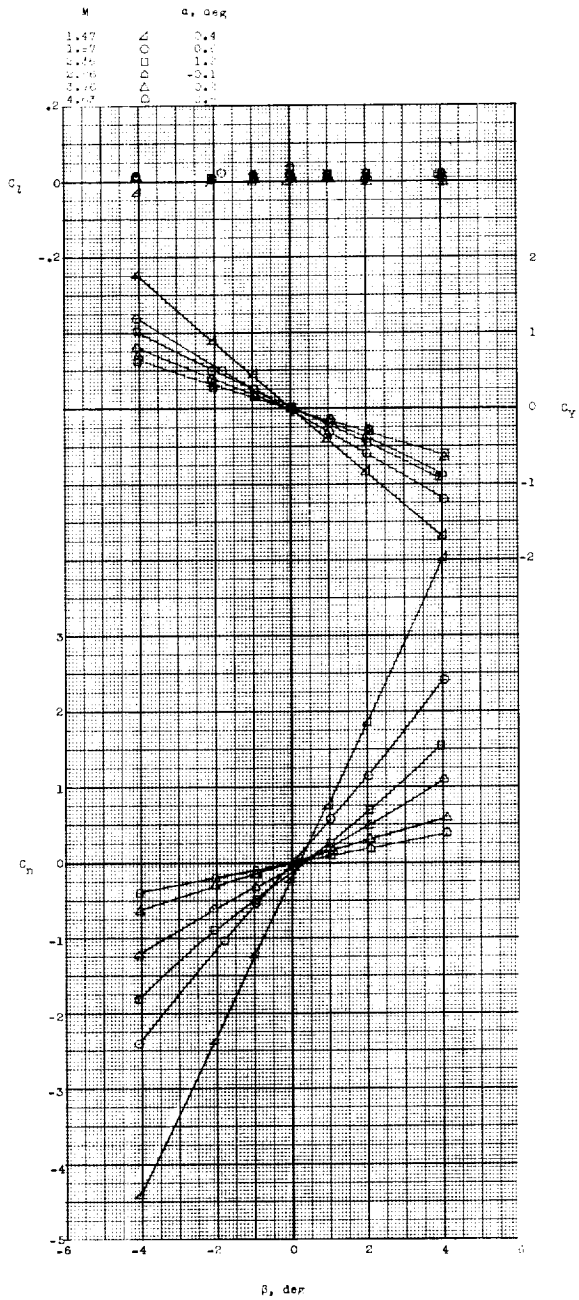

(b) $\delta_I = 0^\circ$; $\alpha \approx 0^\circ$.

Figure 19.- Continued.

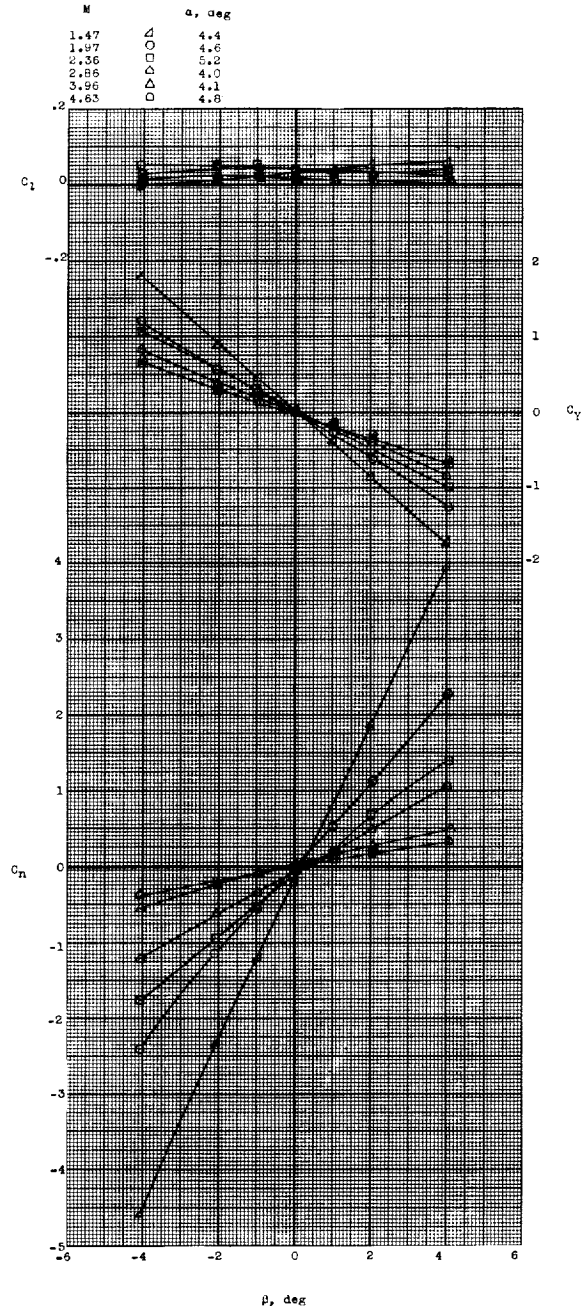

(c) $\delta_I = 0^\circ$; $\alpha \approx 4^\circ$.

Figure 19.- Concluded.

L-1967

L-1967

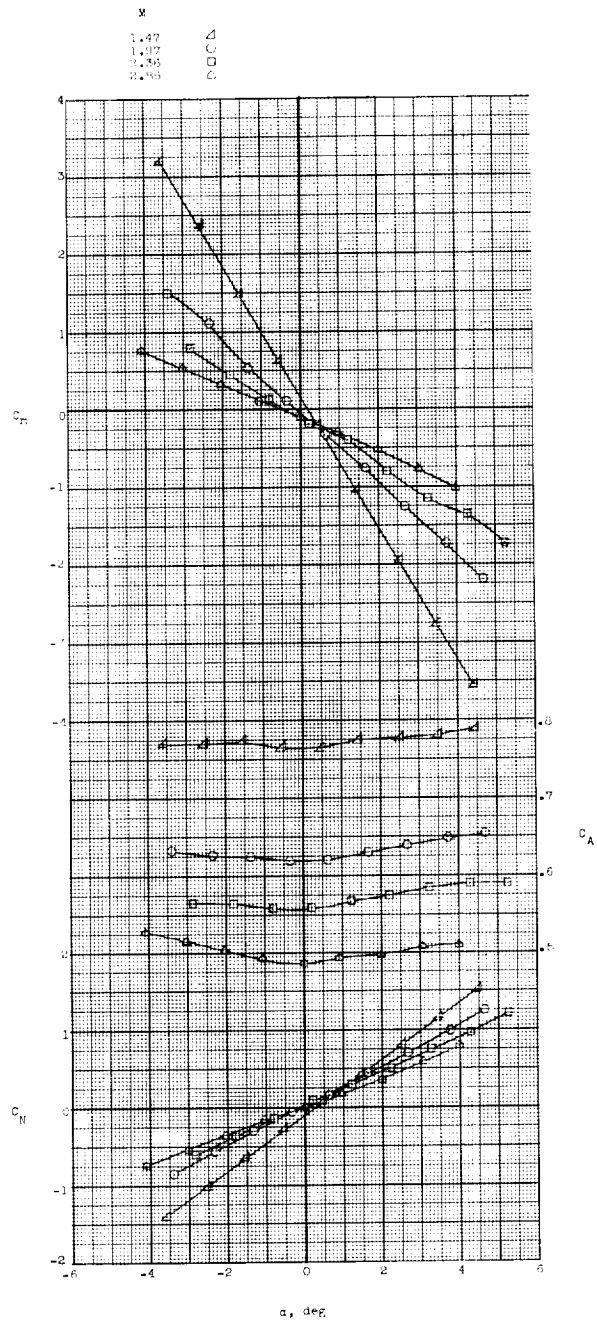

(a) $\delta_I = 0^o$; $\beta = 0^o$.

Figure 20.- Variation of pitch characteristics with angle of attack at four Mach numbers for two-stage configuration. 10-sq-ft, A = 1.5 fins.

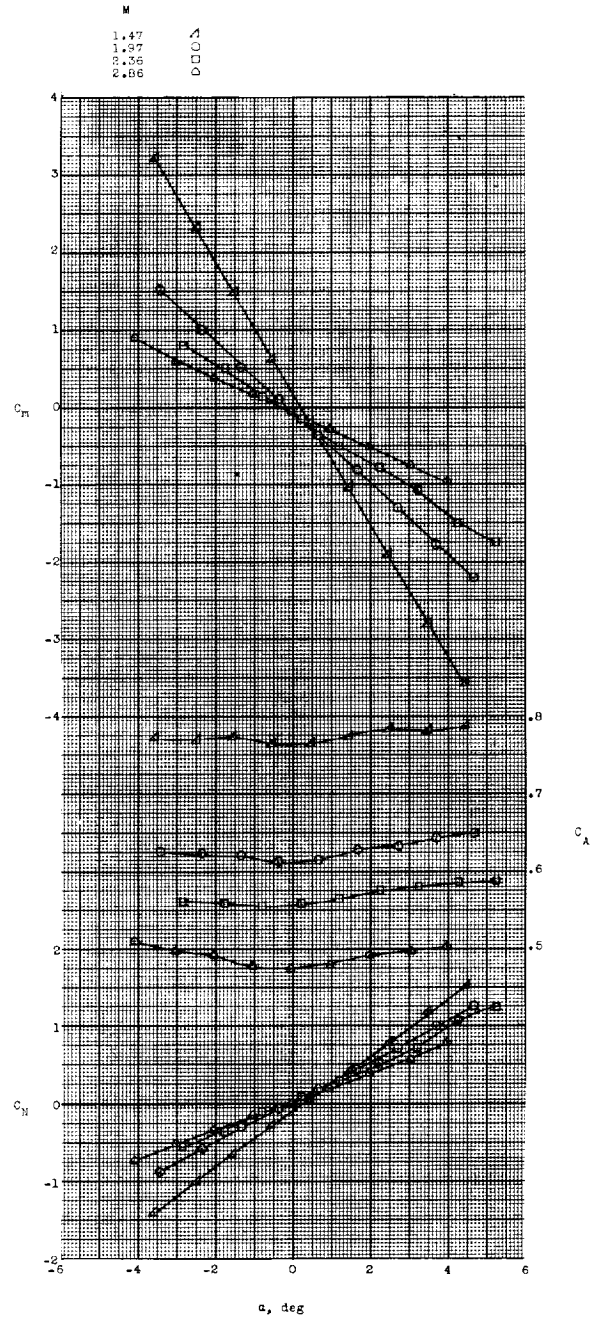

(b) $\delta_I = 2^o$; $\beta = 0^o$.

Figure 20.- Concluded.

L-1967

L-1967

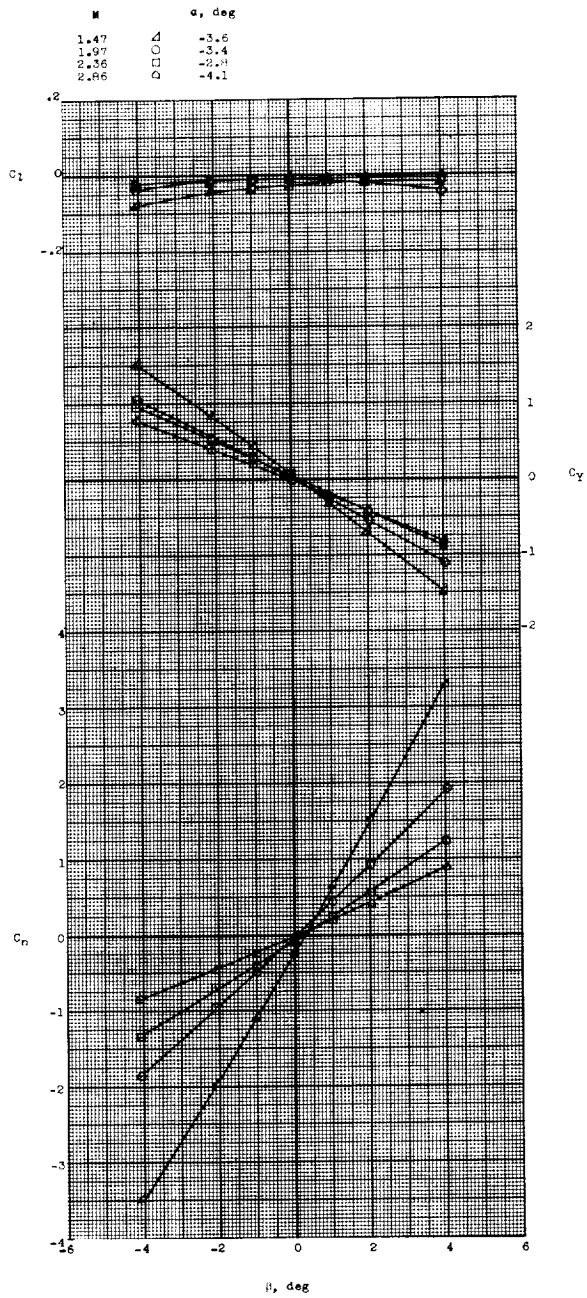

(a) $\delta_I = 0^\circ$; $\alpha \approx -4^\circ$.

Figure 21.- Variation of lateral characteristics with angle of sideslip at four Mach numbers for two-stage configuration. 10-sq-ft, A = 1.5 fins.

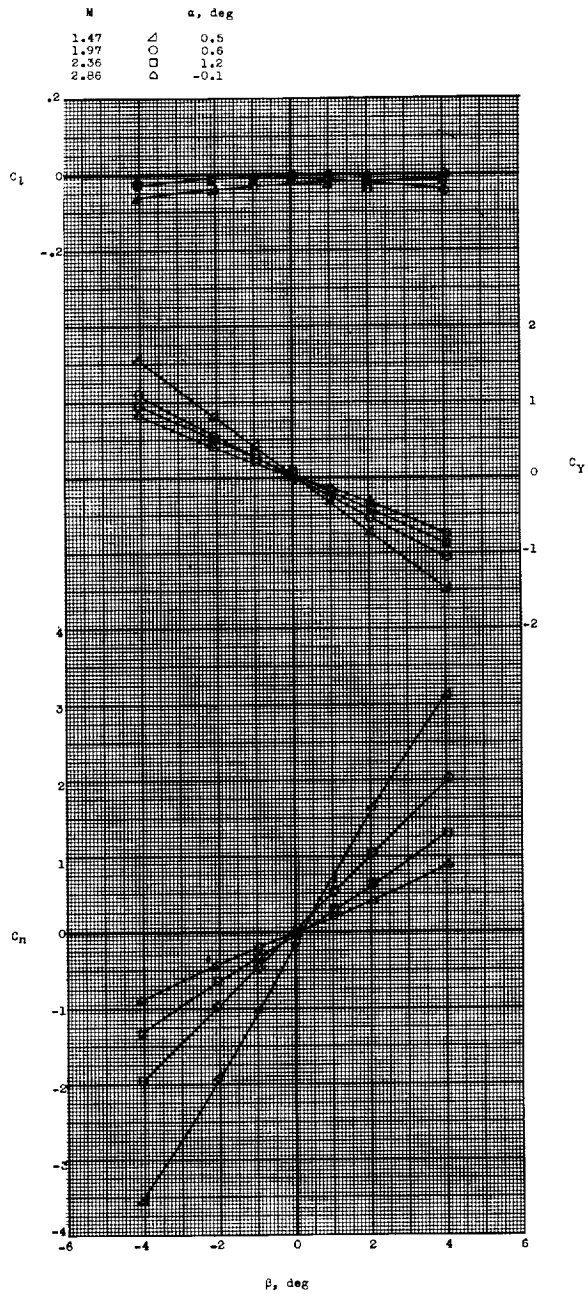

(b) $\delta_I = 0^\circ$; $\alpha \approx 0^\circ$.

Figure 21.- Continued.

L-1967

L-1967

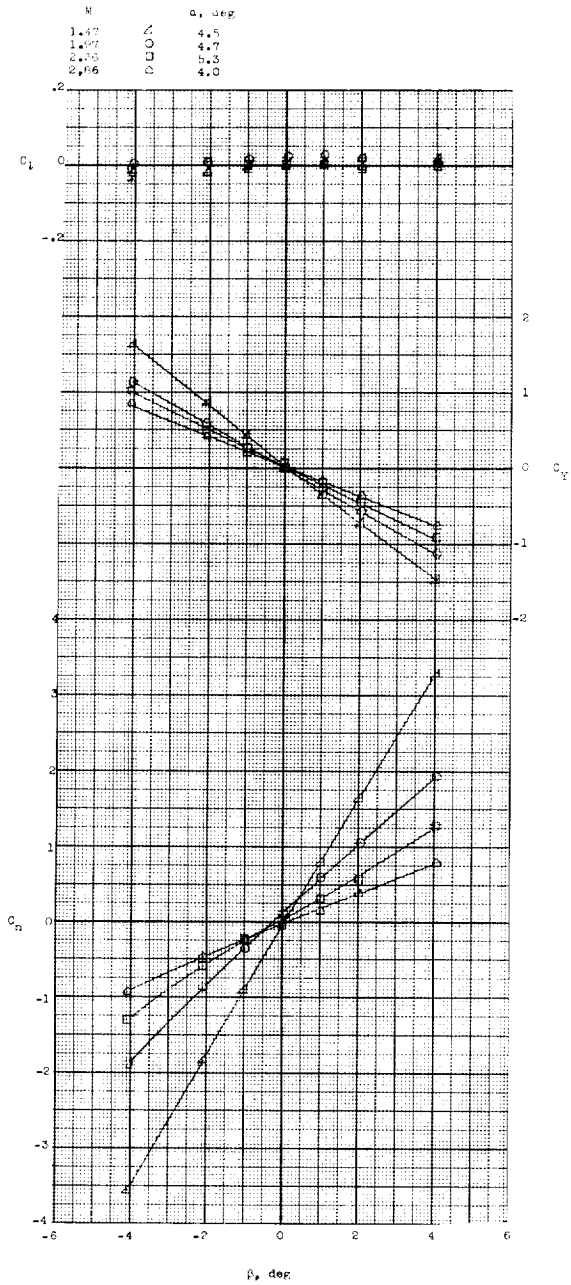

(c) $\delta_I = 0^o$; $\alpha \approx 4^o$.

Figure 21.- Concluded.

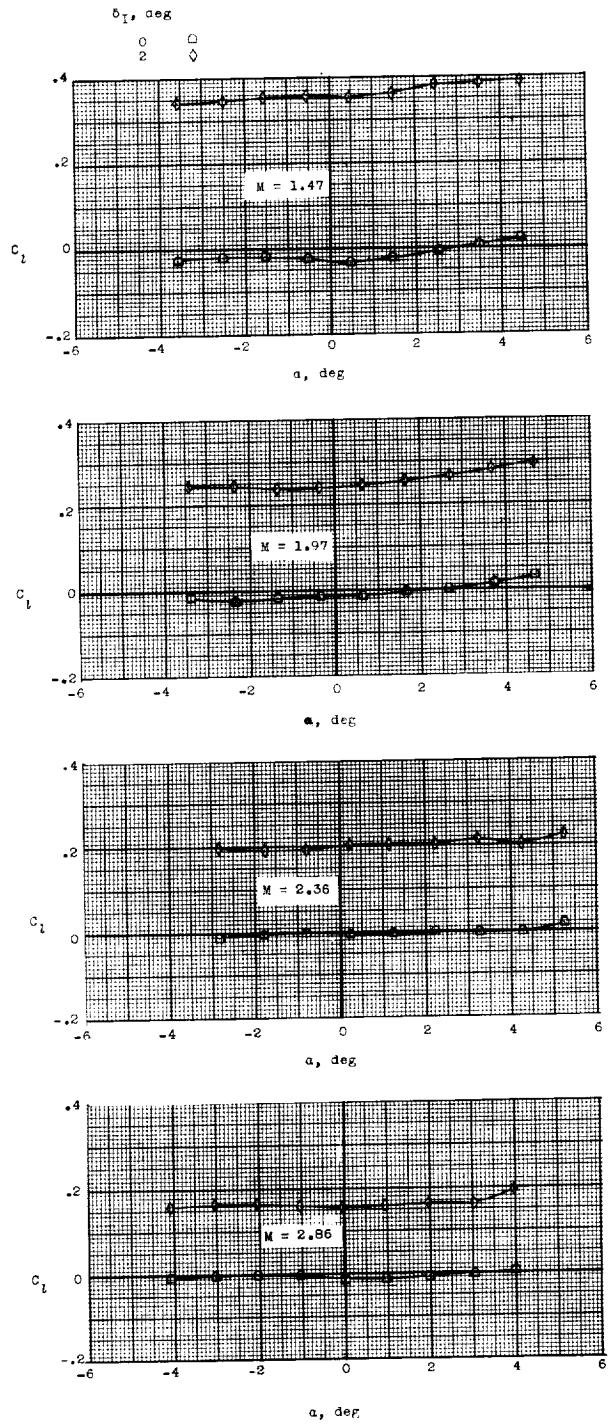

Figure 22.- Variation of rolling moment with angle of attack for two-stage configuration with fin cant. 10-sq-ft, A = 1.5 fins.

L-1967

L-1967

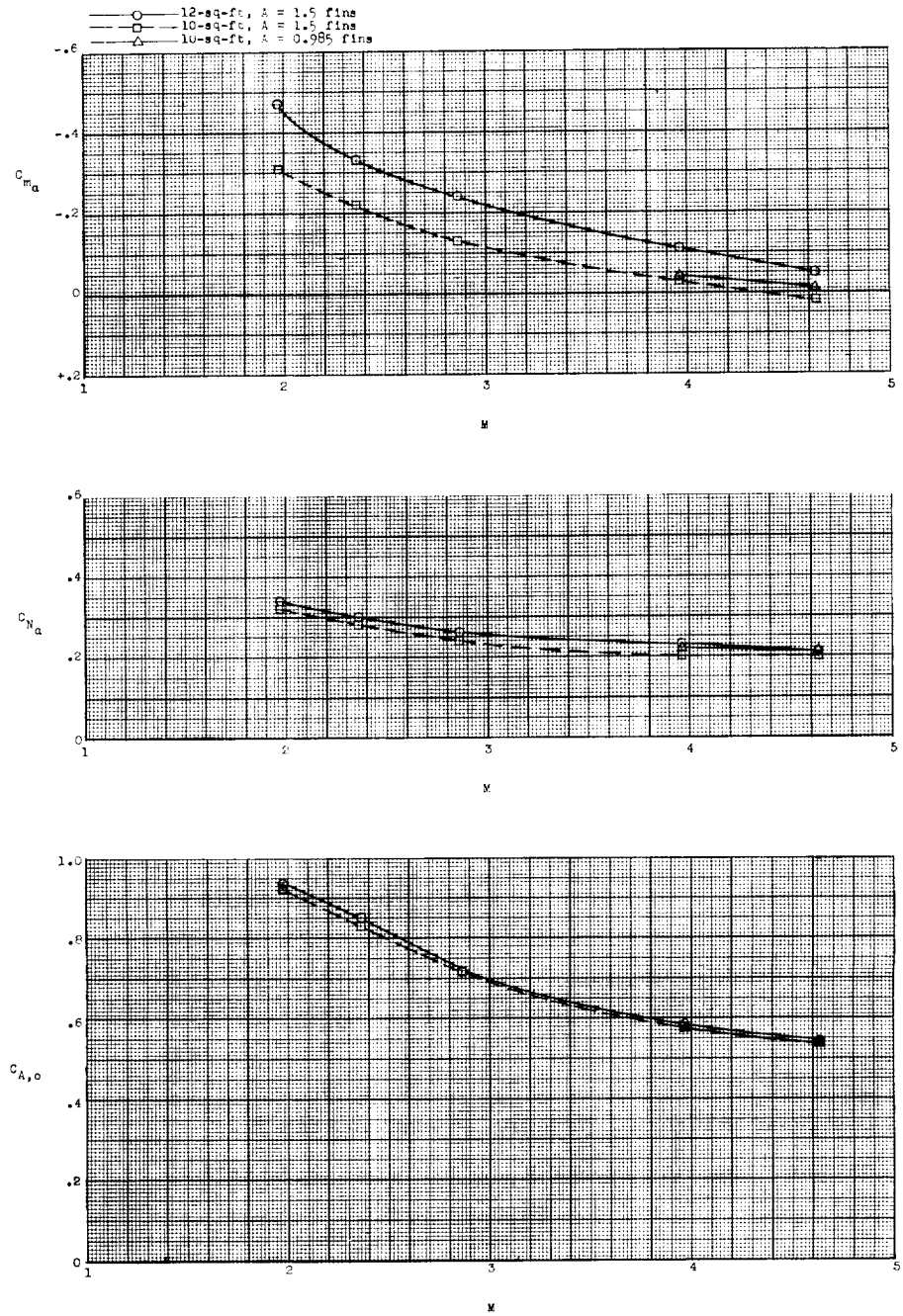

Figure 23.- Variation of pitching-moment derivative C_{m_α}, normal-force derivative C_{N_α}, and axial-force coefficient $C_{A,o}$ with Mach number for three-stage configurations.

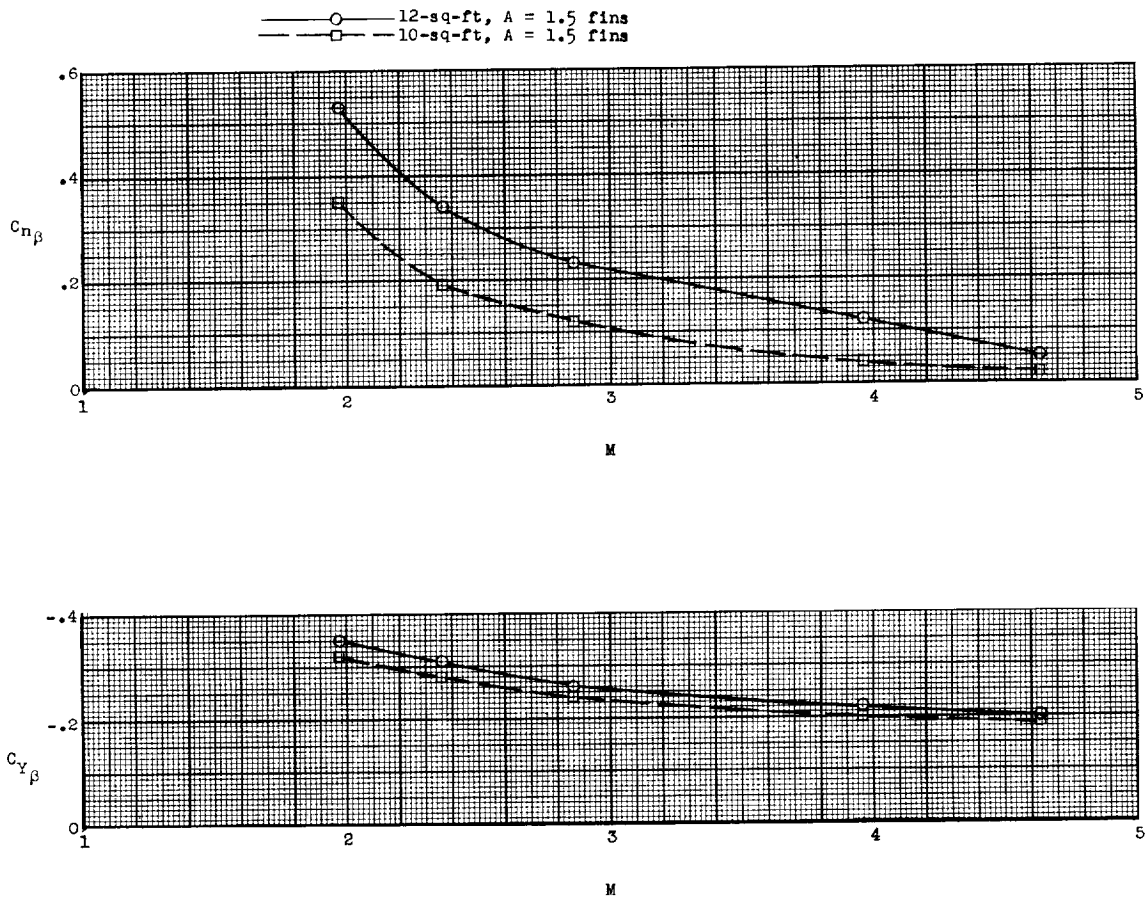

Figure 24.- Variation of yawing-moment derivative C_{n_β} and side-force derivative C_{Y_β} with Mach number for three-stage configurations.

L-1967

L-1967

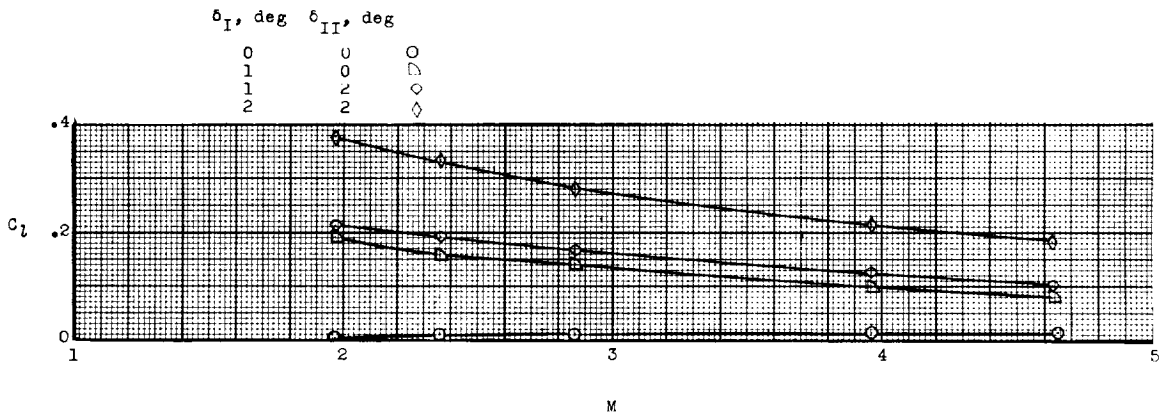

(a) 12-sq-ft, A = 1.5 fins.

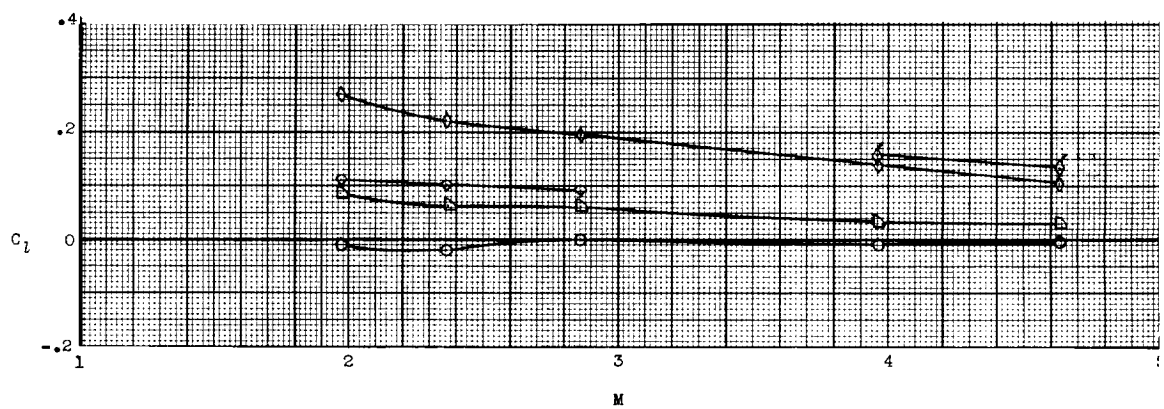

(b) 10-sq-ft, A = 1.5 fins. (Flagged symbols denote 10-sq-ft, A = 0.985 fins.)

Figure 25.- Variation of rolling-moment coefficient C_l with Mach number for three-stage configurations.

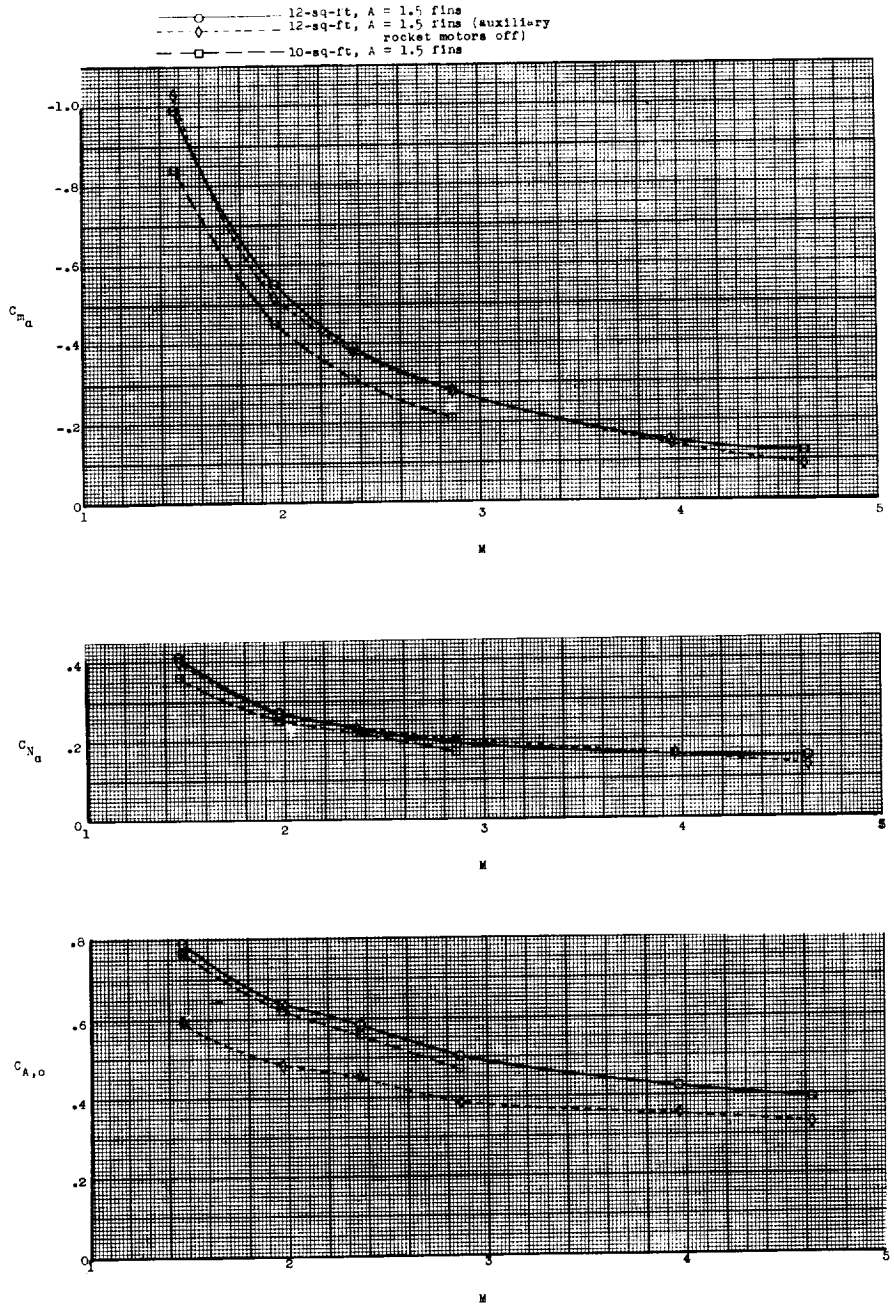

Figure 26.- Variation of pitching-moment derivative C_{m_α}, normal-force derivative C_{N_α}, and axial-force coefficient $C_{A,o}$ with Mach number for two-stage configurations.

L-1967

L-1967

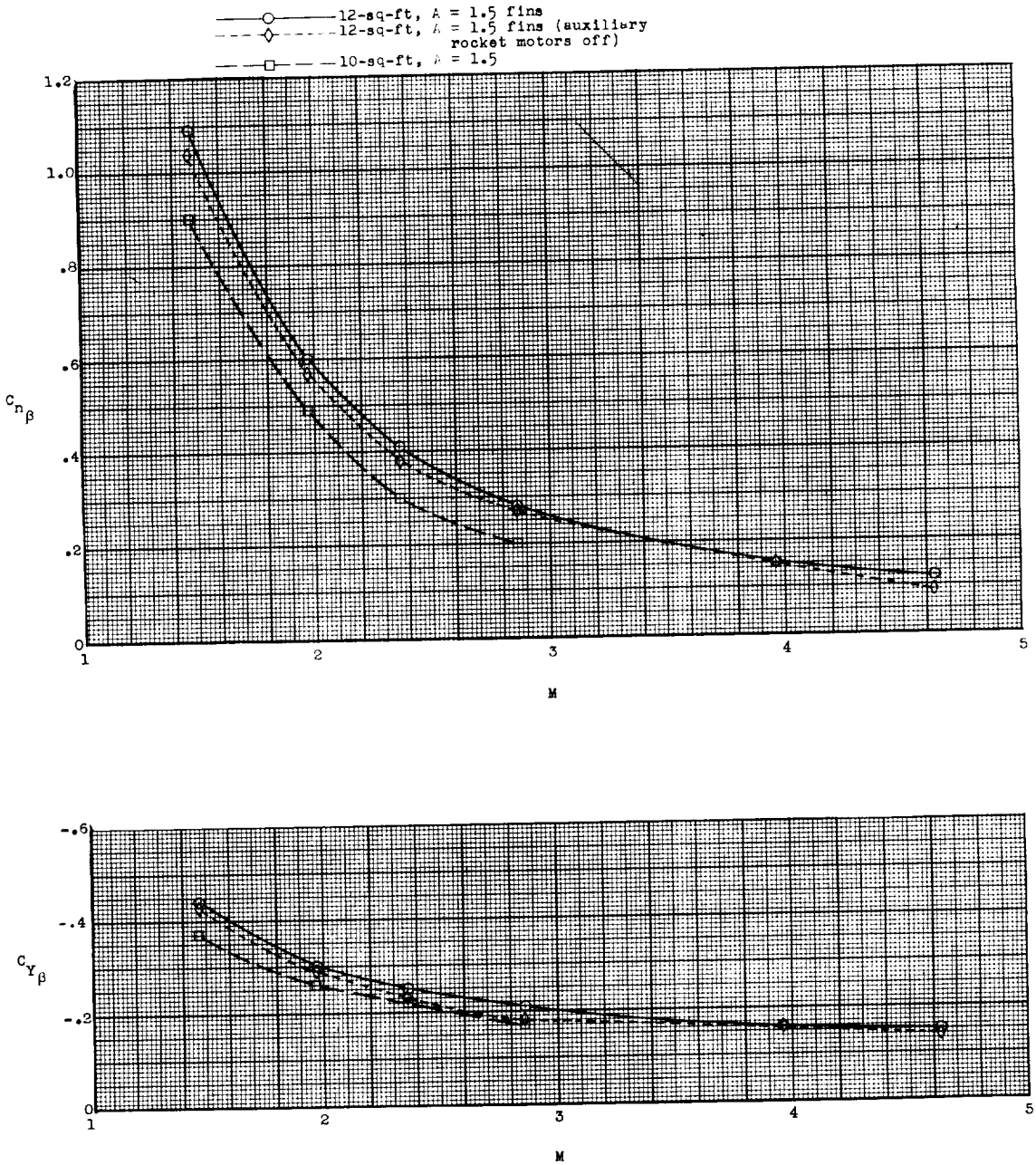

Figure 27.- Variation of yawing-moment derivative C_{n_β} and side-force derivative C_{Y_β} with Mach number for two-stage configurations.

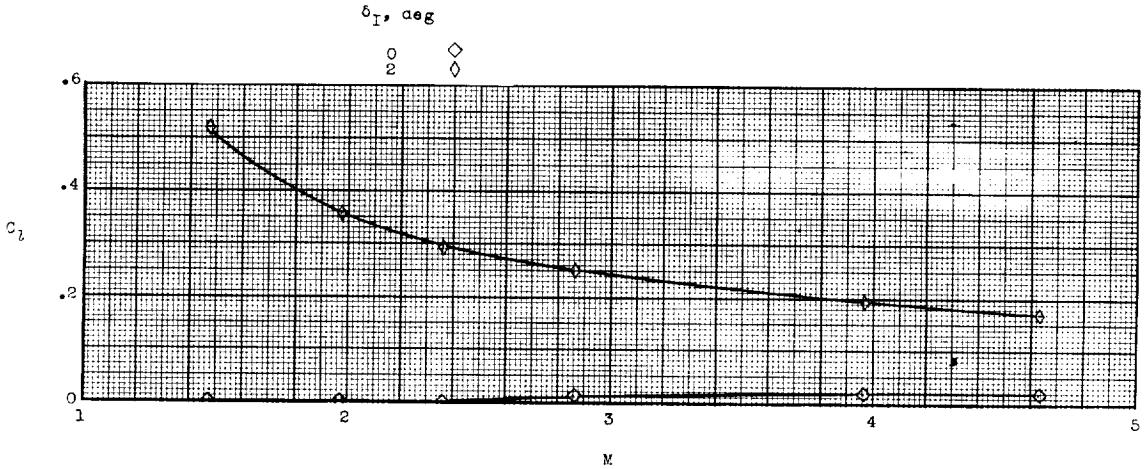

(a) 12-sq-ft, A = 1.5 fins.

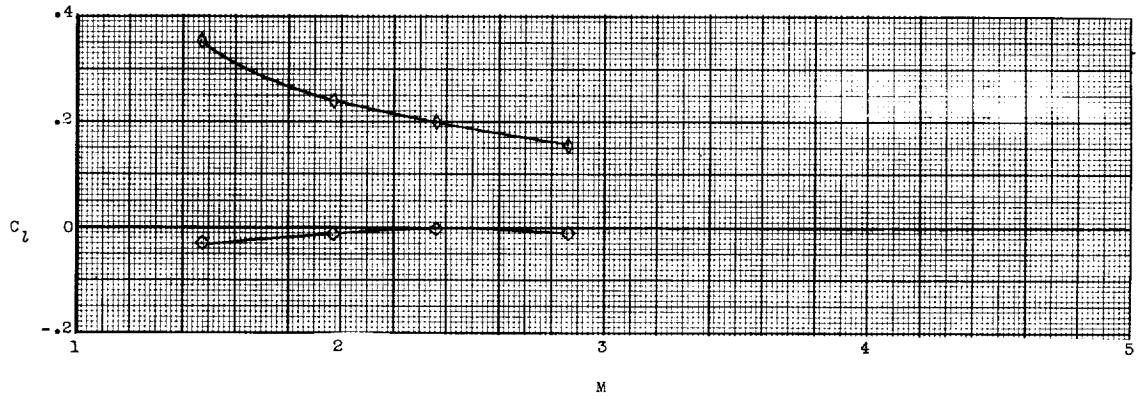

(b) 10-sq-ft, A = 1.5 fins.

Figure 28.- Variation of rolling-moment coefficient C_l with Mach number for two-stage configurations.

L-1967

L-1967

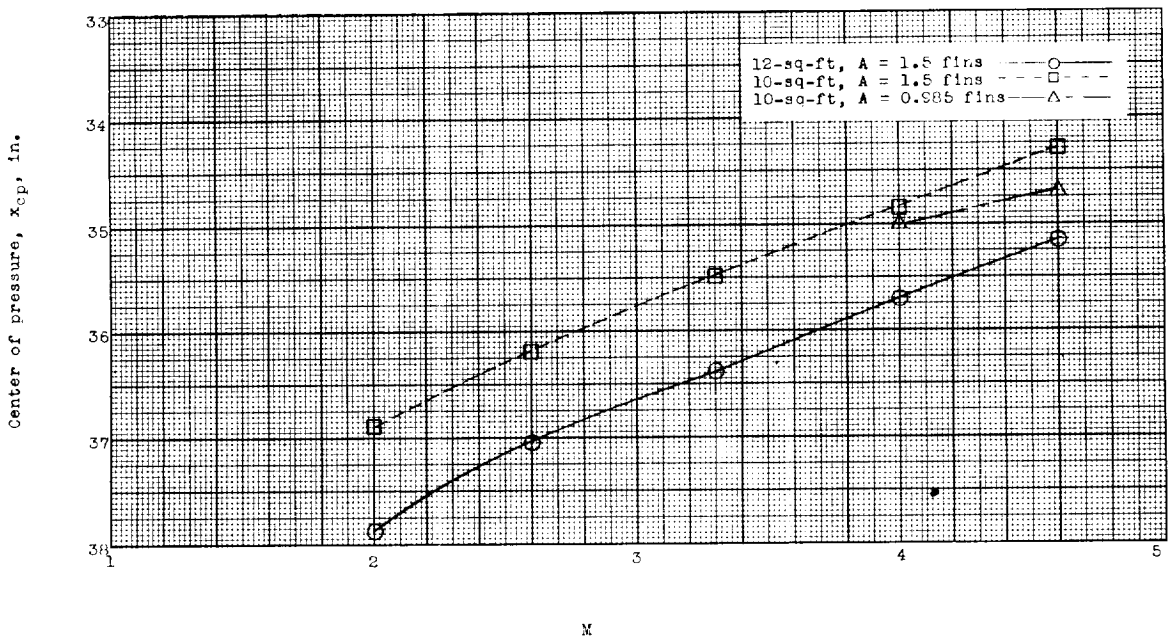

(a) Three-stage configuration.

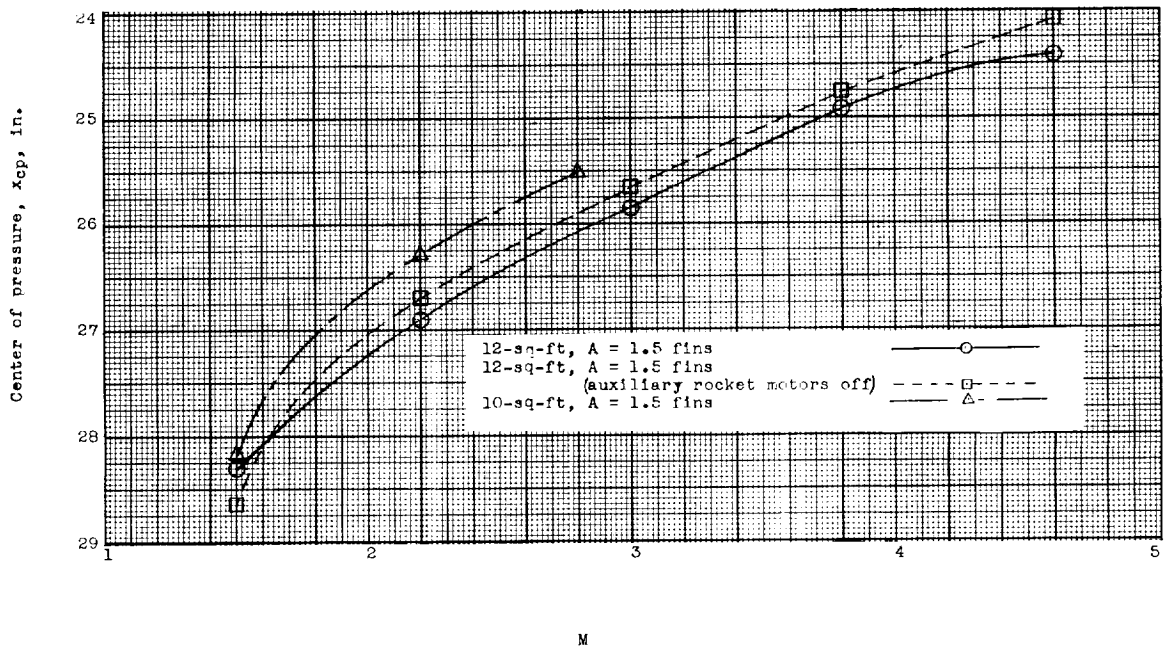

(b) Two-stage configuration.

Figure 29.- Variation of center-of-pressure location with Mach number for all configurations tested.

NASA-Langley, 1962 L-1967